

# Internal tides off the Amazon shelf Part I: importance for the structuring of ocean temperature during two contrasted seasons

Fernand Assene<sup>1</sup>, Ariane Koch-Larrouy<sup>2</sup>, Isabelle Dadou<sup>3</sup>, Michel Tchilibou<sup>4</sup>, Guillaume Morvan<sup>5</sup>, Jérôme Chanut<sup>6</sup>, Alex Costa da Silva<sup>7</sup>, Vincent Vantrepotte<sup>8</sup>, Damien Allain<sup>9</sup>, Trung-Kien Tran<sup>10</sup>

<sup>1,2,3,5,9</sup> Université de Toulouse, LEGOS (CNRS/IRD/UPS/CNES), Toulouse, France

<sup>1,6</sup> Mercator Ocean International, 31400, Toulouse, France

<sup>4</sup> Collecte Localisation Satellites (CLS), 31500, Ramonville Saint-Agne, France

<sup>7</sup> Departamento de Oceanografia da Universidade Federal de Pernambuco, DOCEAN/UFPE, Recife, Brazil

<sup>8,10</sup> Laboratoire d'Océanologie et de Géosciences (LOG), 62930, Wiméreux, France

Correspondence to: Fernand Assene [fassene@mercator-ocean.fr](mailto:fassene@mercator-ocean.fr)

## Abstract

The impact of the tides (internal and ~~barotropic~~external) on the vertical and horizontal structure of temperature off the Amazon River is investigated ~~over~~during two highly ~~contrasting~~contrasted seasons: ~~Twinned (AMJ: April-May-June and ASO: August-September-October) over a three-year period from 2013 to 2015. Twin~~ regional simulations with and without tides are used to highlight the general effect of tides. The tides tend to cool down the ocean from the surface (~0.3 °C) to above the thermocline (~1.2 °C), and to ~~thaw~~warm it up below the thermocline (~1.2 °C). The heat budget analysis leads to the conclusion that vertical mixing ~~could represent~~represents the dominant process that drives these temperature variations within the mixed layer, while it is associated with both horizontal and vertical advection below to explain temperature variations. The intensified mixing in the simulation including tides is attributed to the breaking of internal tides (ITs;IT) on their generation sites over the shelf break and offshore along their propagation pathways. ~~When~~While over the shelf, the mixing is ~~attributed to~~driven by the dissipation of the ~~barotropic~~external tides. ~~Both horizontal and~~In addition, vertical ~~advections exist in simulations without terms of the tides but are strengthened when including it. Furthermore, vertical~~ heat budget equation terms show ~~a~~wavelength patterns of mode-1 horizontal propagation wavelength of ITsIT.

~~In addition~~Moreover, we found ~~that~~ the tides can ~~also have an~~ impact ~~on~~the interactions between the upper ocean interface and the ~~underlying~~overlying atmosphere. They account for

Définition du style : Police par défaut

Définition du style : Commentaire

a mis en forme : Couleur de police : Texte 1

a mis en forme : Couleur de police : Texte 1

a mis en forme : Couleur de police : Texte 1

a mis en forme : Couleur de police : Texte 1

a mis en forme : Couleur de police : Texte 1

a mis en forme : Couleur de police : Texte 1

a mis en forme : Couleur de police : Texte 1

a mis en forme : Couleur de police : Texte 1

a mis en forme : Couleur de police : Texte 1

a mis en forme : Couleur de police : Texte 1

a mis en forme : Couleur de police : Texte 1

a mis en forme : Couleur de police : Texte 1

a mis en forme : Couleur de police : Texte 1

a mis en forme : Couleur de police : Texte 1

a mis en forme : Couleur de police : Texte 1

a mis en forme : Couleur de police : Texte 1

a mis en forme : Couleur de police : Texte 1

a mis en forme : Couleur de police : Texte 1

a mis en forme : Couleur de police : Texte 1

a mis en forme : Couleur de police : Texte 1

a mis en forme : Couleur de police : Texte 1

a mis en forme : Couleur de police : Texte 1

a mis en forme : Couleur de police : Texte 1

a mis en forme : Couleur de police : Texte 1

a mis en forme : Couleur de police : Texte 1

a mis en forme : Couleur de police : Texte 1

33 a significant proportion of the net heat flux between the atmosphere and the ocean, with a  
34 marked seasonal variation of 33.2% ~~in AMJ~~ to 7.4% ~~between the first and second~~ in ASO  
35 seasons. Tidal dynamics ~~could be~~ is therefore critical to understand the climate at regional  
36 climate scale. This study highlights the key role of tides, and particularly, how ITs IT-related  
37 vertical mixing helps to shape ocean temperature off the Amazon.

38 **Keywords:** Amazon shelf break, internal tides, mixing, temperature, heat flux, modeling,  
39 satellite data.

a mis en forme : Couleur de police : Texte 1

## 40 I. Introduction

41 ~~Temperature and its spatial structure carry out a crucial role in ocean dynamics,~~  
42 ~~including water mass formation (Swift and Aagaard, 1981; Lascaratos, 1993; Speer et al.,~~  
43 ~~1995), transport and mixing of other tracers in the ocean and exchanges with other biosphere~~  
44 ~~compartments (Archer et al., 2004; Rosenthal et al., 1997), and most importantly on surface~~  
45 ~~heat exchange at the interface with the atmosphere (Clayson and Bogdanoff, 2013; Mei et al.,~~  
46 ~~2015) and can thus significantly influence the climate (Li et al., 2006; Collins et al., 2010). This~~  
47 ~~oceanic thermal structure can be modified at various spatial and temporal scales. Through~~  
48 ~~different processes external to the ocean like solar radiation, heat exchanges with the~~  
49 ~~atmosphere, winds, precipitation, and freshwater inputs from rivers. And by its internal~~  
50 ~~processes such as mass transport by currents and eddies (e.g., Aguedjou et al., 2021), mixing~~  
51 ~~by turbulent diffusion (Kunze et al., 2012), internal waves and their dissipation (Barton et al.,~~  
52 ~~2001; Smith et al., 2016; Salamena et al., 2021). Finally, bottom friction of the barotropic tidal~~  
53 ~~currents may also produce intensified mixing especially for shallow water condition (e.g., over~~  
54 ~~a shelf, see Lambeck and Runcorn, 1977; Le Provost and Lyard, 1997) and significantly modify~~  
55 ~~ocean temperature in surface layers (Li et al., 2020).~~

56 ~~The key source for internal waves generation is the barotropic or external tides. The~~  
57 ~~external tides when interacting with sharp topography (e.g., ridge, sea mounts, shelf break) in~~  
58 ~~a stratified ocean generate internal tides also called internal tidal/gravity waves, that may~~  
59 ~~propagate and dissipate in the ocean interior causing diapycnal mixing (Baines, 1982; Munk~~  
60 ~~and Wunsch, 1998; Egbert and Ray, 2000). The precise location of this dissipation is a big~~  
61 ~~unknown. But evidence of dissipation at the generation sites, at the reflection to the bottom or~~  
62 ~~close to the surface when the energy rays interact with the thermocline and pycnocline, have~~  
63 ~~been measured and modelled (among others: Laurent and Garrett, 2002; Sharples et al., 2007;~~  
64 ~~2009; Koeh Larrouy et al., 2015; Nugroho et al., 2018; Xu et al., 2020 and Whalen et al., 2020).~~

65 ITs may also dissipate or lose energy when they encounter others or when they interact with  
66 mesoscale or fine scale structures (Vlasenko and Stashchuk, 2006; Dunphy and Lamb, 2014).  
67 Moreover, the surface interactions allow nonlinear internal solitary waves (ISW) to develop and  
68 to propagate usually with phase locked to the ITs troughs (New and Pingree, 1990, 2000;  
69 Azevedo et al., 2006; da Silva et al., 2011). Finally, ISW can dissipate and induce mixing  
70 (Sandstrom and Oakey, 1995; Feng et al., 2021; Purwandana et al., 2022). Moreover, ITs can  
71 vertically advect the water masses following their propagation. The effect is the vertical shifts  
72 in isopycnic levels of few meters to tens of meters, which can be observed in the thermocline  
73 (Wallace et al., 2008; Xu et al., 2020). But over a tidal cycle, the mean effect on temperature is  
74 null except some tidal residual circulation exists (Bessières, 2007).

75 Our study focuses on the oceanic region of northern Brazil off the Amazon River. This  
76 region exhibits a variation in the wind position and hence the position of the Intertropical  
77 Convergence Zone (ITCZ) during the year. This directly influences the discharge of the  
78 Amazon River, oceanic circulation, eddy kinetic energy (EKE) and the stratification (Muller-  
79 Karger et al., 1988; Johns et al., 1998; Xie and Carton, 2004). Hence, two very contrasting  
80 seasons form, April-May-June (AMJ) and August-September-October (ASO). AMJ (vs. ASO)  
81 season is characterized by an increasing (vs. decreasing) river discharge, stronger (vs. smaller)  
82 and shallower (vs. deeper) pycnocline. The North Brazilian Current (NBC) and eddy kinetic  
83 energy (EKE) are weaker (vs. stronger) (Aguedjou et al., 2019, Tchilibou et al., 2022). For the  
84 ASO season, the stronger NBC develops a retroflection (NBCR) between 5°-8° N that feeds  
85 the North Equatorial Counter Current (NECC) transporting the water masses towards the east  
86 of the tropical Atlantic. The retroflexion also generates very large anticyclonic eddies (NBC  
87 Rings) exceeding 450 km in diameter (Didden and Schott, 1993; Richardson et al., 1994;  
88 Garzoli et al., 2004), which in turn transport water masses towards the Northern Hemisphere  
89 (Bourles et al., 1999a; Johns et al., 1998; Schott et al., 2003).

90 Internal tides are generated on the sharp shelf break which possesses a depth decreasing  
91 of 200-2000 m over some tens of kilometers (Fig.1). Six main sites (A to F) have been  
92 identified, with the most intense, A and B, located in the southern part of the region (Fig.1;  
93 Magalhaes et al., 2016, Tchilibou et al., 2022). Previous studies have shown that in this region  
94 ITs propagation is modulated by the seasonal variation of the currents (Magalhaes et al., 2016;  
95 Lentini et al., 2016; Tchilibou et al., 2022; de Macedo et al., 2023). In addition, seasonal  
96 variations in stratification induce changes in the internal tide's activity. With in AMJ (vs. ASO)  
97 a stronger (vs. smaller) energy conversion and a stronger (vs. smaller) local dissipation of ITs

98 energy (Barbot et al., 2021, Tehilibou et al., 2022). Moreover, the interaction between the  
99 weaker (vs. stronger) background circulation and ITs can lead to less (vs. more) incoherent or  
100 non-stationary internal tides (Tehilibou et al., 2022). Incoherent ITs can account for about half  
101 of the total internal tides in the global ocean and much more when looking at some regional  
102 ocean system. For example over 80% in equatorial Pacific (Zaron, 2017) and over 40% off the  
103 Amazon (see Fig. 11e-f in Tehilibou et al., 2022). But quantifying the associated energy is  
104 difficult to determine and is still unknown in our region but is part of the scope of upcoming  
105 studies.

106 The role of ITs on the thermal structure of the ocean is of increasing interest with many  
107 studies in recent years. In the Hawaii shallow shelf surface waters, Smith et al. (2016) report  
108 that ITs can induce surface cooling from 1 °C to 5 °C. For the Indonesian region, IT induce an  
109 annual mean surface cooling of 0.5 °C (Koch-Larrouy et al., 2007, 2008; Nagai and Hibiya,  
110 2015 and Nugroho et al., 2018), that decreases local atmospheric convection, which in turn  
111 reduces precipitation by 20%. They can therefore fulfil a relevant role on regional climate  
112 (Koch-Larrouy et al., 2010, Sprintall et al., 2014, 2019). Furthermore, in the Andaman Sea,  
113 Jithin and Francis (2020) showed that ITs can affect the temperature in deep waters (>1600 m),  
114 leading to a warming of about 1–2 °C. But off the Amazon plateau, the impact of ITs on the  
115 thermal structure of the ocean is still poorly understood.

116 During the ASO season, cold water (< 27.6 °C) associated with the western extension  
117 of the Atlantic Cold water Tongue (ACT) enter the region from the south and run along the  
118 edge of the continental shelf to about 3°N, establishing a cold cell often referred to as seasonal  
119 upwelling (Lentz and Limeburner, 1995; Neto and da Silva, 2014). Modelling studies, with and  
120 without tides, have shown that this upwelling is affected by the tides. Cooling is more realistic  
121 when tides are included (Ruault et al., 2020). However, these analyses cannot determine what  
122 processes are at work. For example, it is not yet explicit whether the tidal-induced cooling is  
123 due to mixing on the shelf produced by barotropic tides, or to the mixing produced by baroclinic  
124 tides at their generation sites and propagation pathways. Neto and da Silva (2014), based on *in*  
125 *situ* observations, suggest instead that it is the vertical advection triggered by the NBC that can  
126 explain the cooling observed at the surface. Following on from the latter, we can also examine  
127 the role of horizontal advection and its contribution relative to vertical advection.

128 Temperature and its spatial structure play a crucial role in ocean, including water mass  
129 formation (Swift and Aagaard, 1981; Lascaratos, 1993; Speer et al., 1995), transport and mixing  
130 of other tracers in the ocean and exchanges with other biosphere compartments (Archer et al.,

131 2004, Rosenthal et al., 1997), and most importantly on surface heat exchange at the interface  
132 with the atmosphere (Clayson and Bogdanoff, 2013; Mei et al., 2015) and can thus significantly  
133 influence the climate (Li et al., 2006; Collins et al., 2010). This oceanic thermal structure can  
134 be modified at various spatial and temporal scales, through different processes external to the  
135 ocean like solar radiation, heat exchanges with the atmosphere, winds, precipitation, and  
136 freshwater inputs from rivers, and by its internal processes such as mass transport by currents  
137 and eddies (e.g., Aguedjou et al., 2021), mixing by turbulent diffusion (Kunze et al., 2012), the  
138 dissipation of internal waves (Barton et al., 2001; Smith et al., 2004; Salamena et al., 2021).  
139 Finally, bottom friction of the barotropic tidal currents may also produce intensified mixing  
140 especially for shallow water conditions (e.g., over a shelf, see Lambeck and Runcorn, 1977; Le  
141 Provost and Lyard, 1997) and significantly modify ocean temperature in surface layers (Li et  
142 al., 2020).

143 The barotropic tides, also called external tides, are the main source for internal waves  
144 generation. The external tides, when interacting with sharp topography (e.g., ridge, sea mounts,  
145 shelf break) in a stratified ocean, generate internal tides, that propagate and dissipate in the  
146 ocean interior causing diapycnal mixing (Baines, 1982; Munk and Wunsch, 1998; Egbert and  
147 Ray, 2000). A number of observational and modelling studies have shown that this dissipation  
148 occurs at the generation sites, at the reflection to the bottom or close to the surface when the  
149 energy rays interact with the thermocline and pycnocline (among others: Laurent and Garrett,  
150 2002; Sharples et al., 2007, 2009; Koch-Larrouy et al., 2015; Nugroho et al., 2018; Whalen et  
151 al., 2012). IT also dissipate or lose energy by wave-wave interactions or when they interact with  
152 mesoscale or fine-scale structures (Vlasenko and Stashchuk, 2006; Dunphy and Lamb, 2014).

153 The role of internal tides on the ocean's thermal structure has been the subject of  
154 growing interest and numerous studies in recent years. In the Hawaii shallow shelf surface  
155 waters, Smith et al. (2016) report that IT can induce surface cooling from 1 °C to 5 °C. For the  
156 Indonesian region, IT induce an annual mean surface cooling of 0.5 °C (Koch-Larrouy et al.,  
157 2007, 2008; Nagai and Hibiya, 2015 and Nugroho et al., 2018) that decreases local atmospheric  
158 convection, which in turn reduces precipitation by 20%. They can therefore fulfil a relevant role  
159 on regional climate (Koch-Larrouy et al., 2010; Sprintall et al., 2014, 2019). Furthermore, in  
160 the Andaman Sea, Jithin and Francis (2020) showed that internal tides can affect the  
161 temperature in deep waters (> 1600 m), leading to a warming of about 1–2 °C. But off the  
162 Amazon plateau, their impact on the thermal structure of the ocean is still poorly understood.

163 Our study focuses on the oceanic region of northern Brazil off the Amazon River. This  
164 region exhibits a variation in the wind position and hence the position of the Intertropical  
165 Convergence Zone (ITCZ) during the year. This directly influences the discharge of the  
166 Amazon River, oceanic circulation, eddy kinetic energy (EKE) and the stratification (Muller-  
167 Karger et al., 1988; Johns et al., 1990; Xie and Carton, 2004). Hence, two very contrasting  
168 seasons form, April-May-June (AMJ) and August-September-October (ASO). AMJ (vs. ASO)  
169 is characterized by an increasing (vs. decreasing) river discharge, stronger (vs. smaller) and  
170 shallower (vs. deeper) pycnocline. The North Brazilian Current (NBC) and eddy kinetic energy  
171 (EKE) are weaker (vs. stronger) (Aguedjou et al., 2019, Tchilibou et al., 2022). For the ASO  
172 season, the stronger NBC develops a retroflection (NBCR) between 5°–8° N that feeds the  
173 North Equatorial Counter-Current (NECC) transporting the water masses towards the east of  
174 the tropical Atlantic. The retroflection also generates very large anticyclonic eddies (NBC  
175 Rings) exceeding 450 km in diameter (Didden and Schott, 1993; Richardson et al., 1994;  
176 Garzoli et al., 2003), which in turn transport water masses towards the Northern Hemisphere  
177 (Bourles et al., 1999; Johns et al., 1998; Schott et al., 2003).

178 Internal tides are generated on the sharp shelf break featured by a depth decreasing from  
179 200-2000 m over some tens of kilometers (Fig.1). Six main sites (A to F) have been identified,  
180 with the most intense, A and B, located in the southern part of the region (Fig.1; Magalhaes et  
181 al., 2016, Tchilibou et al., 2022). Previous studies have shown that in this region IT propagation  
182 is modulated by the seasonal variation of the currents (Magalhaes et al., 2016; Lentini et al.,  
183 2016; Tchilibou et al., 2022). In addition, seasonal variations in stratification induce changes in  
184 the internal tide's activity, with in AMJ (vs. ASO) a stronger (vs. smaller) energy conversion  
185 and a stronger (vs. smaller) local dissipation of IT energy (Barbot et al., 2021, Tchilibou et al.,  
186 2022). The interaction between the weaker (vs. stronger) background circulation and IT leads  
187 to less (vs. more) incoherent or non-stationary internal tides (Tchilibou et al., 2022).

188 During the ASO season, cold water (< 27.6 °C) associated with the western extension  
189 of the Atlantic Cold-water Tongue (ACT) runs the region from the south and run along the edge  
190 of the continental shelf to about 3°N, establishing a cold cell often referred to as seasonal  
191 upwelling (Lentz and Limeburner, 1995; Neto and da Silva, 2014). Modelling studies, with and  
192 without tides, have shown that this upwelling is affected by the tides. Cooling is more realistic  
193 when tides are included (Ruault et al., 2020). However, these analyses cannot determine what  
194 processes are at work. For example, it is not yet explicit whether the tidal-induced cooling is  
195 due to mixing on the shelf produced by barotropic tides, or to the mixing produced by baroclinic

196 ~~tides at their generation sites and propagation pathways. Based on *in situ* observations, Neto~~  
197 ~~and da Silva (2014) suggest instead that it is the vertical advection triggered by the NBC that~~  
198 ~~can explain the cooling observed at the surface.~~

199 To answer the previous questions, we ~~used~~use a high-resolution model ( $1/36^\circ$ ) with and  
200 without explicit tidal forcing and a satellite SST product, with the aim of highlighting the impact  
201 of tides on the temperature structure and quantify the associated processes. We distinguish the  
202 analysis for the two contrasted seasons (AMJ and ASO) described above. The SST product, our  
203 model, and the methods used are described in section II. The validation of certain characteristics  
204 of the barotropic and baroclinic tides and of the temperature is presented in section III. The  
205 impacts of ~~HsIT~~ on the temperature structure, the influence on heat exchange at the  
206 atmosphere-ocean interface, and the processes involved, are analyzed in section IV. The  
207 discussion and the summary of the obtained results are presented in section V and VI  
208 respectively.

## 209 II. Data and Methods

### 210 II.1. Satellite Data ~~used~~: TMI SST

211 This dataset ~~is~~ derived from Tropical Rainfall Measurement Mission (TRMM), which  
212 performs measurements using onboard TRMM Microwave Imager (TMI). The microwaves can  
213 penetrate clouds and are therefore crucially important for data acquisition in low latitude  
214 regions, cloudy covered during long periods of raining seasons. We use ~~Remote Sensing~~  
215 ~~Systems (RSS)~~ TMI data products v7.1, which represents the most recent version of TMI SST.  
216 It contains a daily mean of SST with a  $0.25^\circ \times 0.25^\circ$  grid resolution ( $\sim 25$  km). This SST is  
217 obtained by inter-calibration of TMI data with other microwave radiometers. The TMI SST full  
218 description and inter-calibration algorithm are detailed in ~~Wentz et al., (2015)~~Wentz (2015).

### 219 II.2. The NEMO Model: *AMAZON36* configuration

220 ~~The numerical model used in this study is the Nucleus for European Modelling of the~~  
221 ~~Ocean (NEMOv4.0.2, Madec et al., 2019). The configuration designed for our purpose is called~~  
222 ~~*AMAZON36* and covers the western tropical Atlantic region from the Amazon River mouth to~~  
223 ~~the open ocean. Other configurations exist in this region, but either they have a coarse grid ( $1/4^\circ$~~   
224 ~~, Hernandez et al., 2016), or when the grid is fine ( $1/36^\circ$ ) they do not extend very far eastwards~~  
225 ~~and therefore exclude most of the site B (Ruault et al., 2020). The current configuration avoids~~  
226 ~~these two limitations. The grid resolution is fine ( $1/36^\circ$ ) and the domain lies between  $54.7^\circ W$~~   
227  ~~$35.3^\circ W$  and  $5.5^\circ S$ – $10^\circ N$  (Fig.1). In this way, we can capture the internal tides radiating from~~

a mis en forme : Couleur de police : Texte 1

a mis en forme : Couleur de police : Texte 1

a mis en forme : Couleur de police : Texte 1

a mis en forme : Couleur de police : Texte 1

228 ~~all the generating sites on the Brazilian shelf break. Unlike previous configurations, we do not~~  
229 ~~use multiple nested grids, but a single fine grid. The vertical grid comprises 75 vertically fixed~~  
230 ~~z-coordinates levels, with a narrower grid refinement near the surface with 23 levels in the first~~  
231 ~~100 m. Cell thickness reaches 160 m when approaching the bottom. The horizontal and vertical~~  
232 ~~resolutions of the grid are therefore fine enough to resolve low mode internal tides. This grid~~  
233 ~~resolution has already been used for this purpose in this region (e.g., Tchilibou et al., 2022).~~

234 ~~A third order upstream biased scheme (UP3) with built in diffusion is used for~~  
235 ~~momentum advection, while tracer advection relies on a 2<sup>nd</sup>-order Flux Corrected Transport~~  
236 ~~(FCT) scheme (Zalesak, 1979). The numerical model used in this study is the Nucleus for~~  
237 ~~European Modelling of the Ocean (NEMOv4.0.2, Madec et al., 2019). The configuration~~  
238 ~~designed for our purpose is called *AMAZON36* and covers the western tropical Atlantic region~~  
239 ~~from the Amazon River mouth to the open ocean. Other configurations exist in this region, but~~  
240 ~~either they have a coarse grid ( $1/4^\circ$ , Hernandez et al., 2016), or when the grid is fine ( $1/36^\circ$ ) they~~  
241 ~~do not extend very far eastwards and therefore exclude most of the site B (Ruault et al., 2020).~~  
242 ~~The current configuration avoids these two limitations. The grid resolution is  $1/36^\circ$  and the~~  
243 ~~domain lies between  $54.7^\circ\text{W}$ – $35.3^\circ\text{W}$  and  $5.5^\circ\text{S}$ – $10^\circ\text{N}$  (Fig.1). In this way, we capture the~~  
244 ~~internal tides radiating from all the generating sites on the Brazilian shelf break. The vertical~~  
245 ~~grid comprises 75 vertically fixed z-coordinates levels, with a narrower grid refinement near~~  
246 ~~the surface with 23 levels in the first 100 m. Cell thickness reaches 160 m when approaching~~  
247 ~~the bottom. The horizontal and vertical resolutions of the grid are therefore fine enough to~~  
248 ~~resolve low-mode internal tides. This grid resolution has already been used for this purpose in~~  
249 ~~this region (e.g., Tchilibou et al., 2022).~~

250 ~~A third order upstream biased scheme (UP3) with built-in diffusion is used for~~  
251 ~~momentum advection, while tracer advection relies on a 2<sup>nd</sup> order Flux Corrected Transport~~  
252 ~~(FCT) scheme (Zalesak, 1979). A Laplacian isopycnal diffusion with a constant coefficient of~~  
253  ~~$20\text{ m}^2\cdot\text{s}^{-1}$  is used for tracers. The temporal integration is achieved thanks to a leapfrog scheme~~  
254 ~~combined with an Asselin filter to damp numerical modes, with a baroclinic time step of 150 s.~~  
255 ~~The  $k$ - $\epsilon$  turbulent closure scheme is used for ~~the~~ vertical diffusion ~~coefficients~~. Bottom~~  
256 ~~friction is quadratic with a bottom drag coefficient of  $2.5\times 10^{-3}$ , while lateral wall free-slip~~  
257 ~~boundary conditions are prescribed. A time splitting technique is used to resolve the free~~  
258 ~~surface, with the barotropic part of the dynamical equations integrated explicitly.~~

259 ~~We use the 2020's release of the General Bathymetric Chart of the Oceans (GEBCO~~  
260 ~~2020, ~~see~~ ~~details~~ ~~in~~~~



261 [https://www.gebco.net/data\\_and\\_products/gridded\\_bathymetry\\_data/gebco\\_2020/](https://www.gebco.net/data_and_products/gridded_bathymetry_data/gebco_2020/)  
262 interpolated onto the model horizontal grid, with the minimal depth set to 12.8 m. The model  
263 is forced at the surface by the ERA-5 atmospheric reanalysis (Hersbach et al., 2020). The river  
264 discharges are based on monthly means from hydrology simulation of the Interaction Sol-  
265 Biosphère-Atmosphère model (ISBA, see description in [https://www.umr-  
266 cnrm.fr/spip.php?article146&lang=en](https://www.umr-cnrm.fr/spip.php?article146&lang=en)) and are prescribed as surface mass sources with null  
267 salinity, and we use a multiplicative factor of 90% based on a comparison with the HYBAM  
268 interannual timeseries (HYBAM, 2018). The model is forced at its open boundaries by (i) the  
269 fifteen major tidal constituents (M<sub>2</sub>, S<sub>2</sub>, N<sub>2</sub>, K<sub>2</sub>, 2N<sub>2</sub>, MU<sub>2</sub>, NU<sub>2</sub>, L<sub>2</sub>, T<sub>2</sub>, K<sub>1</sub>, O<sub>1</sub>, Q<sub>1</sub>, P<sub>1</sub>, S<sub>1</sub>,  
270 and M<sub>4</sub>) and (ii) barotropic currents, both derived from FES2014 atlas (Lyard et al., 2021). In  
271 addition to the open boundaries, we prescribe the recent MERCATOR-GLORYS12 v1  
272 assimilation data (Lellouche et al., 2018) for temperature, salinity, sea level, current velocity  
273 and derived baroclinic velocity.

274 We use the 2020's release of the General Bathymetric Chart of the Oceans interpolated  
275 onto the model horizontal grid, with the minimal depth set to 12.8 m. The model is forced at  
276 the surface by the ERA-5 atmospheric reanalysis (Hersbach et al., 2020). The river discharges  
277 are based on monthly means from hydrology simulation of the Interaction Sol-Biosphère-  
278 Atmosphère model (see details in <https://www.umr-cnrm.fr/spip.php?article146&lang=en>) and  
279 are prescribed as surface mass sources with null salinity, and we use a multiplicative factor of  
280 90% based on a comparison with the HYBAM interannual timeseries (see details in  
281 <http://www.ore-hybam.org>). The model is forced at its open boundaries by the fifteen major  
282 tidal constituents (M<sub>2</sub>, S<sub>2</sub>, N<sub>2</sub>, K<sub>2</sub>, 2N<sub>2</sub>, MU<sub>2</sub>, NU<sub>2</sub>, L<sub>2</sub>, T<sub>2</sub>, K<sub>1</sub>, O<sub>1</sub>, Q<sub>1</sub>, P<sub>1</sub>, S<sub>1</sub>, and M<sub>4</sub>) and  
283 barotropic currents, derived from FES2014 atlas (Lyard et al., 2021). In addition to the open  
284 boundaries, we prescribe the recent MERCATOR-GLORYS12 v1 assimilation data (Lellouche  
285 et al., 2018) for temperature, salinity, sea level, current velocity and derived baroclinic velocity.

286 The simulation was initialized on the 1st of January 2005, and ran for 11 years until  
287 December 2015. In this study, we use ~~3-years~~three-year model outputs from January 2013 to  
288 December 2015. Indeed, the model has reached an equilibrium in terms of seasonal cycle after  
289 2 years ~~of run~~. A twin model configuration without ~~the~~tides is used to highlight the influence  
290 of ~~the~~tides on the temperature structure. ~~To assess the realism of the model, we perform~~  
291 ~~validation of various state variables used in this study such as the current's circulation,~~  
292 ~~temperature, salinity, stratification as well as the barotropic and baroclinic tides properties.~~

a mis en forme : Couleur de police : Texte 1

a mis en forme : Espace Après : 12 pt

a mis en forme : Couleur de police : Texte 1

a mis en forme : Couleur de police : Texte 1

a mis en forme : Couleur de police : Texte 1

a mis en forme : Couleur de police : Texte 1

a mis en forme : Couleur de police : Texte 1

## II.3. Methods

### II.3.1. ~~Barotropic/baroclinic tide separation and tide~~Tide energy budget

~~We follow Kelly et al. (2010) to separate barotropic and baroclinic tide constituents: pressure, currents and energy flux. There is no separation following vertical propagation modes. Then we analyze the total energy for all the resolved propagation modes for a given harmonic. Note that the barotropic/baroclinic tide separation is performed directly by the model for better accuracy. Even though, it has the disadvantage of being very costly in terms of computing time. We have therefore only analyzed the M2 harmonic for the single year 2015. Note that M2 is the major tidal constituent in this region (Prestes et al., 2018; Fassoni Andrade et al., 2023). It represents ~70% of the tidal energy (Beardsley et al., 1995; Gabioux et al., 2005).~~

~~The barotropic and baroclinic tide energy budget equations are obtained by ignoring as a first order approximation, the energy tendency, the nonlinear advection and the forcing terms (Wang et al., 2016). Then, the remaining equations are reduced to the balance between the energy dissipation, the divergence of the energy flux, and the energy conversion from barotropic to baroclinic (e.g., Buijsman et al., 2017; Tchilibou et al., 2018, 2020; Jithin and Francis 2020; Peng et al., 2021):~~

$$~~D_{bt} + \nabla_h \cdot F_{bt} + C \approx 0 \quad (1)~~$$

~~We follow Kelly et al. (2010) to separate barotropic and baroclinic tide constituents. There is no separation following vertical modes, then we analyze the total energy for all the resolved propagation modes for a given tidal frequency. Note that the barotropic/baroclinic tide separation is performed directly by the model for better accuracy. We have only analyzed the M<sub>2</sub> harmonic which is the major tidal constituent in this region (Prestes et al., 2018; Fassoni-Andrade et al., 2023), representing ~70% of the tidal energy (Beardsley et al., 1995; Gabioux et al., 2005).~~

~~The barotropic and baroclinic tide energy budget equations are obtained assuming that the energy tendency, the nonlinear advection and the forcing terms are small (Wang et al., 2016). Then, the remaining equations are reduced to the balance between the energy dissipation, the divergence of the energy flux, and the energy conversion from barotropic to baroclinic (e.g., Buijsman et al., 2017; Tchilibou et al., 2018, 2020; Jithin and Francis, 2020; Peng et al., 2021)~~

~~:~~

$$D_{bt} + \nabla_h \cdot F_{bt} + C \approx 0 \quad (1)$$

a mis en forme : Couleur de police : Texte 1

$$D_{bc} + \nabla_h \cdot F_{bc} - C \approx 0 \quad (2)$$

$bt$  and  $bc$  indicate the barotropic and baroclinic terms,  $D$  is the depth-integrated energy dissipation, which can be understood as a proxy of the real dissipation since  $D$  may encompass the energy loss of ~~other tidal harmonics, non-linear terms and/or numerical dissipation (see Nugroho et al., 2018)~~, non-linear terms and/or numerical dissipation (see Nugroho et al., 2018),

$\nabla_h \cdot F$  represents the divergence of the depth-integrated energy flux, whilst  $C$  is the depth-integrated barotropic-to-baroclinic energy conversion, i.e., the amount of incoming barotropic energy converted into internal tides energy over the steep topography, with:

$$C = \langle \nabla H \cdot U_{bt}^* P_{bc}^* \rangle = U_{bt} P_{bc}^* \quad (3)$$

$$F_{bt} = \langle U_{bt}^* P_{bt} \rangle = U_{bt} P_{bt} \quad (4)$$

$$F_{bc} = \int_H^\eta \langle U_{bc}^* P_{bc} \rangle dz = F_{bc} \equiv \int_H^\eta \langle U_{bc} P_{bc} \rangle dz \quad (5)$$

where the angle bracket  $\langle \rangle$  denotes the average over a tidal period,  $\nabla H$  is the slope of the bathymetry,  $U^*U$  is the current velocity ~~( $u, v$ ) respectively in ( $x, y$ ) directions~~,  $P_{bc}^*$  is the baroclinic pressure perturbation at the bottom,  $H$  is the bottom depth,  $\eta$  the surface elevation,  $P$  is the pressure, then  $F$  is the energy flux and emphasizes the ~~pathway~~ path of the ~~respective~~ tides ~~(external or internal)~~.

### H.3.2. 3-D heat budget equation for temperature

~~The three dimensional temperature budget was computed online and further analyzed. It is the balance between the total temperature trend and the sum of the temperature advection, diffusion and solar radiative and non-solar radiative fluxes (e.g., Jouanno et al., 2011; Hernandez et al., 2017):~~

$$\frac{\partial T}{\partial t} = \underbrace{-u \frac{\partial T}{\partial x} - v \frac{\partial T}{\partial y} - w \frac{\partial T}{\partial z}}_{ADV^*} - \underbrace{\frac{\partial}{\partial z} (K_z \frac{\partial T}{\partial z})}_{ZDF} + LDF_x + FOR_z + Numdiff \quad (6)$$

Here  $T$  is the model potential temperature,  $(u, v, w)$  are the velocities component in the  $(x, y, z)$  [respectively eastward, northward and upward] directions,  $ADV^*$  is the 3-D tendency term from the advection routine of the NEMO code (from the left to right: zonal, meridional

a mis en forme : Couleur de police : Texte 1

a mis en forme : Police :12 pt, Couleur de police : Texte 1

a mis en forme : Couleur de police : Texte 1

a mis en forme : Couleur de police : Texte 1

a mis en forme : Police :12 pt

a mis en forme : Police :14 pt

a mis en forme : Police :12 pt

a mis en forme : Police :14 pt

a mis en forme : Police :12 pt

a mis en forme : Police :11 pt

a mis en forme : Couleur de police : Texte 1

a mis en forme : Couleur de police : Texte 1

a mis en forme : Couleur de police : Texte 1

a mis en forme : Couleur de police : Texte 1

and vertical terms). Note that this term hides secondary terms that are important to define here. Hence, the total advection tendency of temperature (ADV) is expressed as follows:

$$ADV = \underbrace{\langle U \cdot \nabla T \rangle}_{ADV*} + \underbrace{\langle U' \cdot \nabla T \rangle + \langle U \cdot \nabla T' \rangle + \langle U' \cdot \nabla T' \rangle + Numdiff_{ADV}}_{Non-Linear\ terms} \quad (7)$$

where  $U'$  is the tidal current, and  $T'$  represents the anomaly of temperature that is produced by the tides apart the advection. When comparing the tidal and non-tidal simulation, the residual term could come from at least three possible tidal impacts:

- 1) The result of the advection is null over a tidal cycle except in some tidal residual circulation. In our region the residual tidal circulation is limited but might be slightly more important on the shelf (Bessières et al., 2008).
- 2) In the nonlinear terms of the previous equation (7), temperature could be modified by other processes than advection, which will count in the total tendency and mark the signature of the impact of the tides.
- 3) Finally, and it might represent the key point, in the model, the advection term leads to some diffusivity of the temperature due to numerical dissipation of the advection scheme ( $Numdiff_{ADV}$ ), in contrast to some non-diffusive advection scheme like in Leclair and Madec (2009). In our case, we are using the FCT advection scheme that includes a diffusive part (Zalesak, 1979). In previous study, this mixing has been quantified to be responsible for 30% of the dissipation (in lower resolution  $1/4^\circ$  resolution, Koch-Larrouy et al., 2008), as part of the high-frequency work of the advection diffusion. We expect here at  $1/36^\circ$  that this effect will be smaller but still non-negligible. Explicit separation of these 3 impacts is beyond the scope of our study but will be discussed in the last section.

Furthermore,  $ZDF$  represents the vertical diffusion,  $LDF_T$  is the lateral diffusion,  $FOR_s$  is the tendency of temperature due to penetrative solar radiation and includes a vertical-decaying structure. At the air-sea interface, the temperature flux is equal to the non-solar heat flux (sum of the latent, sensible, and net infrared fluxes).  $FOR_s$  can modify temperature in the thin surface layer but will be unshown in the following.  $Numdiff$  corresponds to the numerical diffusion for the temperature.

### 380 II.3.2. 3-D heat budget equation for temperature

381 The three-dimensional temperature budget was computed online and further analyzed.  
382 It is the balance between the total temperature trend and the sum of the temperature advection,  
383 diffusion and solar radiative and non-solar radiative fluxes (e.g., Jouanno et al., 2011;  
384 Hernandez et al., 2017):

$$385 \quad \frac{\partial T}{\partial t} = \underbrace{-u\partial_x T - v\partial_y T - w\partial_z T}_{ADV} + LDF - \underbrace{\partial_z(K_z\partial_z T)}_{ZDF} + Forcing + Asselin \quad (6)$$

386 Here  $T$  is the model potential temperature.  $(u, v, w)$  are the velocity components in the  $(x, y, z)$   
387 [respectively eastward, northward and upward] directions.  $ADV$  is the 3-D tendency term from  
388 the advection routine of the NEMO code (from the left to right: zonal, meridional and vertical  
389 terms). Note that in our model,  $ADV$  includes nonlinear effect between the temperature and the  
390 currents and leads to some diffusivity of the temperature due to numerical dissipation of the  
391 FCT advection scheme (Zalesak, 1979) in contrast to some non-diffusive advection scheme like  
392 in Leclair and Madec (2009). In previous studies, for lower resolution ( $1/4^\circ$ ), this mixing has  
393 been quantified to be responsible for 30% of the dissipation as part of the high-frequency work  
394 of the diffusion (Koch-Larrouy et al., 2008). We expect here at  $1/36^\circ$  resolution that this effect  
395 will be smaller but still non negligible. This will be discussed in the last section. Note that  
396 explicit separation of this effect is beyond the scope of our study. Furthermore,  $ZDF$  represents  
397 the vertical diffusion,  $LDF$  is the lateral diffusion,  $Forcing$  is the sum of tendency of  
398 temperature due to penetrative solar radiation, which includes a vertical decaying structure, and  
399 the non-solar heat flux (sum of the latent, sensible, and net infrared fluxes) at the surface layer,  
400 and  $Asselin$  corresponds to the numerical diffusion for the temperature.

## 401 **III. Model validation**

402 In this subsection, we assess the quality of our ~~model's~~ simulations by verifying whether  
403 they are in good agreement with the observations and other reference data. Firstly, for the  
404 barotropic and baroclinic characteristics of the  $M_2$  tides for the year 2015, and finally for the  
405 temperature ~~for the period~~ from 2013 to 2015.

### 406 **III.1. $M_2$ Tides in the model**

407 We initially examined ~~at~~ the barotropic SSH and there is a good agreement in both  
408 amplitude (color shading) and phase (solid contours) between FES2014 and the model,

a mis en forme : Indice

a mis en forme : Indice

409 ~~Fig.2a~~Fig.2a and Fig.2b respectively. Nevertheless, near the coast, some differences are  
410 observed in amplitude. The SSH amplitude of the model is lower ( $\sim +50$  cm) north of the mouth  
411 of the Amazon. However, ~~shorewards~~shoreward and on the southern part of the mouth, the  
412 model overestimates the amplitude by  $\sim +20$  cm and  $\sim +40$  cm respectively. ~~These biases are~~  
413 ~~of the same order of magnitude as Ruault et al. (2020).~~These biases are of the same order of  
414 ~~magnitude as Ruault et al. (2020).~~ The flux of the barotropic tidal energy flowing inshore is  
415 represented by the black arrows in Fig.2c and Fig.2d for FES2014 and the model respectively.  
416 A fraction of this energy is converted into baroclinic tidal energy over the steep slope of the  
417 bathymetry. We compared the depth-integrated barotropic-to-baroclinic energy conversion rate  
418 ( $C$ ) between FES2014 and the model, color shading in Fig.2c and Fig.2d respectively. The  
419 model does reproduce the same conversion patterns of FES2014 over the slope, but hardly  
420 offshore ~~over the Mid-Atlantic Ridge between 42°W–35°W and 7°N–10°N. This leads to an~~  
421 ~~overall underestimate of about 30%. It is worth noting that  $C$  increases with bathymetry~~  
422 ~~resolution. The latter therefore plays a critical role in converting barotropic tidal energy into~~  
423 ~~internal tides (see Niwa and Hibiya, 2011). Compared with FES2014 ( $\sim 1.5$  km), the horizontal~~  
424 ~~grid of our model is coarser ( $\sim 3$  km). Meaning that the difference in bathymetry resolution~~  
425 ~~could explain the difference in energy conversion with FES2014. Later, another part of the~~  
426 ~~barotropic energy is dissipated on the shelf by bottom friction and induces mixing from the~~  
427 ~~bottom (Beardsley et al., 1995; Gabioux et al., 2005; Bessières, 2007; Fontes et al.,~~  
428 ~~2008) between 42°W–35°W and 7°N–10°N. This leads to an overall underestimate of  $C$  of~~  
429 ~~about 30% by our model. Niwa and Hibiya (2011) have shown that  $C$  increases with bathymetry~~  
430 ~~resolution, meaning that there is more conversion with the FES2014 grid ( $\sim 1.5$  km) compared~~  
431 ~~to our grid ( $\sim 3$  km). In addition, FES2014 (vs. our model) is a barotropic (vs. baroclinic) model,~~  
432 ~~which may be a source of some differences since it solves different set of equations.~~

433 ~~Another part of the barotropic energy is dissipated on the shelf by bottom friction and~~  
434 ~~induces mixing from the bottom (Beardsley et al., 1995; Gabioux et al., 2005; Bessières, 2007;~~  
435 ~~Fontes et al. (2008)). Most of the dissipation of barotropic energy ( $D_{bt}$ ) occurs in the middle and~~  
436 ~~inner shelf between 3°S–4°N (Fig.2c) in good agreement with Beardsley et al. (1995) and~~  
437 ~~Bessières (2007). The remaining barotropic energy flows over hundreds of kilometers into the~~  
438 ~~estuarine systems of this region (Kosuth et al., 2009; Beardsley et al. (1995) and Bessières~~  
439 ~~(2007). The remaining barotropic energy propagates over hundreds of kilometers into the~~  
440 ~~estuarine systems of this region (Kosuth et al., 2009; Fassoni-Andrade et al., 2023).~~

a mis en forme : Couleur de police : Texte 1

a mis en forme : Français (France)

a mis en forme : Couleur de police : Texte 1,

a mis en forme : Couleur de police : Texte 1

441 For the baroclinic tides, the critical parameter,  $\gamma = s/\alpha$ , is defined as the ratio between  
442 the slope of the bathymetry,  $s = \nabla H$  (see Fig.1), and the slope of the radiated internal wave,  
443  $\alpha = \sqrt{(\omega^2 - f^2)/(N^2 - \omega^2)}$ , with  $\omega$  the tidal frequency for a given wave,  $f$  is the Coriolis  
444 frequency and  $N^2$  represents the squared Brünt Väisälä frequency near the bottom (e.g., Nash  
445 et al., 2007; Vie et al., 2019). On the slope where ITs are generated,  $\gamma > 1$ , meaning that the  
446 topography is supercritical. Consequently, the baroclinic tides, once generated, will propagate  
447 in the opposite direction to the barotropic tides, i.e., from the slope towards the open ocean, as  
448 shown by the model's baroclinic energy flux ( $F_{bc}$ ), black arrows in Fig.2f.  $F_{bc}$  highlights the  
449 existence of six main sites of ITs generation on the slope. Two of these are more important (A  
450 and B) regarding their higher and far extended energy flux, in good agreement with Magalhaes  
451 et al. (2016), Barbot et al. (2021) and Tchilibou et al. (2022). From these two main sites, ITs  
452 propagate for the nearly 1000 km. Along the propagation pathways, they can dissipate their  
453 energy. Color shading in the Figure 2f shows the model's depth-integrated internal tides energy  
454 dissipation ( $D_{bc}$ ). We first look at the local dissipation of this energy defined as  $q = D_{bc}/C$  (see  
455 Laurent and Garrett, 2002).  $q$  is integrated over the slope in the same boxes as defined in Table  
456 A1 in Tchilibou et al. (2022). This reveals that a significant part of the energy, about 30%, is  
457 dissipated locally in the different boxes in good agreement with the latter study. The remaining  
458 part of the energy is exported offshore, and it is dissipated along the propagation path. This  
459 offshore dissipation is more extensive along path A, ~300 km from the slope, with two patterns  
460 spaced approximately by an average wavelength of 120–150 km corresponding to mode-1  
461 propagation. The offshore dissipation is less extensive along path B, occurring around 100–200  
462 km from the slope (Fig.2f).

463 For the internal tides, their energy flux ( $F_{bc}$ , black arrows in Fig.2f) shows that they  
464 from the slope towards the open ocean.  $F_{bc}$  highlights the existence of six main sites of IT  
465 generation on the slope. Two of these are more important (A and B) regarding their higher and  
466 far extended energy flux, in good agreement with Magalhaes et al. (2016), Barbot et al. (2021)  
467 and Tchilibou et al. (2022). From these two main sites, internal tides spread over nearly 1000  
468 km, and dissipate their energy. Color shading in Figure 2f shows the model's depth-integrated  
469 internal tides energy dissipation ( $D_{bc}$ ). We found that about 30% of the energy is dissipated  
470 locally over generation sites (not shown), in good agreement with Tchilibou et al. (2022). The  
471 remaining part is dissipated offshore along the propagation path. This offshore dissipation is  
472 more extended along path A, ~300 km from the slope, with two patterns spaced approximately

473 ~~by an average wavelength of 120–150 km corresponding to mode-1 propagation. While there~~  
474 ~~is less offshore dissipation along path B, occurring around 100–200 km from the slope (Fig.2f).~~

475 Another critical characteristic of ~~internal tidal waves,IT~~ is their SSH imprints along the  
476 propagation pathway. We compared an estimate of this signature deduced from the altimeter  
477 tracks (Fig.2g) produced by ~~Zaron (2019)~~Zaron (2019) with our model (Fig.2h). ~~The), with~~  
478 ~~shelf masked over 150 m depth. Our~~ model is in good agreement with this product, with an  
479 overestimation of the order of  $\sim +1.5$  cm on the SSH maxima. It is relevant to note ~~that~~ the  
480 baroclinic SSH of ~~theour~~ model is an average over the year 2015, whilst the estimate is an  
481 average over about 20 years. ~~This more extended~~This means that the variability of the altimeter  
482 ~~tracks is greater due to the longer period, which may lowerreduce~~ the amplitude of the ~~signal~~  
483 ~~obtained from the altimetry observations. Furthermore, the variability within the two datasets~~  
484 ~~is not the same. This mayestimates and~~ explain ~~some~~the small differences in the positioning  
485 and amplitude of the maxima.

486 ~~Only the energy dissipation of the M2 tides is presented above. Elsewhere, the harmonic~~  
487 ~~analysis does not consider the incoherent (non-stationary) part of the tidal energy, which has~~  
488 ~~been found to be non-neglectable (Tehilibou et al., 2022). And can therefore influences the~~  
489 ~~structure of the temperature. Further on, the analysis are carried out on a seasonal scale, which~~  
490 ~~means that the mean temperature field obtained could result from the cumulative effect of all~~  
491 ~~coherent and incoherent tidal harmonies.~~

### 492 **III.2. Temperature validation**

493 ~~For the following, it should be noted we obtained the bias between TMI SST and the~~  
494 ~~two model simulations after linear interpolation of the model data into the observation grid.~~

495 ~~Figure 3 shows the mean SST over the entire period 2013–2015 from TMI SST (Fig.3a),~~  
496 ~~the tidal simulation (Fig.3b) and the non-tidal simulation (Fig.3c). The simulation with tides~~  
497 ~~accurately reproduces the spatial distribution of the observations both for cooling on the shelf~~  
498 ~~around  $47.5^{\circ}\text{W}$  and to the southeast between  $40^{\circ}\text{W}$ – $35^{\circ}\text{W}$  and  $2^{\circ}\text{S}$ – $2^{\circ}\text{N}$ , as shown by the weak~~  
499 ~~bias,  $< \pm 0.1^{\circ}\text{C}$ , with TMI (Fig.3d). This cooling is inaccurately reproduced by the non-tidal~~  
500 ~~simulation which exhibits a warm bias of about  $0.3^{\circ}\text{C}$  (Fig.3.e). To the northeast, between~~  
501  ~~$50^{\circ}\text{W}$ – $54^{\circ}\text{W}$  and  $3^{\circ}\text{N}$ – $8^{\circ}\text{N}$  in the Amazon plume, the SST of the non-tidal simulation is in~~  
502 ~~better agreement with the observations, while the SST of the tidal simulation is about  $> 0.6^{\circ}\text{C}$~~   
503 ~~cooler than TIM SST (Fig.3d). Such a difference fits to what is obtained by other models in the~~  
504 ~~same region (e.g., Hernandez et al., 2016, 2017; Gévaudan et al., 2022). Far offshore, between~~  
505  ~~$50^{\circ}\text{W}$ – $40^{\circ}\text{W}$  and  $6^{\circ}\text{N}$ – $10^{\circ}\text{N}$ , both simulations reveal a negative bias of about  $0.2$ – $0.3^{\circ}\text{C}$~~

a mis en forme : Couleur de police : Texte 1



506 (Fig.3d-e). We averaged the observations and the interpolated model data in the corresponding  
507 dashed line box in the upper panels, with depth  $< 200$  m masked. This location is around the  
508 ITs generation sites and on part of their pathways. Then, we compute the seasonal cycle of the  
509 three products (Fig.3f). The tidal and non-tidal simulations of the model reproduce accurately  
510 both the seasonal cycle and the standard deviation of the observations, with a low RMSE of  
511  $\sim 10^{-2}$  °C between each simulation and TMI SST (Fig.3f). This indicates the robustness of our  
512 model simulations. Nevertheless, over the seasonal cycle, it appears that between January-April  
513 and July-December, the tidal simulation is closer to the observations, while the non-tidal  
514 simulation seems moderately warmer than the observations. In May-June, both simulations are  
515 colder than TMI SST (Fig.3f).

516 Figure 3 shows the mean SST over the entire 2013–2015 period for TMI SST (Fig.3a),  
517 the tidal simulation (Fig.3b) and the non-tidal simulation (Fig.3c), then, the bias between TMI  
518 SST and the two simulations is obtained by linear interpolation of the simulations data on the  
519 observation grid. The simulation with tides accurately reproduces the spatial distribution of the  
520 observations both for cooling on the shelf around  $47.5^{\circ}\text{W}$  and to the southeast between  $40^{\circ}\text{W}$   
521  $-35^{\circ}\text{W}$  and  $2^{\circ}\text{S}-2^{\circ}\text{N}$ , as shown by the weak bias,  $< \pm 0.1^{\circ}\text{C}$ , with TMI (Fig.3d). This cooling is  
522 inaccurately reproduced by the non-tidal simulation which exhibits a warm bias of about  $0.3^{\circ}\text{C}$   
523 (Fig.3.e). To the northeast, between  $50^{\circ}\text{W}-54^{\circ}\text{W}$  and  $3^{\circ}\text{N}-8^{\circ}\text{N}$  in the Amazon plume, the SST  
524 of the non-tidal simulation is in better agreement with the observations, while the SST of the  
525 tidal simulation is about  $> 0.6^{\circ}\text{C}$  cooler than TMI SST (Fig.3d). The same bias is obtained in  
526 this northern zone by other models including tides (e.g., Hernandez et al., 2016, 2017;  
527 Gévaudan et al. (2022)). Far offshore, between  $50^{\circ}\text{W}-40^{\circ}\text{W}$  and  $6^{\circ}\text{N}-10^{\circ}\text{N}$ , both simulations  
528 reveal a negative bias of about  $0.2-0.3^{\circ}\text{C}$  (Fig.3d-e). We averaged the observations and the  
529 interpolated simulation data in the dashed box (see Fig.3a-c), with depth  $< 200$  m masked. This  
530 location is around IT generation sites and on part of their pathways. Then, we compute the  
531 seasonal cycle of the three products (Fig.3f). The tidal and non-tidal simulations of the model  
532 reproduce accurately both the seasonal cycle and the standard deviation of the observations,  
533 with a low RMSE of  $\sim 2 \cdot 10^{-2}$  °C and  $\sim 4 \cdot 10^{-2}$  °C, between TMI SST and tidal and non-tidal  
534 simulation respectively, indicating the robustness of our model's simulations. Over the seasonal  
535 cycle, it appears that the tidal simulation is closer to the observations from January to March,  
536 July to September and November to December, while during the rest of the year, either the two  
537 simulations are equally close, or the non-tidal simulation is closer.

538 To gain an insight into our model along the depth, we used the mean ~~model water~~  
539 ~~properties~~ WOA2018 climatology (2005–2017) and simulation data (salinity and temperature)  
540 for the three years 2013–2015 ~~in the same region as in Fig.3f. We compared them with the~~  
541 ~~WOA2018 climatological (2005–2017) data ([https://www.ncei.noaa.gov/access/world-ocean-](https://www.ncei.noaa.gov/access/world-ocean-atlas-2018/)~~  
542 ~~atlas-2018/)~~. We used hereabove and elsewhere  $\sigma_\theta[\rho - 1000]$  to represent the density, with  $\rho$   
543 ~~the water density~~, averaged in the same region as in Fig.3f. Figure 3g shows the Temperature-  
544 Salinity (T-S) diagram, with equal density ( $\sigma_\theta$ ) contours, for WOA2018 (black line), tidal  
545 simulation (blue line) and non-tidal simulation (red line) and the two simulations. The data are  
546 averaged in the box as before, and we use  $\sigma_\theta[\rho - 1000]$  to represent the density contours, with  
547  $\rho$  the water density. Both simulations exhibit similar ~~pattern~~ patterns with WOA2018 for deeper  
548 waters, i.e.,  $T < 17^\circ\text{C}$  and  $\sigma_\theta > 25.6 \text{ kg.m}^{-3}$ . However, there exist minor discrepancies for the  
549 surface layer waters, i.e.,  $T > 17^\circ\text{C}$  and  $22.4 > \sigma_\theta < 25.6 \text{ kg.m}^{-3}$ . At that level, the tidal  
550 simulation better reproduces the T-S profiles. ~~The water is slightly more eroded in profile of the~~  
551 ~~non-tidal simulation observations~~. These ~~petty~~ small differences between WOA2018  
552 observations and the ~~model, even more~~ two simulations, especially with the tidal simulation,  
553 further demonstrate the ability of our model to reproduce the observed water mass properties.

a mis en forme : Espace Après : 0 pt

## 554 IV. Results

555 In this section, we present the influence of tides on the temperature, the associated  
556 processes, and the impact on the atmosphere-ocean net heat exchange. The analyses were  
557 performed on a seasonal scale between April-May-June (AMJ) and August-September-October  
558 (ASO) for the three years 2013–2015.

### 559 IV.1. Tide-enhanced surface cooling

560 During the first season, warm waters, ~~which are defined as~~  $> 27.6^\circ\text{C}$ , dominate near the  
561 coast, especially in the middle shelf and in the south-east. ~~While, and~~ cold waters are present  
562 offshore north of  $6^\circ\text{N}$  (Fig.4a-c). Off the mouth of the Amazon River, water colder than  $28.2$   
563  $^\circ\text{C}$  ~~spreads~~ spreads between  $43^\circ\text{W}$ – $51^\circ\text{W}$  for TMI SST (Fig.4a) and the tidal simulation (Fig.4b),  
564 ~~whilst~~ while warmer waters are present in the same area for the simulation without the tides  
565 (Fig.4c). Figures 4d-f show the SST, averaged over the ASO season. The TMI SST observations  
566 (Fig.4d) shows an upwelling cell represented by the extension of the  $27.2^\circ\text{C}$  isotherm (white  
567 dashed contour) along the slope to about  $49^\circ\text{W}$ – $3^\circ\text{N}$  towards the north-east of the region, which  
568 forms the extension of the ACT. This extension also exists in the tidal simulation (Fig.4e),  
569 whereas  $\leq 27.2^\circ\text{C}$  waters are not crossing  $45.5^\circ\text{W}$  and remain in the southern hemisphere in

a mis en forme : Couleur de police : Texte 1

a mis en forme : Couleur de police : Texte 1

a mis en forme : Couleur de police : Texte 1

570 the simulation without the tides (Fig.4f). ~~Which~~This means that ~~a lesser upwelling cell may~~  
571 ~~exist without the tides, and it is enhanced by 0.3°C in average due to tidal effect. The tides~~  
572 ~~allow~~ waters colder than 27.2°C ~~to form~~can only extend further ~~north-east. Finally into the~~  
573 ~~northeast because of tides. In addition~~, we can note that the mean SST shows a very contrasting  
574 distribution between the two seasons. There are warm waters along the shelf and cold waters  
575 offshore during the AMJ season (Fig.4a-c). This is followed by warming along the Amazon  
576 plume and offshore, and ~~an~~ upwelling ~~cells~~cell in the south-east (Fig.4d-f).

577 The general impact of the tides, illustrated by the SST anomaly between the tidal and  
578 the non-tidal simulation, is a cooling over a large part of the study area with maxima up to 0.3  
579 °C (Fig. 5a-b). For ASO, tides induce a warming ( $> 0.3$  °C) on the shelf at the mouth of the  
580 Amazon River (Fig.5b), while for AMJ it is a cooling of the same intensity (Fig.5a). That  
581 difference will be further discussed. Out of the shelf, the temperature anomaly for each season  
582 has different spatial structures. This is probably due to a different mesoscale variability between  
583 the two seasons.

#### 584 **IV.2. Impact of the tides in the atmosphere-to-ocean net heat flux**

585 The atmosphere–ocean net heat flux ( $Q_t$ ) reflects the balance of incoming and outgoing  
586 heat fluxes across the atmosphere-ocean interface (see details on ~~Moisan and Niiler, 1998;~~  
587 ~~Jayakrishnan and Babu, 2013~~); Moisan and Niiler, 1998; Jayakrishnan and Babu, 2013). During  
588 AMJ, the tides mainly induce positive  $Q_t$  anomalies over the whole domain. The average values  
589 are around 25  $W.m^{-2}$  in the plume and the Amazon retroflection to the northeast and along A  
590 and B (Fig.5c). Negative SST anomalies ( $\sim 0.3^\circ C$ ) occur throughout the domain in the same  
591 location. During the ASO season, at the mouth of the Amazon, there are negative  $Q_t$  anomalies  
592 but of the same magnitude as during the previous season (Fig.5d). At this location, positive  
593 temperature anomalies ( $\sim 0.3^\circ C$ ) are observed (Fig.5b). Elsewhere, there are positive  $Q_t$   
594 anomalies and negative SST anomalies. It therefore appears that negative SST anomalies induce  
595 positive  $Q_t$  anomalies and vice versa. Hence, the spatial structures of  $Q_t$  anomalies and SST  
596 anomalies fit almost perfectly together for the ~~respective season. As it is shown by the~~  
597 ~~correlation among them two season~~. There is a strong negative correlation of 0.97 with a  
598 significance of  $R^2 = 0.95$  for the AMJ season. And roughly the same intensity and sign for the  
599 ASO season with 0.98 and 0.96, respectively for the correlation and its significance (Fig.5e).  
600 This is consistent with the fact that the atmosphere and the underlying ocean are balanced. Then,  
601 the SST cooling induced by upwelled cold water will try upset this balance. As a result of this,

a mis en forme : Couleur de police : Texte 1

a mis en forme : Couleur de police : Texte 1

602 an equivalent variation in the net heat flux from the atmosphere to the ocean will attempt to  
603 restore it.

604 The integral over the entire domain of the net heat flux for each season and for each  
605 simulation is shown in Figure 5f. During the AMJ season,  $Q_t$  increases from 23.85 TW (1 TW  
606 =  $10^{12}$  W) for the non-tidal simulation to 35.7 TW for the tidal simulation, i.e., an increase of  
607 33.2 %. ~~The tides are behind a third of  $Q_t$  variation. This is very large compared to what is~~  
608 ~~observed elsewhere in other ITs hotspots (e.g., 15% in Solomon Sea, Tchilibou et al.,~~  
609 ~~2020). That is, the tides are responsible for a third of  $Q_t$  variation. This is very large compared~~  
610 ~~to what is observed elsewhere in other IT hotspots (e.g., 15% in Solomon Sea, Tchilibou et al.,~~  
611 ~~2020).~~ During the second season, there is a smaller increase in  $Q_t$  of about 7.4% between the  
612 two simulations, i.e., from 73.03 TW to 78.83 TW for the non-tidal and tidal simulations  
613 respectively (Fig.5f).

614 ~~Moreover, it~~ is also worth noting the significant difference in integrated  $Q_t$  between  
615 the two seasons. The values are less than 36 TW during the AMJ season, whereas they are  
616 around twice as high, > 73 TW, during the ASO season. Given that colder SST induce a stronger  
617  $Q_t$ , these higher values are likely related to the arrival of water from ACT, which forms  
618 upwelling cells (Fig.4d-f) with a secondary tidal effect.

### 619 **IV.3. Vertical structure of Temperature along internal tides pathway**

620 To further analyze the temperature changes between both simulations, we made vertical  
621 sections following the path of ~~ITs emanating from sites A and B (respectively black and red~~  
622 ~~line in Fig.2e). Hereunder, (i) only the transects following the pathway A will be shown, since~~  
623 ~~the vertical structure is similar following pathway B especially for AMJ season, or because~~  
624 ~~some processes tend to be null along pathway B during the ASO season. (ii) The mixed layer~~  
625 ~~refers to a quasi-homogenous surface layer of temperature-dependent density that interacts with~~  
626 ~~the atmosphere (Kara et al., 2003). Its maximum depth also known as mixed-layer depth (MLD)~~  
627 ~~is defined as the depth where the density increases from the surface value, due to temperature~~  
628 ~~change of  $|\Delta T| = 0.2$  °C with constant salinity (e.g., Dong et al., 2008; Varona et al., 2019). IT~~  
629 ~~radiating from sites A and B (respectively black and red line in Fig.2f). Hereunder, only the~~  
630 ~~transects following the pathway A will be shown, since the vertical structure is similar following~~  
631 ~~pathway B especially for AMJ season and because some processes tend to be null along~~  
632 ~~pathway B during the ASO season. The mixed layer refers to a quasi-homogenous surface layer~~  
633 ~~of temperature-dependent density that interacts with the atmosphere (Kara et al., 2003). Its~~  
634 ~~maximum depth, also known as mixed-layer depth (MLD), is defined as the depth where the~~

a mis en forme : Couleur de police : Texte 1

a mis en forme : Couleur de police : Texte 1

a mis en forme : Couleur de police : Texte 1

635 density increases from the surface value, due to temperature change of  $|\Delta T| = 0.2 \text{ }^\circ\text{C}$  with  
636 constant salinity (e.g., Dong et al., 2008; Varona et al., 2019).

637 Figure 6 shows the vertical sections of temperature for the two seasons following A. For  
638 the AMJ season, over the slope and near the coast, cold waters ( $< 27.6 \text{ }^\circ\text{C}$ ) remain below the  
639 surface at  $\sim 20 \text{ m}$  for the tidal simulation (Fig.6a) and deeper at  $\sim 60 \text{ m}$  for the non-tidal  
640 simulation (not shown). Then, cold waters rise to the surface more than 400 km offshore for  
641 both simulations. ~~Although at A,~~ the surface the SST anomaly is relatively small ( $\sim -0.3 \text{ }^\circ\text{C}$ ,  
642 Fig.5a), because the SST ~~is anomalies are~~ likely damped by the heat fluxes, further down the  
643 water column, this anomaly becomes much larger (Fig.6b). ~~Note that cyan and yellow dashed~~  
644 ~~lines in Fig.6b and Fig.7b refer to thermocline for tidal and non-tidal simulations respectively.~~  
645 Above that thermocline ( $< 120 \text{ m}$ ), the simulation with the tides is colder by  $1.2 \text{ }^\circ\text{C}$  from the  
646 slope where ~~the ITsIT~~ are generated to the open ocean following their propagation path.  
647 Conversely, below the thermocline, the tidal simulation is warmer by approximately the same  
648 intensity ( $1.2 \text{ }^\circ\text{C}$ ) up to  $\sim 300 \text{ m}$  depth and along the propagation path (Fig.6b). During this AMJ  
649 season, the thermocline is  $\sim 100 \text{ m} \pm 15 \text{ m}$  deep and the MLD is  $\sim 40 \text{ m} \pm 20 \text{ m}$  deep (dashed  
650 white line, Fig.6a). They both have a very weak slope between the coast and the open ocean.  
651 Over the whole domain, the thermocline is deeper by about 15 m on average in the non-tidal  
652 simulation, following the propagation paths of ~~the ITsinternal tides~~, on the Amazon shelf and  
653 plume (Fig.6c). Whilst MLD in the non-tidal simulation is deeper by an average of 10 m over  
654 the shelf, 4 m on average along ~~the ITsIT~~ propagation paths and close to zero in the Amazon  
655 plume (Fig.6d).

656 During the ASO season, cold waters previously confined below the surface during the  
657 previous season (AMJ) rise to the surface. These cold waters extend over the slope and up to  
658 about 150 km offshore in the non-tidal simulation (not shown) and up to 250 km offshore in the  
659 tidal simulation (Fig.7a). The  $27.2 \text{ }^\circ\text{C}$  isotherm only reaches the surface above the slope in the  
660 tidal simulation and remains below the surface ( $\sim 30 \text{ m}$ ) in the non-tidal simulation- ~~(not shown)~~.  
661 This aligns with the missing of that isotherm at this location in the corresponding SST map  
662 (Fig.4e4f). For the tidal simulation, ~~at the surface,~~ the temperature ~~is therefore colder than in~~  
663 ~~previous season. The temperature~~ anomaly in the ASO season is smaller ( $< 0.4 \text{ }^\circ\text{C}$ , Fig.7b) in  
664 the surface layers ( $< 40 \text{ m}$ ) near the coast compared to the AMJ season (Fig.6b). In contrast,  
665 during the ASO season, this cooling can ~~reach the surface and results in a colder drive more~~ SST  
666 ~~anomalies~~ along A ( $-0.3 \text{ }^\circ\text{C}$ , Fig.5a). ~~The strongest~~5b). A stronger cooling of  $\sim -1.2 \text{ }^\circ\text{C}$  ~~is occurs~~  
667 deeper between 60 and 140 m depth. ~~Below the thermocline,~~ and a warming of about  $1.2 \text{ }^\circ\text{C}$

a mis en forme : Couleur de police : Texte 1

a mis en forme : Couleur de police : Texte 1

a mis en forme : Couleur de police : Texte 1

a mis en forme : Couleur de police : Texte 1

a mis en forme : Couleur de police : Texte 1

a mis en forme : Couleur de police : Texte 1

a mis en forme : Couleur de police : Texte 1

a mis en forme : Couleur de police : Texte 1

a mis en forme : Couleur de police : Texte 1

a mis en forme : Couleur de police : Texte 1

a mis en forme : Couleur de police : Texte 1

a mis en forme : Couleur de police : Texte 1

a mis en forme : Couleur de police : Texte 1

a mis en forme : Couleur de police : Texte 1

a mis en forme : Couleur de police : Texte 1

a mis en forme : Couleur de police : Texte 1

668 ~~is also present but below, which~~ extends less offshore ~~to about than during AMJ season,~~ 650  
669 km, ~~Fig.7b (vs. ~1000 km, Fig.6b).~~ During this ASO season, the coastward slope of the  
670 thermocline and MLD becomes somewhat steeper compared to the other season. In both  
671 simulations, there is a dip of ~80 m, i.e., ~60 m offshore and ~140 m inshore, for the thermocline  
672 (dashed black line, Fig.7a). And a dip of ~40 m, i.e., ~30 m offshore and ~70 m inshore, for  
673 MLD (dashed white line, Fig.7a). Over the entire domain, the tides ~~shallow~~reduce the  
674 thermocline depth by ~6 m on the shelf and ~12 m at the plume and far offshore along the  
675 propagation path of A (Fig.7c). They ~~shallow~~reduce the MLD in the tidal run by about 10 m  
676 along the shelf and ~4 m along the propagation path of A (Fig.7d).

677 ~~Between the two seasons, there is also a change in the vertical density gradient~~  
678 ~~(Stratification) between the coast and the open sea. In the tidal simulation, during the AMJ~~  
679 ~~season, the isodensities are tight near the coast and thicken towards the open sea (Fig.6a). This~~  
680 ~~means that a strong stratification is present near the coast and decreases towards the open sea.~~  
681 ~~In contrast, during the second ASO season, the isodensities are thicker near the coast and tight~~  
682 ~~offshore (Fig.7a). As the result of this, the stratification is weaker inshore than offshore. This~~  
683 ~~clearly highlights a seasonality in the vertical density gradient profile in agreement with~~  
684 ~~Tchilibou et al. (2022). Note that, this behavior also appears in the simulation without the tides~~  
685 ~~(not shown). The transects of the temperature anomaly, Fig.6b and 7b, show that ITs and likely~~  
686 ~~the barotropic tides can influence the temperature in the ocean from the surface to the deep~~  
687 ~~layers, with a greater effect on the first 300 meters. One question we address in this paper is to~~  
688 ~~better understand what processes are at work that explain these temperature changes.~~

#### 689 **IV.4. What are the processes involved?**

690 ~~To explain the observed surface and water column temperature changes, we computed~~  
691 ~~and analyzed the terms of the heat balance equation (see Section II.3.2, Equation 6) for both~~  
692 ~~seasons (AMJ and ASO) averaged over the three years from 2013 to 2015.~~

693 ~~Between the two seasons, there is also a change in the vertical density gradient between~~  
694 ~~the coast and the open sea. In the tidal simulation, during the AMJ season, the isopycnals layers~~  
695 ~~are tight near the coast and thicken towards the open sea (Fig.6a). This means that a strong~~  
696 ~~stratification is present near the coast and decreases towards the open sea. In contrast, during~~  
697 ~~the second ASO season, the isopycnals layers are thicker near the coast and tight offshore~~  
698 ~~(Fig.7a). As the result of this, the stratification is weaker inshore than offshore. This clearly~~  
699 ~~highlights a seasonality in the vertical density gradient profile in agreement with Tchilibou et~~

a mis en forme : Couleur de police : Texte 1

a mis en forme : Couleur de police : Texte 1

a mis en forme : Couleur de police : Texte 1

a mis en forme : Couleur de police : Texte 1

a mis en forme : Couleur de police : Texte 1

a mis en forme : Couleur de police : Texte 1

al. (2022). Note that this behavior also appears in the simulation without the tides (not shown). The transects of the temperature anomaly, Fig.6b and 7b, show that the tides influence the temperature in the ocean from the surface to the deep layers, with a greater effect on the first 300 meters. One question we address in this paper is to better understand what processes are at work that explain these temperature changes.

#### IV.4. What are the processes involved?

To explain the observed surface and water column temperature changes, we computed and analyzed the terms of the heat balance equation (see Section II.3.2, Equation 6) for both seasons (AMJ and ASO).

##### IV.4.1. Vertical diffusion of Temperature

Figure 8 shows the vertical temperature diffusion tendency (ZDF). ZDF is averaged between 2–20 m, i.e., within the mixed-layer. For the AMJ season, ZDF in the tidal simulation (Fig.8a) shows a negative trend (cooling) in the whole domain. The maximum values ( $> |0.4|$  °C.day<sup>-1</sup>) are located along the slope where the ITs are generated and on their propagation path. There is a larger horizontal extent along A of ~700 km from the coasts compared to B, where it is ~300 km from the coasts. Elsewhere, it remains very low,  $> -0.1$  °C.day<sup>-1</sup>. For the non-tidal simulation (Fig.8b), the ZDF is very weak over the entire domain ( $> > -0.1$  °C.day<sup>-1</sup>). For the ASO season, the tidal simulation (Fig.8c) shows a decrease of the ZDF near the coast ( $< 100$  km) and a strengthening offshore along A compared to the previous season, but with the same cooling trend ( $< -0.4$  °C.day<sup>-1</sup>). Along B, it tends to be null, both at the coast and offshore (Fig.8c). In addition, the mesoscale circulation and eddy activity intensify during this season. To the northeast, approximately between 4°N–8°N, and 47°W–53°W, there is a cooling on the shelf of ~0.3 °C.day<sup>-1</sup> with eddy-like patterns in the tidal simulation (Fig.8c). The processes by which these features might arise will be examined/discussed in more detail/details in the section V. Unsurprisingly, ZDF is very weak elsewhere for the non-tidal simulation (Fig.8d). Whatever, the ITs could be/Internal tides are, the dominant driver of vertical diffusion of temperature along the shelf break and offshore, while the mixing induced by barotropic tides could prevail on the shelf to explain the weak ZDF values.

On the vertical following A, we have noted inverted there are opposite sign ZDF values, with mean magnitude of  $\sim |0.4|$  °C.day<sup>-1</sup>. These values are centered around the thermocline for the simulation with tides in the two seasons AMJ and ASO (respectively Fig.8e and 8f). There is a cooling trend above the thermocline and a warming trend below. The average vertical

a mis en forme : Couleur de police : Texte 1

a mis en forme : Couleur de police : Texte 1

a mis en forme : Couleur de police : Texte 1

a mis en forme : Couleur de police : Texte 1

a mis en forme : Couleur de police : Texte 1

a mis en forme : Couleur de police : Texte 1

a mis en forme : Couleur de police : Texte 1

a mis en forme : Couleur de police : Texte 1

a mis en forme : Couleur de police : Texte 1

a mis en forme : Couleur de police : Texte 1

732 ~~extension~~ extent is up to ~350 m depth for the maximum values but exceeds 500 m depth for  
733 the low values ( $< 0.1 \text{ }^\circ\text{C}\cdot\text{day}^{-1}$ ). As for the horizontal averages (Fig. ~~8a9a~~ and ~~8e9c~~), from one  
734 season to another there is a weakening of ZDF above the slope and a strengthening offshore,  
735 Fig. 8e and 8f, for AMJ and ASO respectively. Furthermore, offshore ZDF maxima seem to be  
736 discontinuous and spaced of about 140–160 km during the AMJ season (Fig. 8e) but are more  
737 continuous for the ASO season (Fig. 8f). For the non-tidal simulation, the mean ZDF tends to  
738 be null in the ocean interior but remains quite large ( $> -0.2 \text{ }^\circ\text{C}\cdot\text{day}^{-1}$ ) in the thin surface layer  
739 during the two seasons (Fig. 8g-h).

740 Furthermore, it is worth to ~~notenoting~~ that along ~~the ITsIT~~ propagation's pathway, the  
741 maximum of the ZDF follows the maxima of the baroclinic tidal energy dissipation (color  
742 shading in Fig. 2f). Thus, the dissipation of ~~ITsIT~~ causes vertical mixing that enhances the  
743 cooling ~~observed atof~~ the sea surface. In addition, this temperature diffusion contributes to  
744 greater subsurface cooling, within the mixed-layer and warming in the deeper layers beneath  
745 the thermocline.

746 ~~In section IV.3, the~~ The seasonality of the stratification ~~was~~, highlighted, ~~which we~~  
747 ~~recall is stronger at the coast relative to the open ocean during the AMJ season, and reverses~~  
748 ~~during the ASO season to become stronger offshore relative to the coast. This above~~, could  
749 explain why the ZDF is stronger along the slope and the near-coastal pathway B during the  
750 AMJ season (Fig. 8a and 8e). ~~And~~, and why ~~#ZDF~~ is weaker along the slope, close to zero  
751 following B, and reinforce offshore of A during the ASO season (Fig. 8c and 8f). Previous  
752 studies have shown that stratification influences the generation of ~~ITsinternal tides~~ and controls  
753 their ~~propagation modes: modal distribution~~. Here we show that stratification also plays a role  
754 on the fate of these ~~ITsinternal tides~~, in this case on their dissipation. The stratification could  
755 determine where ~~ITs wavesIT~~ dissipate their energy in the water column, as mentioned by ~~de~~  
756 ~~Lavergne et al. (2020)~~ de Lavergne et al. (2020).

#### 757 IV.4.2. Advection of temperature

758 The vertical (z-ADV) ~~orand the~~ horizontal (h-ADV) terms of the temperature advection  
759 tendency are ~~also~~ averaged ~~between 2–20m~~, for each season over the three years. ~~Remember~~  
760 ~~that when comparing the tidal and non-tidal simulation, a residual term may arise (see equation~~  
761 ~~7 in the section II.3.2) and must be considered for the following terms, even if it is expected to~~  
762 ~~be low~~ same depth-range as above for the two seasons.

a mis en forme : Couleur de police : Texte 1

a mis en forme : Couleur de police : Texte 1

a mis en forme : Couleur de police : Texte 1

a mis en forme : Couleur de police : Texte 1

a mis en forme : Couleur de police : Texte 1

a mis en forme : Couleur de police : Texte 1

a mis en forme : Couleur de police : Texte 1

a mis en forme : Couleur de police : Texte 1

a mis en forme : Couleur de police : Texte 1

a mis en forme : Couleur de police : Texte 1

a mis en forme : Couleur de police : Texte 1

a mis en forme : Couleur de police : Texte 1

a mis en forme : Couleur de police : Texte 1

a mis en forme : Couleur de police : Texte 1

a mis en forme : Couleur de police : Texte 1

a mis en forme : Couleur de police : Texte 1

a mis en forme : Couleur de police : Texte 1

a mis en forme : Couleur de police : Texte 1

a mis en forme : Couleur de police : Texte 1

a mis en forme : Couleur de police : Texte 1



#### 763 IV.4.2.a Vertical advection of Temperature

764 z-ADV is almost null in these surface layers throughout the region (Fig.9a-d). For both  
765 seasons, some weak extreme values are in the northwest on the plateau between 54°W–50°W  
766 and 3°N–3°N and are for the same intensity between the two simulations with and without tides.  
767 This result suggests that, overall, the tides fail to generate vertical temperature advection within  
768 these ~~ocean surface layers. At, but deeper depth, z-ADV tendency term is non-negligible, and~~  
769 ~~clearly become~~ higher in tidal simulation than in non-tidal one. Vertical sections (Fig.9a-h)  
770 show an intensification of z-ADV of about  $\pm 0.8$  °C.day<sup>-1</sup> located below the MLD (~~magenta~~  
771 ~~dashed line~~) and seems to be centered around the thermocline (~~black dashed line~~), with a  
772 vertical extension from 20–200 m depth. z-ADV is stronger in tidal simulation during ~~the~~ both  
773 seasons (Fig.9e-f), and mainly presents sparse extrema offshore (> 300 km) for the non-tidal  
774 simulation (Fig.9g-h). For the simulation with the tides, z-ADV appears to be rather dominated  
775 by a cooling trend, with a marked hotspot on the slope followed by other hotspots offshore.  
776 These extreme values are spaced about 120–150 km apart, i.e., ~~the imprint of a mode-1~~  
777 ~~propagation wavelength as for the baroclinic tidal energy dissipation (Fig.2f). For the~~ Note that  
778 ~~for~~ both simulations (Fig.9e10e-h), the extreme values are located within the narrow density  
779 ( $\sigma_\theta$ ) contours [23.8–26.2 kg.m<sup>-3</sup>], i.e., ~~they follow the maximum of the stratification,~~  
780 ~~namely within~~ the pycnocline. ~~The location of the extreme values of z-ADV at the shelf break~~  
781 ~~and along IT propagation's pathway and its negative sign suggest that the diffusive part of the~~  
782 ~~advection scheme might be the dominant process compared to nonlinear effects.~~

#### 783 IV.4.2.b Horizontal advection of temperature

784 Horizontal advection of temperature (h-ADV) is defined as the sum of the zonal (x-  
785 ADV) and meridional (y-ADV) terms of temperature advection tendency. As for z-ADV, the  
786 mean of h-ADV tends to be null over the entire domain in the surface layers for both seasons  
787 in both simulations (Fig.10a-d). Nevertheless, some weak extreme values are in the northwest  
788 of the plateau between 54°W–50°W and 3°N–3°N. ~~That, that~~ intensify during the ASO season  
789 in both simulations,  $\sim \pm 0.2$  °C.day<sup>-1</sup>, Fig.10c and 10d for the tidal and non-tidal simulations  
790 respectively. During AMJ, h-ADV is slightly stronger,  $\sim 0.1$  °C.day<sup>-1</sup>, around sites A and B in  
791 the tidal simulation (Fig.10a) ~~than in the non-tidal simulation (Fig.10b). This, which~~ appears  
792 to be related to ~~the ITs/IT~~ generated along the slope. On the other hand, the small difference  
793 between the two simulations in the surface layers shows that the tides hardly generate h-ADV.  
794 Then, h-ADV ~~could not~~ hardly influence the cold-water tongue observed over the surface SST

a mis en forme : Couleur de police : Texte 1

a mis en forme : Espace Avant : 6 pt

a mis en forme : Couleur de police : Texte 1

a mis en forme : Couleur de police : Texte 1

a mis en forme : Couleur de police : Texte 1

a mis en forme : Couleur de police : Texte 1

a mis en forme : Couleur de police : Texte 1

a mis en forme : Couleur de police : Texte 1

a mis en forme : Couleur de police : Texte 1

a mis en forme : Couleur de police : Texte 1

a mis en forme : Couleur de police : Texte 1

a mis en forme : Couleur de police : Texte 1

a mis en forme : Couleur de police : Texte 1

a mis en forme : Couleur de police : Texte 1

a mis en forme : Couleur de police : Texte 1

a mis en forme : Couleur de police : Texte 1

a mis en forme : Couleur de police : Texte 1

a mis en forme : Couleur de police : Texte 1

a mis en forme : Couleur de police : Texte 1

a mis en forme : Couleur de police : Texte 1

a mis en forme : Couleur de police : Texte 1

a mis en forme : Couleur de police : Texte 1

a mis en forme : Espace Avant : 6 pt

a mis en forme : Couleur de police : Texte 1

a mis en forme : Couleur de police : Texte 1

a mis en forme : Couleur de police : Texte 1

a mis en forme : Couleur de police : Texte 1

795 during the ASO season (Fig.4d-f). ~~This result aligns with Bessières et al. (2008), which had~~  
796 ~~previously shown that the tidal residual mean transport is null in the upwelling region in the~~  
797 ~~south east and low ( $< |0.1|$  Sverdrup) over the whole shelf.~~

798 Along the vertical following A, h-ADV maxima remain essentially confined below the  
799 mixed-layer depth, with much more intense values in the tidal simulation (Fig.10e-f) compared  
800 to the non-tidal simulation (Fig.10g-h). h-ADV contributes to both warming and cooling of the  
801 temperature of  $\sim \pm 0.4$  °C.day<sup>-1</sup> from the slope to more than 500 km offshore. During both  
802 seasons, the average vertical extension lies between the surface and 400 m depth for the tidal  
803 simulation and a little less extended between 20–300 m depth for the non-tidal simulation. As  
804 for z-ADV, h-ADV is also stronger within the pycnocline. For the tidal simulation, there is a  
805 warming above the slope (0.4 °C.day<sup>-1</sup>) reaching the surface in both seasons. This vertical  
806 excursion is observed elsewhere for ZDF and z-ADV, and it is probably a marker of local  
807 dissipation of ~~ITs~~IT at their generation site. ~~The~~This local dissipation of ~~ITs~~ITs clearly affects both  
808 advection and vertical diffusion of the temperature. ~~But~~ but there are very low values along the  
809 slope when averaging h-ADV or z-ADV between 2–20 m and much more strong values for  
810 the ZDF. This means that the energy dissipated by ~~ITs~~internal tides is mostly transferred to  
811 mixing. In addition, unlike ZDF and z-ADV, the (horizontal) location of h-ADV maxima  
812 mismatch IT dissipation hotspots.

813 ~~Furthermore, unlike ZDF and z-ADV, the (horizontal) location of h-ADV maxima~~  
814 ~~mismatch the dissipation hotspots. It is difficult to identify the wave-like characteristic of the~~  
815 ~~propagation of ITs in h-ADV. This probably means that ITs hardly induce any horizontal~~  
816 ~~motion of water mass. We can therefore deduce that the observed increase in h-ADV is mainly~~  
817 ~~because of the barotropic tides.~~

## 818 **V. Discussion**

### 819 **V.1. Vertical advection tendency term**

820 Results showed that z-ADV is stronger in the deeper layer, below the MLD and within the  
821 pycnocline (Fig.9e h). As mentioned above, this tendency term includes both nonlinear effect  
822 between the temperature and the currents and numerical dissipation of the diffusive part of  
823 advection scheme working at high frequencies. The location of the maxima of the vertical  
824 advection tendency at the shelf break and along the ITs propagation pathway and its negative  
825 sign, suggest that the diffusive part of the advection scheme might be the dominant process

a mis en forme : Couleur de police : Texte 1

a mis en forme : Couleur de police : Texte 1

a mis en forme : Couleur de police : Texte 1

a mis en forme : Couleur de police : Texte 1

a mis en forme : Couleur de police : Texte 1

a mis en forme : Couleur de police : Texte 1

a mis en forme : Couleur de police : Texte 1

826 compared to nonlinear effects, as the velocity of the (mode-1) internal tidal waves is maximum  
827 in the thermocline where exactly z-ADV term is working harder.

### 828 V.2.-IV.4.3. Heat budget balance

829 Figure 10 shows the terms of the heat balance equation averaged below the MLD  
830 between 60 and 400 m depth in a region around the IT trajectories emanating from A and B  
831 between 40°W-48°W and 0°N-6°N. During the AMJ season, advection (ADV) dominates over  
832 diffusion terms for both tidal (Fig.11a) and non-tidal (Fig.11b) simulations, while during the  
833 ASO season, advection dominates only in tidal simulations (Fig.11c) and ZDF dominates in  
834 non-tidal simulations (Fig.11d). We show here that advection terms dominate under the MLD,  
835 while from the two sections above, in the tidal simulation, ZDF dominates the advection terms  
836 at surface and within the mixed-layer and is the main contributor within the ocean processes to  
837 explain SST changes. That vertical profile is probably the case in the real ocean since the tidal  
838 simulation is more representative of reality.

## 839 V. Discussion

### 840 V.1. On the role of advection in coastal upwelling

841 To explain the cooling of the SST at the surface, ~~Neto and da Silva (2014)~~Neto and da  
842 Silva (2014) indicated that the steady flow of the NBC induces northward transport of water  
843 masses. This transport is in turn offset by a vertical advection of cool water towards the surface.  
844 We demonstrate with our model that the vertical advection hardly modifies the SST. But it is  
845 rather working below the mixed layer (Fig.9e-h). The tides-induced vertical diffusion (mixing)  
846 extends from the mixed-layer to deeper layers (Fig.8e-f). It is ~~therefore possible for that~~ the  
847 vertical mixing ~~to bring up~~upwells to the surface the water masses that are advected into the  
848 layers below the mixed layer. The ~~change in SST and~~temperature change at the surface and  
849 within the mixed-layer can then be ~~influence in~~influenced to first order by (i) the vertical  
850 diffusion of temperature and ~~secondary by~~(ii) a cross effect between the latter and the advection  
851 (vertical and horizontal) of temperature that mainly takes place below ~~the mixed layer~~MLD.

### 852 V.32. The mode-1 wave-like patterns wavelenth in the vertical terms of the 853 heat budget equation

854 Along the vertical and toward the open ocean, both ZDF and z-ADV tendencies are found  
855 to have a wave-like structure. For z-ADV, patches are spaced apart by about 120–150 km and  
856 140–160 km for the AMJ and ASO seasons respectively. Whilst for z-ADV, this wavelength is

a mis en forme : Couleur de police : Texte 1

a mis en forme : Couleur de police : Texte 1

a mis en forme : Couleur de police : Texte 1

a mis en forme : Couleur de police : Texte 1

a mis en forme : Couleur de police : Texte 1

a mis en forme : Couleur de police : Texte 1

a mis en forme : Couleur de police : Texte 1

a mis en forme : Couleur de police : Texte 1

a mis en forme : Couleur de police : Texte 1

a mis en forme : Couleur de police : Texte 1

a mis en forme : Couleur de police : Texte 1

a mis en forme : Couleur de police : Texte 1

857 about 140–160 km during the AMJ season and more continuous patches for the ASO season.  
858 The wavelength ranges found in ~~temperature tendency~~ heat budget terms (~~3T~~) are slightly wider  
859 (~~±~~ 10–20 km, for z-ADV in ASO season and for ZDF) than the purely dynamic tidal coherent  
860 wavelength (~ 120–150 km, see section III.1). The difference can be understood as the effect  
861 of incoherent ITs, i.e., ITs that are not captured by the harmonic analysis because they are  
862 deviated or diffracted by the currents and/or eddies, and for which dissipation occurs around  
863 where coherent ITs dissipate. ~~They are uncaptured by the harmonic analysis.~~ Hence, the total  
864 (coherent + incoherent) dissipation pattern of ITs could be wider than in Figure 2f. When  
865 integrating ~~3T~~ heat budget terms over the season, this cumulative effect is considered and  
866 therefore leads to diffused ~~diffusive~~ patterns and wider wavelength. This diffusive effect  
867 increases during the ASO season when both background circulation and eddy activity increase.

868 ~~Recently, de Macedo et al. (2023) gave a detailed description of ISW in this region. They~~  
869 ~~showed an intensification of ISW occurrences along A and B pathways, whose inter packet~~  
870 ~~distance corresponds to the wavelength of mode 1 ITs. These ISW packets are also colocalized~~  
871 ~~(horizontally) with the deeper 3T patches. Our results are therefore consistent with the~~  
872 ~~observations of the latter study regarding the localization of IT dissipation, particularly where~~  
873 ~~they can generate ISW.~~

874 Recently, de Macedo et al. (2023) gave a detailed description of internal solitary waves  
875 (ISW) in this region from remote sensing data. These ISW originate from instabilities and  
876 energy loss or dissipation of IT radiating from the slope, mainly along the pathways A and B  
877 (Magalhaes et al., 2016). The first have shown that inter-packet distance of ISW corresponds  
878 to mode-1 wavelength. IT dissipation and deeper heat budget terms patches of our simulations  
879 are colocalized horizontally with observed ISW packets. This means that our model well  
880 reproduces the location of IT dissipation.

### 881 **V.43. Tidal impact at the mouth of the Amazon River and on the southern** 882 **shelf: two main competitive processes**

883 ~~Depending on the season, the mean SST anomaly [Tide — No Tide] at the mouth of the~~  
884 ~~Amazon and southeast of the plateau is either negative (AMJ, fig.5a) or positive (ASO, fig.5b).~~  
885 ~~What we found can be explained by a combination of processes. Note that seasonal variations~~  
886 ~~in solar radiation, river flow and stratification over the shelf can also play significant roles.~~

887 ~~In the simulation without the tides, there is a strong along-coast-parallel current exiting~~  
888 ~~northwesterly the mouth of the Amazon River (black arrows in Fig.11a, 11b; Ruault et al.,~~  
889 ~~2020)e.g., Ruault et al., 2020) with an average intensity > 0.5 m.s<sup>-1</sup> in the first 50 meters (color~~

a mis en forme : Couleur de police : Texte 1

a mis en forme : Couleur de police : Texte 1

a mis en forme : Couleur de police : Texte 1

a mis en forme : Couleur de police : Texte 1

a mis en forme : Couleur de police : Texte 1

a mis en forme : Couleur de police : Texte 1

890 ~~shading in for both seasons (Fig.11a, 11b|2a-b)~~. When including the tides in the model, the  
891 latter study ~~had shown~~ showed that there is an increase in the vertical mixing in the water column  
892 due to stratified-shear flow instability. ~~They then show that this, which weakens and deflects~~  
893 ~~the along-coast parallel, current and favors north-eastwards at the mouth of the Amazon River~~  
894 ~~(Fig.12c-d) and favours cross-shore export of water (color shading in Fig.11c, 11d), which is~~  
895 ~~then diverted to the north west (black arrows in Fig.11c, 11d).~~ We can therefore establish that  
896 there are at least two processes at work ~~in producing SST anomalies~~: (i) vertical mixing and (ii)  
897 horizontal transport, ~~reflected~~ backed respectively by ZDF and h-ADV. We then looked at the  
898 latter two processes along the vertical following the cross-shore transect (C-S) defined in Figure  
899 10b. Hereinafter, “inner mouth” refers to the part of the transect before 200 km, whereas “outer  
900 shelf” refers to the part beyond.

901 During the AMJ season, in the inner mouth, river flow dominates and tide-induced vertical  
902 mixing in the narrow water column leads to warming and deepening of the thermocline (~~cyan~~  
903 ~~and black lines in Fig.12a|3a-b)~~. On the outer shelf, this mixing in the thicker water column  
904 leads to cooling above the thermocline and warming below (Fig.12a). ~~Which~~ 13a), which in turn  
905 extends across the shelf and along the pathways of ~~ITsIT~~ as shown in section IV.4.1 (see Fig.8a,  
906 ~~8c, and 8e-f)~~. At the same time, the SST on the shelf is somewhat homogeneous (see Fig.4a-c)  
907 and solar radiation is lower than  $190 \text{ W.m}^{-2}$  (not shown). As a result, waters of similar  
908 temperature are advected horizontally, i.e., ~~the~~ h-ADV is low (Fig.12b|3b). Thus, for the first  
909 season, vertical mixing seems to be the dominant process explaining the average negative SST  
910 anomaly on the plateau.

911 For the second season, solar radiation on the shelf rose sharply with an average value of  $60$   
912  $\text{W.m}^{-2}$  compared with the previous season (Fig.12c). ~~The average depth of the thermocline~~  
913 ~~deepens offshore (cyan and black lines Fig.12d and 12e)~~. Here, mixing leads to warming in the  
914 thin surface layer ( $< 2\text{m}$ , Fig.12d). In contrast to AMJ, there is a significant horizontal variation  
915 in SST on the plateau (see Fig.4d-f). The NBC is stronger and can influence transport over the  
916 shelf (Prestes et al., 2018). Even it is small, the mean tidal residual transport is added and should  
917 be taken into account (Bessières et al., 2008). Warm waters can therefore be advected across  
918 the shelf. Consequently, h-ADV is stronger and positive (Fig.12e) and plays a greater role in  
919 the fate of SST. For this season, ZDF and h-ADV add to explain the positive SST anomaly on  
920 the shelf|3c) and the average depth of the thermocline deepens offshore (Fig.13d and 13e). In  
921 this season, mixing leads to warming in the thin surface layer ( $< 2\text{m}$ , Fig.13d). The NBC is  
922 stronger and can influence transport over the shelf (Prestes et al., 2018) and the small mean

a mis en forme : Couleur de police : Texte 1

a mis en forme : Couleur de police : Texte 1

a mis en forme : Couleur de police : Texte 1

a mis en forme : Couleur de police : Texte 1

a mis en forme : Couleur de police : Texte 1

a mis en forme : Couleur de police : Texte 1

a mis en forme : Couleur de police : Texte 1

a mis en forme : Couleur de police : Texte 1

a mis en forme : Couleur de police : Texte 1

a mis en forme : Couleur de police : Texte 1

a mis en forme : Couleur de police : Texte 1

a mis en forme : Couleur de police : Texte 1

a mis en forme : Couleur de police : Texte 1

a mis en forme : Couleur de police : Texte 1

a mis en forme : Couleur de police : Texte 1

a mis en forme : Couleur de police : Texte 1

a mis en forme : Couleur de police : Texte 1

a mis en forme : Couleur de police : Texte 1

a mis en forme : Couleur de police : Texte 1

a mis en forme : Couleur de police : Texte 1

a mis en forme : Couleur de police : Texte 1

a mis en forme : Couleur de police : Texte 1

a mis en forme : Couleur de police : Texte 1

923 tidal residual transport should also be considered (Bessières et al., 2008). The region is more  
924 dynamic, and waters of distinct temperatures are advected over the shelf. Consequently, h-ADV  
925 is stronger and positive (Fig.13e) and then plays a greater role in the fate of SST. For this season,  
926 ZDF and h-ADV add to explain the positive SST anomaly on the shelf. In addition, from AMJ  
927 to ASO, we noted the deepening of the thermocline depth on the outer shelf. This was  
928 previously highlighted by Silva et al. (2005) from REVIZEE (Recursos Vivos da Zona  
929 Econômica Exclusiva ) campaign data and is a further contribution to the validation of our  
930 simulations.

931 ~~From AMJ to ASO, we can note the deepening of the thermocline depth on the outer shelf.~~  
932 ~~This was previously highlighted by Silva et al. (2005) from REVIZEE (Recursos Vivos da Zona~~  
933 ~~Econômica Exclusiva ) campaign data. This is a further contribution to the validation of our~~  
934 ~~model in the section III.2.~~

#### 935 **V.5. Tidal impact4. Mixing in the NBC retroflection area**

936 To the north-west of the domain [3°N–9°N and 53°W–45°W], in the surface layers (2–  
937 20m), eddy-like or circular patterns exist in ZDF during the ASO season for the simulation  
938 including tides (Fig.8c). ~~It should be remembered that during this season the NBC intensifies~~  
939 ~~and retroflects, and strong eddy activity takes place there. We therefore assume that they may~~  
940 ~~be the driving force behind these ZDF patterns. However, it is not yet clear how these mesoscale~~  
941 ~~features produce vertical mixing. They may be involved either by fronts or trapping the internal~~  
942 ~~tidal waves.~~

943 ~~1) Fronts: they exist in such a intensively active mesoscale region. They are associated~~  
944 ~~with significant vertical mixing (see Chapman et al., 2020). We therefore looked at the~~  
945 ~~horizontal temperature gradient ( $\nabla T$ ) averaged over the same depth range (2–20m) as the ZDF~~  
946 ~~(Fig.8a-d). During the AMJ season, it is on average equal to  $4 \cdot 10^{-2} \text{ }^\circ\text{C}/10 \text{ km}$ .NBC intensifies~~  
947 ~~and retroflects, and strong eddy activity takes place there during ASO. We can assume that this~~  
948 ~~intense mesoscale activity influences the mixing and subsequent temperature diffusion.~~  
949 ~~However, it is not yet clear how these mesoscale features produce mixing. Fronts exist in such~~  
950 ~~region and are associated with high horizontal temperature gradient ( $\nabla T$ ) and significant vertical~~  
951 ~~mixing (see Chapman et al., 2020). We therefore examined the mean  $\nabla T$  in the same depth~~  
952 ~~range (2–20m) as ZDF (Fig.8a-d). During the AMJ season, it is on average equal to  $4 \cdot 10^{-2} \text{ }^\circ\text{C}/10$~~   
953 ~~km. As expected, it does not reveal any circular fronts for the two simulations (Fig.13a,14a-b)~~  
954 ~~since mesoscale activity is low. Secondly, the horizontal gradient of the temperature Then  $\nabla T$ .~~

a mis en forme : Couleur de police : Texte 1

a mis en forme : Couleur de police : Texte 1

a mis en forme : Normal, Retrait : Première ligne : 0,63 cm, Espace Avant : 0 pt, Sans numérotation ni puces

a mis en forme : Couleur de police : Texte 1

a mis en forme : Couleur de police : Texte 1

a mis en forme : Couleur de police : Texte 1

955 increases during the ASO season [ $> 5 \cdot 10^{-2} \text{ }^\circ\text{C}/10 \text{ km}$ ] in the north-west and exhibits circular  
956 and filamentary fronts in both the non-tidal (Fig.13e14c) and tidal (Fig.13d14d) simulations.  
957 Therefore, one would expect to see the same circular patterns in the ZDF for both simulations.  
958 ~~This, this is not actually the case (see Fig.8c and 8d) and invalidates this statement. Furthermore,~~  
959 ~~these values are at least three times smaller compared to other oceanic regions (e.g., Kostianoy~~  
960 ~~et al., 2004 and Bouali et al., 2017), meaning). Another hypothesis is that these fronts are less~~  
961 ~~pronounced circular patterns could be originated from the interaction between IT and near-~~  
962 ~~inertial oscillations, which can enhance mixing and vertical transport processes in the ocean.~~  
963 ~~But quantifying this interaction requires further analysis and is beyond the scope this study.~~

964 ~~2) Trapping internal tidal waves: stronger mesoscale activity which occurs during this~~  
965 ~~season implies more interaction between the background circulation and ITs (Buijsman~~  
966 ~~et al., 2017 and Tehilibou et al., 2022). The NBC flows along the coast and crosses the~~  
967 ~~sites where ITs are generated (see schematic view in Fig.1). This means that ITs can be~~  
968 ~~trapped and advected along the NBC pathway. When this current destabilizes and~~  
969 ~~retroreflects in the north west, these trapped waves dissipate and therefore generate~~  
970 ~~vertical mixing. This hits the high fraction of the incoherent ITs found here (Tehilibou~~  
971 ~~et al., 2022). But quantifying the impact on temperature of such a wave-mean flow~~  
972 ~~interaction process requires further analysis and is beyond the scope of this study.~~

973 ~~Nevertheless, we believe that this second process could be the main cause of vertical~~  
974 ~~diffusion of temperature in that region. Thus, from the section V.3 and the latter, we can~~  
975 ~~conclude that incoherent ITs represent a significant part of the total energy of internal tides. But~~  
976 ~~remains to be quantified in future work. In addition, in parallel with coherent ITs, they might~~  
977 ~~play a critical role on the fate of the temperature in this region.~~

## 978 VI. Summary

979 In this paper, we used twin oceanic simulations (with and without tides) from a realistic  
980 model to explore the impact of internal tidal waves (ITs) on temperature and associated  
981 processes. The impact on the atmosphere-to-ocean net heat fluxes is also covered.

982 The AMAZON36 configuration can reproduce the generation of ITs from two most  
983 energetic sites A and B, in good agreement with previous studies. The model well reproduces  
984 ~~the~~their local, on-shelf, and offshore dissipation ~~of ITs~~ with two beams of mode-1 propagation  
985 (120–150 km). This dissipation occurs less than 300 km from the slope. Then, we assess the  
986 ability of the model to reproduce temperature structure. The simulations including tides is in

a mis en forme : Couleur de police : Texte 1

a mis en forme : Couleur de police : Texte 1

a mis en forme : Couleur de police : Texte 1

a mis en forme : Couleur de police : Texte 1

a mis en forme : Couleur de police : Texte 1

a mis en forme : Numéros + Niveau : 1 + Style de numérotation : I, II, III, ... + Commencer à : 6 + Alignement : Gauche + Alignement : 0,63 cm + Retrait : 1,9 cm

987 better agreement with SST observations and better reproduce water mass properties along the  
988 vertical.

989 Our analyses were based on three years (2013 ~~to~~ 2015) of data averaged over two  
990 seasons, AMJ (April-May-June) and ASO (August-September-October). That are highly  
991 contrasted in terms of stratification, background circulation and EKE. Results show that for  
992 both seasons, the tides create SST cooling of about 0.3 °C in the plume of the Amazon offshore  
993 and along the paths of ~~propagation A and B of ITs internal tides~~. During ASO, the cold waters  
994 of the ACT enter our domain along the coast and are affected by the tides. This enhances that  
995 seasonal upwelling and leads to cooler SST. Over the Amazon shelf, the tides induce the same  
996 magnitude cooling in AMJ and in turn induce an opposite anomaly (warming) in ASO. These  
997 cooling/warming are responsible in the same location for an increase/decrease in the net heat  
998 flux from the atmosphere to the ocean (Qt). However, the overall effect of the tides is an  
999 increase of Qt, which lies between [33.2% – 7.4%] from AMJ to ASO. ~~And can be and is~~ larger  
1000 than ~~what obtained elsewhere (e.g., in the Solomon Sea). In other regions. When increasing the~~  
1001 ~~atmosphere-to-ocean net heat flux in~~ such ~~a region with~~ large atmospheric convection (~~region,~~  
1002 ~~marked by the ITCZ), when increasing the atmosphere-to-ocean net heat flux,~~ the tides  
1003 ~~might can~~ reduce the cloud convection into the atmosphere (~~Koch-Larrouy et al., 2010~~)(~~Koch-~~  
1004 ~~Larrouy et al., 2010~~). Therefore, this tidal effect on the climate might have a key importance  
1005 for the future, taking the climate change into account (~~Yadidya and Rao, 2022~~)(~~Yadidya and~~  
1006 ~~Rao, 2022~~).

1007 In the subsurface, above the thermocline (< 120 m), the tides induce a stronger cooling  
1008 (~1.2 °C) than at the surface. And an associated warming of the same magnitude under the  
1009 thermocline (> 120-300 m). We analyzed the terms of the heat budget equation to identify to  
1010 processes that modify the temperature. We found that the vertical diffusion of temperature  
1011 (ZDF) is mainly caused by the dissipation of the tides. Horizontal (h-ADV) and vertical (z-  
1012 ADV) advection can be driven by non-tidal processes but increase when including the tides in  
1013 the model.

1014 Over the shelf, barotropic tidal mixing increases ZDF (> |-0.4| °C.day<sup>-1</sup>) and explain the  
1015 cooling of the water column in AMJ season. During the second season, it combines with h-  
1016 ADV and to cause a warming. Off the shelf, the (baroclinic) mixing takes place from the slope  
1017 to about 700 km following the path A, and 300 km following the path B. That mixing induces  
1018 ZDF with values of about -0.4 °C.day<sup>-1</sup>, which is the main process in the upper layer above the  
1019 mixed layer. ~~But but~~ could combine with advection terms (z-ADV and h-ADV) to explain the

a mis en forme : Police :Italique

a mis en forme : Couleur de police : Texte 1



1020 temperature changes below the mixed layer. ~~Along ITs propagation pathways, some~~ ZDF  
1021 and z-ADV patches ~~follow the~~ are colocalized with dissipation hotspots along the trajectory of  
1022 the ITs, i.e., they exhibit the mode 1 propagation of ITs.

1023 ~~This study highlights the key role of ITs in creating intensified mixing which is~~  
1024 ~~important for temperature structure. Other analysis we performed with our simulations show~~  
1025 ~~that this mixing can also impacts salinity. Furthermore, they might be seen as a source of~~  
1026 ~~nutrient uptake at tidal frequency and can have an impact on the spatial distribution of~~  
1027 ~~phytoplankton and zooplankton, and therefore on the entire food chain (Sharples et al., 2007,~~  
1028 ~~2009; Xu et al., 2020). These other impacts can be studied through a combined model-in situ~~  
1029 ~~data approach. A long-term PIRATA (PredIction and Research moored Array in the Tropical~~  
1030 ~~Atlantic) mooring data are available for this goal (Bourlès et al., 2019). In addition, recently in~~  
1031 ~~late 2021, the AMAZOn MIXing (“AMAZOMIX”) campaign took place in this region. Among~~  
1032 ~~other things, this campaign was dedicated to ITs. It provided a huge set of data, with the aim of~~  
1033 ~~understanding their impact on marine ecosystems (see details in [https://en.ird.fr/amazomix-](https://en.ird.fr/amazomix-campaign-impact-physical-processes-marine-ecosystem-mouth-amazon)~~  
1034 ~~[campaign-impact-physical-processes-marine-ecosystem-mouth-amazon](https://en.ird.fr/amazomix-campaign-impact-physical-processes-marine-ecosystem-mouth-amazon)).~~ ~~In the meantime, a~~  
1035 ~~coupled physical/biogeochemistry simulation (NEMO/PISCES) is currently under analysis and~~  
1036 ~~will begin to answer these crucial questions.~~

1037 This study highlights the key role of internal tides in creating intensified mixing which  
1038 is important for temperature structure. Other analysis we performed with our simulations show  
1039 that this mixing can also impact salinity. Furthermore, they might be seen as a source of nutrient  
1040 uptake at tidal frequency and can have an impact on the spatial distribution of phytoplankton  
1041 and zooplankton, and therefore on the entire food chain (Sharples et al., 2007, 2009; Xu et al.,  
1042 2020). These other impacts can be studied through a combined model-in situ data approach.  
1043 Long-term PIRATA (PredIction and Research moored Array in the Tropical Atlantic) mooring  
1044 data are available for this goal (Bourlès et al., 2019). In addition, recently in late 2021, the  
1045 AMAZOn MIXing (“AMAZOMIX”) campaign took place in this region. Among other things,  
1046 this campaign was dedicated to internal tides. It provided a huge set of data, with the aim of  
1047 understanding their impact on marine ecosystems (see details in [https://en.ird.fr/amazomix-](https://en.ird.fr/amazomix-campaign-impact-physical-processes-marine-ecosystem-mouth-amazon)  
1048 [campaign-impact-physical-processes-marine-ecosystem-mouth-amazon](https://en.ird.fr/amazomix-campaign-impact-physical-processes-marine-ecosystem-mouth-amazon)). In the meantime, a  
1049 coupled physical/biogeochemistry simulation (NEMO/PISCES) is being analyzed and will  
1050 begin to answer these crucial questions.

1051 Finally, we focused hereabove on describing the impacts of tides on a seasonal scale. A  
1052 companion paper will then analyze the variability of temperature at tidal and subtidal scales  
1053 using our model simulations and two observational data.

1054  
1055

a mis en forme : Non Surlignage

a mis en forme : Espace Après : 0 pt

### 1056 **Data availability statements**

1057 The 2020's release of GEBCO bathymetry is publicly available online through:  
1058 [https://www.gebco.net/data\\_and\\_products/gridded\\_bathymetry\\_data/gebco\\_2020/](https://www.gebco.net/data_and_products/gridded_bathymetry_data/gebco_2020/). The TMI  
1059 SST v7.1 data are publicly available online from the REMSS platform:  
1060 <https://www.remss.com/missions/tmi/>, was accessed on 27 June 2022. WOA2018 climatology  
1061 is publicly available online at: <https://www.ncei.noaa.gov/access/world-ocean-atlas-2018/>, was  
1062 accessed on 27 June 2022. The model simulations are available upon request by contacting the  
1063 corresponding author.

a mis en forme : Couleur de police : Texte 1

a mis en forme : Soulignement , Couleur de police : Lien  
hypertexte

### 1064 **Authors contributions**

1065 Funding acquisition, AKL; Conceptualization and methodology, FA, AKL and ID.  
1066 Numerical simulations, GM and FA. Formal analysis, FA; FA prepared the paper with  
1067 contribution from all co-authors.

a mis en forme : Espace Avant : 6 pt

a mis en forme : Espace Après : 0 pt

### 1068 **Competing interests**

1069 The authors declare that they have no conflict of interest.

1070

a mis en forme : Espace Avant : 6 pt

### 1071 **Funding**

1072 This work is part of the PhD Thesis of ~~Fernand Assene~~FA, cofounded by Institut de  
1073 Recherche pour le Développement (IRD) and Mercator Ocean International (MOi), under the  
1074 ~~co~~badging supervision of ~~Ariane Koch Larrouy~~AKL and ~~Isabelle Dado~~ID. The numerical  
1075 simulations were founded by CNRS/CNES/IRD via the projects A0080111357 and  
1076 A0130111357 and were performed thank to “Jean-Zay”, the CNRS/GENCI/IDRIS platform for  
1077 modelling and computing.

a mis en forme : Espace Avant : 6 pt

a mis en forme : Espace Après : 0 pt, Interligne : 1,5  
ligne

### 1078 **Acknowledgments**

1079 The authors would like to thank the Editorial team for their availability, and the two  
1080 reviewers Clément Vic and Nicolas Grissouard for their valuable comments, which enhanced

a mis en forme : Espace Avant : 6 pt

a mis en forme : Espace Après : 0 pt

1081 the quality of the present work. ~~We also thank the NOAA Ocean Climate Laboratory for making~~  
1082 ~~the WOA2018 products available.~~

a mis en forme : Retrait : Première ligne : 1,27 cm

## 1084 References

- 1085 ~~Aguedjou, H.M.A., Dadou, I., Chaigneau, A., Morel, Y., Alory, G., 2019. Eddies in the Tropical~~  
1086 ~~Atlantic Ocean and Their Seasonal Variability. Geophys. Res. Lett. 46, 12156–12164.~~  
1087 ~~<https://doi.org/10.1029/2019GL083925>~~
- 1088 ~~Aguedjou, H.M.A., Chaigneau, A., Dadou, I., Morel, Y., Pegliasco, C., Da Allada, C.Y.,~~  
1089 ~~Baloïteha, E., 2021. What Can We Learn From Observed Temperature and Salinity~~  
1090 ~~Isopycnal Anomalies at Eddy Generation Sites? Application in the Tropical Atlantic~~  
1091 ~~Ocean. J. Geophys. Res. Oceans 126, e2021JC017630.~~  
1092 ~~<https://doi.org/10.1029/2021JC017630>~~
- 1093 ~~Areher, D., Martin, P., Buffett, B., Brovkin, V., Rahmstorf, S., Ganopolski, A., 2004. The~~  
1094 ~~importance of ocean temperature to global biogeochemistry. Earth Planet. Sci. Lett. 222,~~  
1095 ~~333–348. <https://doi.org/10.1016/j.epsl.2004.03.011>~~
- 1096 ~~Azevedo, A., da Silva, J.C.B., New, A.L., 2006. On the generation and propagation of internal~~  
1097 ~~solitary waves in the southern Bay of Biscay. Deep Sea Res. Part Oceanogr. Res. Pap.~~  
1098 ~~53, 927–941. <https://doi.org/10.1016/j.dsr.2006.01.013>~~
- 1099 ~~Baines, P.G., 1982. On internal tide generation models. Deep Sea Res. Part Oceanogr. Res. Pap.~~  
1100 ~~29, 307–338. [https://doi.org/10.1016/0198-0149\(82\)90098-X](https://doi.org/10.1016/0198-0149(82)90098-X)~~
- 1101 ~~Barbot, S., Lyard, F., Tchilibou, M., Carrere, L., 2021. Background stratification impacts on~~  
1102 ~~internal tide generation and abyssal propagation in the western equatorial Atlantic and~~  
1103 ~~the Bay of Biscay. Ocean Sci. 17, 1563–1583. <https://doi.org/10.5194/os-17-1563-2021>~~
- 1104 ~~Barton, E.D., Inall, M.E., Sherwin, T.J., Torres, R., 2001. Vertical structure, turbulent mixing~~  
1105 ~~and fluxes during Lagrangian observations of an upwelling filament system off~~  
1106 ~~Northwest Iberia. Prog. Oceanogr., Lagrangian studies of the Iberian upwelling system~~  
1107 ~~51, 249–267. [https://doi.org/10.1016/S0079-6611\(01\)00069-6](https://doi.org/10.1016/S0079-6611(01)00069-6)~~
- 1108 ~~Beardsley, R.C., Candela, J., Limeburner, R., Geyer, W.R., Lentz, S.J., Castro, B.M.,~~  
1109 ~~Cacchione, D., Carneiro, N., 1995. The M2 tide on the Amazon Shelf. J. Geophys. Res.~~  
1110 ~~Oceans 100, 2283–2319. <https://doi.org/10.1029/94JC01688>~~
- 1111 ~~Bessières, L., 2007. Impact des marées sur la circulation générale océanique dans une~~  
1112 ~~perspective climatique (phdthesis). Université Paul Sabatier—Toulouse III.~~
- 1113 ~~Bessières, L., Madec, G., Lyard, F., 2008. Global tidal residual mean circulation: Does it affect~~  
1114 ~~a climate OGCM? Geophys. Res. Lett. 35. <https://doi.org/10.1029/2007GL032644>~~
- 1115 ~~Bouali, M., Sato, O.T., Polito, P.S., 2017. Temporal trends in sea surface temperature gradients~~  
1116 ~~in the South Atlantic Ocean. Remote Sens. Environ. 194, 100–114.~~  
1117 ~~<https://doi.org/10.1016/j.rse.2017.03.008>~~

1118 Bourlès, B., Molinari, R.L., Johns, E., Wilson, W.D., Leaman, K.D., 1999. Upper layer currents  
1119 in the western tropical North Atlantic (1989–1991). *J. Geophys. Res. Oceans* 104, 1361–  
1120 1375. <https://doi.org/10.1029/1998JC900025>

1121 Bourlès, B., Araujo, M., McPhaden, M.J., Brandt, P., Foltz, G.R., Lumpkin, R., Giordani, H.,  
1122 Hernandez, F., Lefèvre, N., Nobre, P., Campos, E., Saravanan, R., Trotte-Duhà, J.,  
1123 Dengler, M., Hahn, J., Hummels, R., Lübbecke, J.F., Rouault, M., Cotrim, L., Sutton,  
1124 A., Jochum, M., Perez, R.C., 2019. PIRATA: A Sustained Observing System for  
1125 Tropical Atlantic Climate Research and Forecasting. *Earth Space Sci.* 6, 577–616.  
1126 <https://doi.org/10.1029/2018EA000428>

1127 Buijsman, M.C., Arbic, B.K., Richman, J.G., Shriver, J.F., Wallcraft, A.J., Zamudio, L., 2017.  
1128 Semidiurnal internal tide incoherence in the equatorial Pacific. *J. Geophys. Res. Oceans*  
1129 122, 5286–5305. <https://doi.org/10.1002/2016JC012590>

1130 C.,—Le Provost, Florent, Lyard, 1997. Energetics of the M2 barotropic ocean tides: an estimate  
1131 of bottom friction dissipation from a hydrodynamic model — *ScienceDirect. Prog.*  
1132 *Oceanogr.* 37–52.

1133 Chapman, C.C., Lea, M. A., Meyer, A., Sallée, J. B., Hindell, M., 2020. Defining Southern  
1134 Ocean fronts and their influence on biological and physical processes in a changing  
1135 climate. *Nat. Clim. Change* 10, 209–219. <https://doi.org/10.1038/s41558-020-0705-4>

1136 Clayson, C.A., Bogdanoff, A.S., 2013. The Effect of Diurnal Sea Surface Temperature  
1137 Warming on Climatological Air-Sea Fluxes. *J. Clim.* 26, 2546–2556.  
1138 <https://doi.org/10.1175/JCLI-D-12-00062.1>

1139 Collins, M., An, S.-I., Cai, W., Ganachaud, A., Guilyardi, E., Jin, F. F., Jochum, M., Lengaigne,  
1140 M., Power, S., Timmermann, A., Vecchi, G., Wittenberg, A., 2010. The impact of global  
1141 warming on the tropical Pacific Ocean and El Niño. *Nat. Geosci.* 3, 391–397.  
1142 <https://doi.org/10.1038/ngeo868>

1143 da Silva, J.C.B., New, A.L., Magalhaes, J.M., 2011. On the structure and propagation of internal  
1144 solitary waves generated at the Mascarene Plateau in the Indian Ocean. *Deep Sea Res.*  
1145 *Part Oceanogr. Res. Pap.* 58, 229–240. <https://doi.org/10.1016/j.dsr.2010.12.003>

1146 de Lavergne, C., Vic, C., Madec, G., Roquet, F., Waterhouse, A.F., Whalen, C.B., Cuypers, Y.,  
1147 Bouruet Aubertot, P., Ferron, B., Hibiya, T., 2020. A Parameterization of Local and  
1148 Remote Tidal Mixing. *J. Adv. Model. Earth Syst.* 12, e2020MS002065.  
1149 <https://doi.org/10.1029/2020MS002065>

1150 de Macedo, C.R., Koch-Larrouy, A., da Silva, J.C.B., Magalhães, J.M., Lentini, C.A.D., Tran,  
1151 T.K., Rosa, M.C.B., Vantrepotte, V., 2023. Spatial and temporal variability of mode-1  
1152 and mode-2 internal solitary waves from MODIS/TERRA sunglint off the Amazon  
1153 shelf. *EGUsphere* 1–27. <https://doi.org/10.5194/egusphere-2022-1482>

1154 Didden, N., Schott, F., 1993. Eddies in the North Brazil Current retroflection region observed  
1155 by Geosat altimetry. *J. Geophys. Res. Oceans* 98, 20121–20131.  
1156 <https://doi.org/10.1029/93JC01184>

1157 Dong, S., Sprintall, J., Gille, S.T., Talley, L., 2008. Southern Ocean mixed layer depth from  
 1158 Argo float profiles. *J. Geophys. Res. Oceans* 113.  
 1159 <https://doi.org/10.1029/2006JC004051>

1160 Dunphy, M., Lamb, K.G., 2014. Focusing and vertical mode scattering of the first mode internal  
 1161 tide by mesoscale eddy interaction. *J. Geophys. Res. Oceans* 119, 523–536.  
 1162 <https://doi.org/10.1002/2013JC009293>

1163 Egbert, G.D., Ray, R.D., 2000. Significant dissipation of tidal energy in the deep ocean inferred  
 1164 from satellite altimeter data. *Nature* 405, 775–778. <https://doi.org/10.1038/35015531>

1165 Fassoni Andrade, A.C., Durand, F., Azevedo, A., Bertin, X., Santos, L.G., Khan, J.U., Testut,  
 1166 L., Moreira, D.M., 2023. Seasonal to interannual variability of the tide in the Amazon  
 1167 estuary. *Cont. Shelf Res.* 255, 104945. <https://doi.org/10.1016/j.csr.2023.104945>

1168 Feng, Y., Tang, Q., Li, J., Sun, J., Zhan, W., 2021. Internal Solitary Waves Observed on the  
 1169 Continental Shelf in the Northern South China Sea From Acoustic Backscatter Data.  
 1170 *Front. Mar. Sci.* 8.

1171 Fontes, R.F.C., Castro, B.M., Beardsley, R.C., 2008. Numerical study of circulation on the inner  
 1172 Amazon Shelf. *Ocean Dyn.* 58, 187–198. <https://doi.org/10.1007/s10236-008-0139-4>

1173 Gabioux, M., Vinzon, S.B., Paiva, A.M., 2005. Tidal propagation over fluid mud layers on the  
 1174 Amazon shelf. *Cont. Shelf Res.* 25, 113–125. <https://doi.org/10.1016/j.csr.2004.09.001>

1175 Garzoli, S.L., Field, A., Johns, W.E., Yao, Q., 2004. North Brazil Current retroflexion and  
 1176 transports. *J. Geophys. Res. Oceans* 109. <https://doi.org/10.1029/2003JC001775>

1177 Gévaudan, M., Durand, F., Jouanno, J., 2022. Influence of the Amazon-Orinoco Discharge  
 1178 Interannual Variability on the Western Tropical Atlantic Salinity and Temperature. *J.*  
 1179 *Geophys. Res. Oceans* 127, e2022JC018495. <https://doi.org/10.1029/2022JC018495>

1180 Hernandez, O., Jouanno, J., Durand, F., 2016. Do the Amazon and Orinoco freshwater plumes  
 1181 really matter for hurricane-induced ocean surface cooling? *J. Geophys. Res. Oceans*  
 1182 121, 2119–2141. <https://doi.org/10.1002/2015JC011021>

1183 Hernandez, O., Jouanno, J., Echevin, V., Aumont, O., 2017. Modification of sea surface  
 1184 temperature by chlorophyll concentration in the Atlantic upwelling systems. *J. Geophys.*  
 1185 *Res. Oceans* 122, 5367–5389. <https://doi.org/10.1002/2016JC012330>

1186 Hersbach, H., Bell, B., Berrisford, P., Hirahara, S., Horányi, A., Muñoz-Sabater, J., Nicolas, J.,  
 1187 Peubey, C., Radu, R., Schepers, D., Simmons, A., Soci, C., Abdalla, S., Abellan, X.,  
 1188 Balsamo, G., Bechtold, P., Biavati, G., Bidlot, J., Bonavita, M., De Chiara, G.,  
 1189 Dahlgren, P., Dee, D., Diamantakis, M., Dragani, R., Flemming, J., Forbes, R., Fuentes,  
 1190 M., Geer, A., Haimberger, L., Healy, S., Hogan, R.J., Hólm, E., Janisková, M., Keeley,  
 1191 S., Laloyaux, P., Lopez, P., Lupu, C., Radnoti, G., de Rosnay, P., Rozum, I., Vamborg,  
 1192 F., Villaume, S., Thépaut, J.-N., 2020. The ERA5 global reanalysis. *Q. J. R. Meteorol.*  
 1193 *Soc.* 146, 1999–2049. <https://doi.org/10.1002/qj.3803>

1194 ~~HYBAM (2018) Contrôles géodynamique, hydrologique et biogéochimique de~~  
1195 ~~l'érosion/altération et des transferts de matière dans les bassins de l'Amazone, de~~  
1196 ~~l'Orénoque et du Congo. <http://www.ore-hybam.org>. Accessed 10 December 2021~~

1197 Jayakrishnan, P.R., Babu, C.A., 2013. Study of the Oceanic Heat Budget Components over the  
1198 Arabian Sea during the Formation and Evolution of Super Cyclone, Gonu 2013.  
1199 <https://doi.org/10.4236/acs.2013.33030>

1200 Jithin, A.K., Francis, P.A., 2020. Role of internal tide mixing in keeping the deep Andaman Sea  
1201 warmer than the Bay of Bengal. *Sci. Rep.* 10, 11982. [https://doi.org/10.1038/s41598-](https://doi.org/10.1038/s41598-020-68708-6)  
1202 [020-68708-6](https://doi.org/10.1038/s41598-020-68708-6)

1203 Johns, W.E., Lee, T.N., Beardsley, R.C., Candela, J., Limeburner, R., Castro, B., 1998. Annual  
1204 Cycle and Variability of the North Brazil Current. *J. Phys. Oceanogr.* 28, 103–128.  
1205 [https://doi.org/10.1175/1520-0485\(1998\)028<0103:ACAVOT>2.0.CO;2](https://doi.org/10.1175/1520-0485(1998)028<0103:ACAVOT>2.0.CO;2)

1206 Jouanno, J., Marin, F., du Penhoat, Y., Sheinbaum, J., Molines, J.-M., 2011. Seasonal heat  
1207 balance in the upper 100 m of the equatorial Atlantic Ocean. *J. Geophys. Res. Oceans*  
1208 116. <https://doi.org/10.1029/2010JC006912>

1209 Kara, A.B., Rochford, P.A., Hurlburt, H.E., 2003. Mixed layer depth variability over the global  
1210 ocean. *J. Geophys. Res. Oceans* 108. <https://doi.org/10.1029/2000JC000736>

1211 Kelly, S.M., Nash, J.D., Kunze, E., 2010. Internal tide energy over topography. *J. Geophys.*  
1212 *Res. Oceans* 115. <https://doi.org/10.1029/2009JC005618>

1213 Koch-Larrouy, A., Madec, G., Bouruet-Aubertot, P., Gerkema, T., Bessières, L., Molcard, R.,  
1214 2007. On the transformation of Pacific Water into Indonesian Throughflow Water by  
1215 internal tidal mixing. *Geophys. Res. Lett.* 34. <https://doi.org/10.1029/2006GL028405>

1216 Koch-Larrouy, A., Madec, G., Iudicone, D., Atmadipoera, A., Molcard, R., 2008. Physical  
1217 processes contributing to the water mass transformation of the Indonesian Throughflow.  
1218 *Ocean Dyn.* 58, 275–288. <https://doi.org/10.1007/s10236-008-0154-5>

1219 Koch-Larrouy, A., Lengaigne, M., Terray, P., Madec, G., Masson, S., 2010. Tidal mixing in the  
1220 Indonesian Seas and its effect on the tropical climate system. *Clim. Dyn.* 34, 891–904.  
1221 <https://doi.org/10.1007/s00382-009-0642-4>

1222 Koch-Larrouy, A., Atmadipoera, A., van Beek, P., Madec, G., Auean, J., Lyard, F., Grelet, J.,  
1223 Souhaut, M., 2015. Estimates of tidal mixing in the Indonesian archipelago from  
1224 multidisciplinary INDOMIX in situ data. *Deep Sea Res. Part Oceanogr. Res. Pap.* 106,  
1225 136–153. <https://doi.org/10.1016/j.dsr.2015.09.007>

1226 Kostianoy, A.G., Ginzburg, A.I., Frankignoulle, M., Delille, B., 2004. Fronts in the Southern  
1227 Indian Ocean as inferred from satellite sea surface temperature data. *J. Mar. Syst.* 45,  
1228 55–73. <https://doi.org/10.1016/j.jmarsys.2003.09.004>

1229 Kosuth, P., Callède, J., Laraque, A., Filizola, N., Guyot, J.L., Seyler, P., Fritsch, J.M.,  
1230 Guimaraes, V., 2009. Sea tide effects on flows in the lower reaches of the Amazon  
1231 River. *Hydrol. Process.* 23, 3141–3150. <https://doi.org/10.1002/hyp.7387>

1232 ~~Kunze, E., MacKay, C., McPhee-Shaw, E.E., Morrice, K., Girton, J.B., Terker, S.R., 2012.~~  
1233 ~~Turbulent Mixing and Exchange with Interior Waters on Sloping Boundaries. *J. Phys.*~~  
1234 ~~*Oceanogr.* 42, 910–927. <https://doi.org/10.1175/JPO-D-11-075.1>~~

1235 ~~Lambeck, K., Runcorn, S.K., 1977. Tidal dissipation in the oceans: astronomical, geophysical~~  
1236 ~~and oceanographic consequences. *Philos. Trans. R. Soc. Lond. Ser. Math. Phys. Sci.*~~  
1237 ~~287, 545–594. <https://doi.org/10.1098/rsta.1977.0159>~~

1238 ~~Lascaratos, A., 1993. Estimation of deep and intermediate water mass formation rates in the~~  
1239 ~~Mediterranean Sea. *Deep Sea Res. Part II Top. Stud. Oceanogr.* 40, 1327–1332.~~  
1240 ~~[https://doi.org/10.1016/0967-0645\(93\)90072-U](https://doi.org/10.1016/0967-0645(93)90072-U)~~

1241 ~~Laurent, L.S., Garrett, C., 2002. The Role of Internal Tides in Mixing the Deep Ocean. *J. Phys.*~~  
1242 ~~*Oceanogr.* 32, 2882–2899. [https://doi.org/10.1175/1520-](https://doi.org/10.1175/1520-0485(2002)032<2882:TROIT>2.0.CO;2)~~  
1243 ~~[0485\(2002\)032<2882:TROIT>2.0.CO;2](https://doi.org/10.1175/1520-0485(2002)032<2882:TROIT>2.0.CO;2)~~

1244 ~~Leclair, M., Madec, G., 2009. A conservative leapfrog time stepping method. *Ocean Model.*~~  
1245 ~~30, 88–94. <https://doi.org/10.1016/j.ocemod.2009.06.006>~~

1246 ~~Lellouche, J. M., Greiner, E., Le Galloudec, O., Garric, G., Regnier, C., Drevillon, M.,~~  
1247 ~~Benkiran, M., Testut, C. E., Bourdalle-Badie, R., Gasparin, F., Hernandez, O., Levier,~~  
1248 ~~B., Drillet, Y., Remy, E., Le Traon, P. Y., 2018. Recent updates to the Copernicus~~  
1249 ~~Marine Service global ocean monitoring and forecasting real-time 1/42° high-resolution~~  
1250 ~~system. *Ocean Sci.* 14, 1093–1126. <https://doi.org/10.5194/os-14-1093-2018>~~

1251 ~~Lentini, C.A.D., Magalhães, J.M., da Silva, J.C.B., Lorenzetti, J.A., 2016. Transcritical Flow~~  
1252 ~~and Generation of Internal Solitary Waves off the Amazon River: Synthetic Aperture~~  
1253 ~~Radar Observations and Interpretation. *Oceanography* 29, 187–195.~~

1254 ~~Lentz, S.J., Limeburner, R., 1995. The Amazon River Plume during AMASSEDS: Spatial~~  
1255 ~~characteristics and salinity variability. *J. Geophys. Res. Oceans* 100, 2355–2375.~~  
1256 ~~<https://doi.org/10.1029/94JC01411>~~

1257 ~~Li, C., Zhou, W., Jia, X., Wang, X., 2006. Decadal/interdecadal variations of the ocean~~  
1258 ~~temperature and its impacts on climate. *Adv. Atmospheric Sci.* 23, 964–981.~~  
1259 ~~<https://doi.org/10.1007/s00376-006-0964-7>~~

1260 ~~Li, Y., Curchitser, E.N., Wang, J., Peng, S., 2020. Tidal Effects on the Surface Water Cooling~~  
1261 ~~Northeast of Hainan Island, South China Sea. *J. Geophys. Res. Oceans* 125,~~  
1262 ~~[e2019JC016016. <https://doi.org/10.1029/2019JC016016>](https://doi.org/10.1029/2019JC016016)~~

1263 ~~Lyard, F.H., Allain, D.J., Cancet, M., Carrère, L., Picot, N., 2021. FES2014 global ocean tide~~  
1264 ~~atlas: design and performance. *Ocean Sci.* 17, 615–649. [https://doi.org/10.5194/os-17-](https://doi.org/10.5194/os-17-615-2021)~~  
1265 ~~[615-2021](https://doi.org/10.5194/os-17-615-2021)~~

1266 ~~Madec, G., Bourdalle-Badie, R., Chanut, J., Clementi, E., Coward, A., Ethé, C., Iovino, D., Lea,~~  
1267 ~~D., Lévy, C., Lovato, T., Martin, N., Masson, S., Mocavero, S., Rousset, C., Storkey,~~  
1268 ~~D., Vancoppenolle, M., Müeller, S., Nurser, G., Bell, M., & Samson, G., (2019). NEMO~~  
1269 ~~ocean engine. In *Notes du Pôle de modélisation de l'Institut Pierre Simon Laplace*~~  
1270 ~~(IPSL) (v4.0, Number 27). Zenodo. <https://doi.org/10.5281/zenodo.3878122>~~

- 1271 [Magalhaes, J.M., da Silva, J.C.B., Buijsman, M.C., Garcia, C. a. E., 2016. Effect of the North](#)  
1272 [Equatorial Counter Current on the generation and propagation of internal solitary waves](#)  
1273 [off the Amazon shelf \(SAR observations\). Ocean Sci. 12, 243–255.](#)  
1274 <https://doi.org/10.5194/os-12-243-2016>
- 1275 [Mei, W., Xie, S. P., Primeau, F., McWilliams, J.C., Pasquero, C., 2015. Northwestern Pacific](#)  
1276 [typhoon intensity controlled by changes in ocean temperatures. Sci. Adv. 1, e1500014.](#)  
1277 <https://doi.org/10.1126/sciadv.1500014>
- 1278 [Moisan, J.R., Niiler, P.P., 1998. The Seasonal Heat Budget of the North Pacific: Net Heat Flux](#)  
1279 [and Heat Storage Rates \(1950–1990\). J. Phys. Oceanogr. 28, 401–421.](#)  
1280 [https://doi.org/10.1175/1520-0485\(1998\)028<0401:TSHBOT>2.0.CO;2](https://doi.org/10.1175/1520-0485(1998)028<0401:TSHBOT>2.0.CO;2)
- 1281 [Muller-Karger, F.E., McClain, C.R., Richardson, P.L., 1988. The dispersal of the Amazon's](#)  
1282 [water. Nature 333, 56–59. https://doi.org/10.1038/333056a0](#)
- 1283 [Munk, W., Wunsch, C., 1998. Abyssal recipes II: energetics of tidal and wind mixing. Deep](#)  
1284 [Sea Res. Part Oceanogr. Res. Pap. 45, 1977–2010. https://doi.org/10.1016/S0967-](#)  
1285 [0637\(98\)00070-3](#)
- 1286 [Nagai, T., Hibiya, T., 2015. Internal tides and associated vertical mixing in the Indonesian](#)  
1287 [Archipelago. J. Geophys. Res. Oceans 120, 3373–3390.](#)  
1288 <https://doi.org/10.1002/2014JC010592>
- 1289 [Nash, J.D., Alford, M.H., Kunze, E., Martini, K., Kelly, S., 2007. Hotspots of deep ocean](#)  
1290 [mixing on the Oregon continental slope. Geophys. Res. Lett. 34.](#)  
1291 <https://doi.org/10.1029/2006GL028170>
- 1292 [Neto, A.V.N., da Silva, A.C., 2014. Seawater temperature changes associated with the North](#)  
1293 [Brazil current dynamics. Ocean Dyn. 64, 13–27. https://doi.org/10.1007/s10236-013-](#)  
1294 [0667-4](#)
- 1295 [New, A.L., Pingree, R.D., 2000. An intercomparison of internal solitary waves in the Bay of](#)  
1296 [Biscay and resulting from Korteweg-de Vries Type theory. Prog. Oceanogr. 45, 1–38.](#)  
1297 [https://doi.org/10.1016/S0079-6611\(99\)00049-X](https://doi.org/10.1016/S0079-6611(99)00049-X)
- 1298 [New, A.L., Pingree, R.D., 1990. Large amplitude internal soliton packets in the central Bay of](#)  
1299 [Biscay. Deep Sea Res. Part Oceanogr. Res. Pap. 37, 513–524.](#)  
1300 [https://doi.org/10.1016/0198-0149\(90\)90022-N](https://doi.org/10.1016/0198-0149(90)90022-N)
- 1301 [Niwa, Y., Hibiya, T., 2011. Estimation of baroclinic tide energy available for deep ocean mixing](#)  
1302 [based on three dimensional global numerical simulations. J. Oceanogr. 67, 493–502.](#)  
1303 <https://doi.org/10.1007/s10872-011-0052-1>
- 1304 [Nugroho, D., Koch-Larrouy, A., Gaspar, P., Lyard, F., Reffray, G., Tranchant, B., 2018.](#)  
1305 [Modelling explicit tides in the Indonesian seas: An important process for surface sea](#)  
1306 [water properties. Mar. Pollut. Bull., Special Issue: Indonesia seas management 131, 7–](#)  
1307 [18. https://doi.org/10.1016/j.marpolbul.2017.06.033](#)



- 1308 Peng, S., Liao, J., Wang, X., Liu, Z., Liu, Y., Zhu, Y., Li, B., Khokiattiwong, S., Yu, W., 2021.  
 1309 Energetics Based Estimation of the Diapycnal Mixing Induced by Internal Tides in the  
 1310 Andaman Sea. *J. Geophys. Res. Oceans* 126. <https://doi.org/10.1029/2020JC016521>
- 1311 Prestes, Y.O., Silva, A.C. da, Jeandel, C., 2018. Amazon water lenses and the influence of the  
 1312 North Brazil Current on the continental shelf. *Cont. Shelf Res.* 160, 36–48.  
 1313 <https://doi.org/10.1016/j.csr.2018.04.002>
- 1314 Purwandana, A., Cuyppers, Y., Bourgault, D., Bouruet-Aubertot, P., Santoso, P.D., 2022. Fate  
 1315 of internal solitary wave and enhanced mixing in Manado Bay, North Sulawesi,  
 1316 Indonesia. *Cont. Shelf Res.* 245, 104801. <https://doi.org/10.1016/j.csr.2022.104801>
- 1317 Richardson, P.L., Hufford, G.E., Limeburner, R., Brown, W.S., 1994. North Brazil Current  
 1318 retroreflection eddies. *J. Geophys. Res. Oceans* 99, 5081–5093.  
 1319 <https://doi.org/10.1029/93JC03486>
- 1320 Rosenthal, Y., Boyle, E.A., Slowey, N., 1997. Temperature control on the incorporation of  
 1321 magnesium, strontium, fluorine, and cadmium into benthic foraminiferal shells from  
 1322 Little Bahama Bank: Prospects for thermocline paleoceanography. *Geochim.  
 1323 Cosmochim. Acta* 61, 3633–3643. [https://doi.org/10.1016/S0016-7037\(97\)00181-6](https://doi.org/10.1016/S0016-7037(97)00181-6)
- 1324 Ruault, V., Jouanno, J., Durand, F., Chanut, J., Benshila, R., 2020. Role of the Tide on the  
 1325 Structure of the Amazon Plume: A Numerical Modeling Approach. *J. Geophys. Res.  
 1326 Oceans* 125, e2019JC015495. <https://doi.org/10.1029/2019JC015495>
- 1327 Salamena, G.G., Whinney, J.C., Heron, S.F., Ridd, P.V., 2021. Internal tidal waves and deep-  
 1328 water renewal in a tropical fjord: Lessons from Ambon Bay, eastern Indonesia. *Estuar.  
 1329 Coast. Shelf Sci.* 253, 107291. <https://doi.org/10.1016/j.eess.2021.107291>
- 1330 Sandstrom, H., Oakey, N.S., 1995. Dissipation in Internal Tides and Solitary Waves. *J. Phys.  
 1331 Oceanogr.* 25, 604–614. [https://doi.org/10.1175/1520-0485\(1995\)025<0604:DIITAS>2.0.CO;2](https://doi.org/10.1175/1520-0485(1995)025<0604:DIITAS>2.0.CO;2)
- 1333 Schott, F.A., Dengler, M., Brandt, P., Affler, K., Fischer, J., Bourlès, B., Gouriou, Y., Molinari,  
 1334 R.L., Rhein, M., 2003. The zonal currents and transports at 35°W in the tropical  
 1335 Atlantic. *Geophys. Res. Lett.* 30. <https://doi.org/10.1029/2002GL016849>
- 1336 Sharples, J., Moore, C.M., Hickman, A.E., Holligan, P.M., Tweddle, J.F., Palmer, M.R.,  
 1337 Simpson, J.H., 2009. Internal tidal mixing as a control on continental margin  
 1338 ecosystems. *Geophys. Res. Lett.* 36. <https://doi.org/10.1029/2009GL040683>
- 1339 Sharples, J., Tweddle, J.F., Green, J.A.M., Palmer, M.R., Kim, Y. N., Hickman, A.E., Holligan,  
 1340 P.M., Moore, C.M., Rippeth, T.P., Simpson, J.H., Krivtsov, V., 2007. Spring neap  
 1341 modulation of internal tide mixing and vertical nitrate fluxes at a shelf edge in summer.  
 1342 *Limnol. Oceanogr.* 52, 1735–1747. <https://doi.org/10.4319/lo.2007.52.5.1735>
- 1343 Silva, A., Araujo, M., Medeiros, C., Silva, M., Bourlès, B., 2005. Seasonal changes in the mixed  
 1344 and barrier layers in the western Equatorial Atlantic. *Braz. J. Oceanogr.* 53, 83–98.

1345 [Smith, K.A., Rocheleau, G., Merrifield, M.A., Jaramillo, S., Pawlak, G., 2016. Temperature](#)  
1346 [variability caused by internal tides in the coral reef ecosystem of Hanauma bay, Hawai'i.](#)  
1347 [Cont. Shelf Res. 116, 1–12. <https://doi.org/10.1016/j.csr.2016.01.004>](#)

1348 [Speer, K.G., Isemer, H. J., Biastoch, A., 1995. Water mass formation from revised COADS](#)  
1349 [data. J. Phys. Oceanogr. 25, 2444–2457.](#)

1350 [Sprintall, J., Gordon, A.L., Koch-Larrouy, A., Lee, T., Potemra, J.T., Pujiana, K., Wijffels, S.E.,](#)  
1351 [2014. The Indonesian seas and their role in the coupled ocean-climate system. Nat.](#)  
1352 [Geosci. 7, 487–492. <https://doi.org/10.1038/ngeo2188>](#)

1353 [Sprintall, J., Gordon, A.L., Wijffels, S.E., Feng, M., Hu, S., Koch-Larrouy, A., Phillips, H.,](#)  
1354 [Nugroho, D., Napitu, A., Pujiana, K., Susanto, R.D., Sloyan, B., Peña-Molino, B., Yuan,](#)  
1355 [D., Riama, N.F., Siswanto, S., Kuswardani, A., Arifin, Z., Wahyudi, A.J., Zhou, H.,](#)  
1356 [Nagai, T., Ansong, J.K., Bourdalle-Badié, R., Chanut, J., Lyard, F., Arbie, B.K.,](#)  
1357 [Ramdhani, A., Setiawan, A., 2019. Detecting Change in the Indonesian Seas. Front.](#)  
1358 [Mar. Sci. 6.](#)

1359 [Swift, J.H., Aagaard, K., 1981. Seasonal transitions and water mass formation in the Iceland](#)  
1360 [and Greenland seas. Deep-Sea Res. Part Oceanogr. Res. Pap. 28, 1107–1129.](#)  
1361 [https://doi.org/10.1016/0198-0149\(81\)90050-9](#)

1362 [Tehilibou, M., Gourdeau, L., Lyard, F., Morrow, R., Koch-Larrouy, A., Allain, D., Djath, B.,](#)  
1363 [2020. Internal tides in the Solomon Sea in contrasted ENSO conditions. Ocean Sci. 16,](#)  
1364 [615–635. <https://doi.org/10.5194/os-16-615-2020>](#)

1365 [Tehilibou, M., Gourdeau, L., Morrow, R., Serazin, G., Djath, B., Lyard, F., 2018. Spectral](#)  
1366 [signatures of the tropical Pacific dynamics from model and altimetry: a focus on the](#)  
1367 [meso-/submesoscale range. Ocean Sci. 14, 1283–1301. \[https://doi.org/10.5194/os-14-\]\(https://doi.org/10.5194/os-14-1283-2018\)](#)  
1368 [1283-2018](#)

1369 [Tehilibou, M., Koch-Larrouy, A., Barbot, S., Lyard, F., Morel, Y., Jouanno, J., Morrow, R.,](#)  
1370 [2022. Internal tides off the Amazon shelf during two contrasted seasons: interactions](#)  
1371 [with background circulation and SSH imprints. Ocean Sci. 18, 1591–1618.](#)  
1372 [https://doi.org/10.5194/os-18-1591-2022](#)

1373 [Varona, H.L., Veleda, D., Silva, M., Cintra, M., Araujo, M., 2019. Amazon River plume](#)  
1374 [influence on Western Tropical Atlantic dynamic variability. Dyn. Atmospheres Oceans](#)  
1375 [85, 1–15. <https://doi.org/10.1016/j.dynatmoe.2018.10.002>](#)

1376 [Vic, C., Naveira-Garabato, A.C., Green, J.A.M., Waterhouse, A.F., Zhao, Z., Melet, A., de](#)  
1377 [Lavergne, C., Buijsman, M.C., Stephenson, G.R., 2019. Deep-ocean mixing driven by](#)  
1378 [small-scale internal tides. Nat. Commun. 10, 2099. \[https://doi.org/10.1038/s41467-019-\]\(https://doi.org/10.1038/s41467-019-10149-5\)](#)  
1379 [10149-5](#)

1380 [Vlasenko, V., Stashchuk, N., 2006. Amplification and Suppression of Internal Waves by Tides](#)  
1381 [over Variable Bottom Topography. J. Phys. Oceanogr. 36, 1959–1973.](#)  
1382 [https://doi.org/10.1175/JPO2958.1](#)

1383 [Wallace, M.I., Meredith, M.P., Brandon, M.A., Sherwin, T.J., Dale, A., Clarke, A., 2008. On](#)  
1384 [the characteristics of internal tides and coastal upwelling behaviour in Marguerite Bay,](#)

1385 [west Antarctic Peninsula. Deep Sea Res. Part II Top. Stud. Oceanogr. 55, 2023–2040.](https://doi.org/10.1016/j.dsr2.2008.04.033)  
1386 <https://doi.org/10.1016/j.dsr2.2008.04.033>

1387 [Wang, X., Peng, S., Liu, Z., Huang, R.X., Qian, Y. K., Li, Y., 2016. Tidal Mixing in the South  
1388 China Sea: An Estimate Based on the Internal Tide Energetics. J. Phys. Oceanogr. 46,  
1389 107–124. <https://doi.org/10.1175/JPO-D-15-0082.1>](https://doi.org/10.1175/JPO-D-15-0082.1)

1390 [Wentz, F.J., C. Gentemann, K.A. Hilburn, 2015: Remote Sensing Systems TRMM TMI \[Daily\]  
1391 Environmental Suite on 0.25 deg grid, Version 7.1. Remote Sensing Systems, Santa  
1392 Rosa, CA. Available online at \[www.remss.com/missions/tmi\]\(http://www.remss.com/missions/tmi\).](http://www.remss.com/missions/tmi)

1393 [Whalen, C.B., de Lavergne, C., Naveira Garabato, A.C., Klymak, J.M., MacKinnon, J.A.,  
1394 Sheen, K.L., 2020. Internal wave driven mixing: governing processes and consequences  
1395 for climate. Nat. Rev. Earth Environ. 1, 606–621. \[https://doi.org/10.1038/s43017-020-  
1396 0097-z\]\(https://doi.org/10.1038/s43017-020-<br/>
1396 0097-z\)](https://doi.org/10.1038/s43017-020-0097-z)

1397 [Xie, S.-P., Carton, J.A., 2004. Tropical Atlantic variability: Patterns, mechanisms, and impacts.  
1398 Wash. DC Am. Geophys. Union Geophys. Monogr. Ser. 147, 121–142.  
1399 <https://doi.org/10.1029/147GM07>](https://doi.org/10.1029/147GM07)

1400 [Xu, P., Yang, W., Zhu, B., Wei, H., Zhao, L., Nie, H., 2020. Turbulent mixing and vertical  
1401 nitrate flux induced by the semidiurnal internal tides in the southern Yellow Sea. Cont.  
1402 Shelf Res. 208, 104240. <https://doi.org/10.1016/j.csr.2020.104240>](https://doi.org/10.1016/j.csr.2020.104240)

1403 [Yadidya, B., Rao, A.D., 2022. Projected climate variability of internal waves in the Andaman  
1404 Sea. Commun. Earth Environ. 3, 1–12. <https://doi.org/10.1038/s43247-022-00574-8>](https://doi.org/10.1038/s43247-022-00574-8)

1405 [Zalesak, S.T., 1979. Fully multidimensional flux corrected transport algorithms for fluids. J.  
1406 Comput. Phys. 31, 335–362. \[https://doi.org/10.1016/0021-9991\\(79\\)90051-2\]\(https://doi.org/10.1016/0021-9991\(79\)90051-2\)](https://doi.org/10.1016/0021-9991(79)90051-2)

1407 [Zaron, E.D., 2017. Mapping the nonstationary internal tide with satellite altimetry. J. Geophys.  
1408 Res. Oceans 122, 539–554. <https://doi.org/10.1002/2016JC012487>](https://doi.org/10.1002/2016JC012487)

1409 [Zaron, E.D., 2019. Baroclinic Tidal Sea Level from Exact Repeat Mission Altimetry. J. Phys.  
1410 Oceanogr. 49, 193–210. <https://doi.org/10.1175/JPO-D-18-0127.1>](https://doi.org/10.1175/JPO-D-18-0127.1)

1411 [Aguedjou, H.M.A., Chaigneau, A., Dadou, I., Morel, Y., Pegliasco, C., Da-Allada, C.Y., Baloitcha, E.,  
1412 2021. What Can We Learn From Observed Temperature and Salinity Isopycnal  
1413 Anomalies at Eddy Generation Sites? Application in the Tropical Atlantic Ocean. J.  
1414 Geophys. Res. Oceans 126, e2021JC017630. <https://doi.org/10.1029/2021JC017630>](https://doi.org/10.1029/2021JC017630)

1415 [Aguedjou, H.M.A., Dadou, I., Chaigneau, A., Morel, Y., Alory, G., 2019. Eddies in the Tropical  
1416 Atlantic Ocean and Their Seasonal Variability. Geophys. Res. Lett. 46, 12156–12164.  
1417 <https://doi.org/10.1029/2019GL083925>](https://doi.org/10.1029/2019GL083925)

1418 [Archer, D., Martin, P., Buffett, B., Brovkin, V., Rahmstorf, S., Ganopolski, A., 2004. The  
1419 importance of ocean temperature to global biogeochemistry. Earth Planet. Sci. Lett. 222,  
1420 333–348. <https://doi.org/10.1016/j.epsl.2004.03.011>](https://doi.org/10.1016/j.epsl.2004.03.011)

1421 [Baines, P.G., 1982. On internal tide generation models. Deep Sea Res. Part Oceanogr. Res. Pap.  
1422 29, 307–338. \[https://doi.org/10.1016/0198-0149\\(82\\)90098-X\]\(https://doi.org/10.1016/0198-0149\(82\)90098-X\)](https://doi.org/10.1016/0198-0149(82)90098-X)

1423 [Barbot, S., Lyard, F., Tchilibou, M., Carrere, L., 2021. Background stratification impacts on  
1424 internal tide generation and abyssal propagation in the western equatorial Atlantic and  
1425 the Bay of Biscay. Ocean Sci. 17, 1563–1583. <https://doi.org/10.5194/os-17-1563-2021>](https://doi.org/10.5194/os-17-1563-2021)

1426 [Barton, E.D., Inall, M.E., Sherwin, T.J., Torres, R., 2001. Vertical structure, turbulent mixing  
1427 and fluxes during Lagrangian observations of an upwelling filament system off](https://doi.org/10.1016/j.jo.2001.03.001)

1428 [Northwest Iberia. Prog. Oceanogr., Lagrangian studies of the Iberian upwelling system](#)  
1429 [51, 249–267. https://doi.org/10.1016/S0079-6611\(01\)00069-6](#)  
1430 [Beardsley, R.C., Candela, J., Limeburner, R., Geyer, W.R., Lentz, S.J., Castro, B.M.,](#)  
1431 [Cacchione, D., Carneiro, N., 1995. The M2 tide on the Amazon Shelf. \*J. Geophys. Res.\*](#)  
1432 [Oceans 100, 2283–2319. https://doi.org/10.1029/94JC01688](#)  
1433 [Bessières, L., 2007. Impact des marées sur la circulation générale océanique dans une](#)  
1434 [perspective climatique \(phdthesis\). Université Paul Sabatier - Toulouse III.](#)  
1435 [Bessières, L., Madec, G., Lyard, F., 2008. Global tidal residual mean circulation: Does it affect](#)  
1436 [a climate OGCM? \*Geophys. Res. Lett.\* 35. https://doi.org/10.1029/2007GL032644](#)  
1437 [Bourlès, B., Araujo, M., McPhaden, M.J., Brandt, P., Foltz, G.R., Lumpkin, R., Giordani, H.,](#)  
1438 [Hernandez, F., Lefèvre, N., Nobre, P., Campos, E., Saravanan, R., Trotte-Duhà, J.,](#)  
1439 [Dengler, M., Hahn, J., Hummels, R., Lübbecke, J.F., Rouault, M., Cotrim, L., Sutton,](#)  
1440 [A., Jochum, M., Perez, R.C., 2019. PIRATA: A Sustained Observing System for](#)  
1441 [Tropical Atlantic Climate Research and Forecasting. \*Earth Space Sci.\* 6, 577–616.](#)  
1442 [https://doi.org/10.1029/2018EA000428](#)  
1443 [Bourles, B., Molinari, R.L., Johns, E., Wilson, W.D., Leaman, K.D., 1999. Upper layer currents](#)  
1444 [in the western tropical North Atlantic \(1989–1991\). \*J. Geophys. Res. Oceans\* 104, 1361–](#)  
1445 [1375. https://doi.org/10.1029/1998JC900025](#)  
1446 [Buijsman, M.C., Arbic, B.K., Richman, J.G., Shriver, J.F., Wallcraft, A.J., Zamudio, L., 2017.](#)  
1447 [Semidiurnal internal tide incoherence in the equatorial Pacific. \*J. Geophys. Res. Oceans\*](#)  
1448 [122, 5286–5305. https://doi.org/10.1002/2016JC012590](#)  
1449 [C., Le Provost, Florent, Lyard, 1997. Energetics of the M2 barotropic ocean tides: an estimate](#)  
1450 [of bottom friction dissipation from a hydrodynamic model - ScienceDirect. \*Prog.\*](#)  
1451 [Oceano. 37–52.](#)  
1452 [Chapman, C.C., Lea, M.-A., Meyer, A., Sallée, J.-B., Hindell, M., 2020. Defining Southern](#)  
1453 [Ocean fronts and their influence on biological and physical processes in a changing](#)  
1454 [climate. \*Nat. Clim. Change\* 10, 209–219. https://doi.org/10.1038/s41558-020-0705-4](#)  
1455 [Clayson, C.A., Bogdanoff, A.S., 2013. The Effect of Diurnal Sea Surface Temperature](#)  
1456 [Warming on Climatological Air–Sea Fluxes. \*Am. Meteorol. Soc.\*](#)  
1457 [Collins, M., An, S.-I., Cai, W., Ganachaud, A., Guilyardi, E., Jin, F.-F., Jochum, M., Lengaigne,](#)  
1458 [M., Power, S., Timmermann, A., Vecchi, G., Wittenberg, A., 2010. The impact of global](#)  
1459 [warming on the tropical Pacific Ocean and El Niño. \*Nat. Geosci.\* 3, 391–397.](#)  
1460 [https://doi.org/10.1038/ngeo868](#)  
1461 [de Lavergne, C., Vic, C., Madec, G., Roquet, F., Waterhouse, A.F., Whalen, C.B., Cuypers, Y.,](#)  
1462 [Bouruet-Aubertot, P., Ferron, B., Hibiya, T., 2020. A Parameterization of Local and](#)  
1463 [Remote Tidal Mixing. \*J. Adv. Model. Earth Syst.\* 12, e2020MS002065.](#)  
1464 [https://doi.org/10.1029/2020MS002065](#)  
1465 [de Macedo, C.R., Koch-Larrouy, A., da Silva, J.C.B., Magalhães, J.M., Lentini, C.A.D., Tran,](#)  
1466 [T.K., Rosa, M.C.B., Vantrepotte, V., 2023. Spatial and temporal variability of mode-1](#)  
1467 [and mode-2 internal solitary waves from MODIS/TERRA sunglint off the Amazon shelf](#)  
1468 [\(preprint\). \*Remote Sensing/Internal waves/Surface/Deep Seas: Equatorial Ocean/Other.\*](#)  
1469 [https://doi.org/10.5194/egusphere-2022-1482](#)  
1470 [Didden, N., Schott, F., 1993. Eddies in the North Brazil Current retroflection region observed](#)  
1471 [by Geosat altimetry. \*J. Geophys. Res. Oceans\* 98, 20121–20131.](#)  
1472 [https://doi.org/10.1029/93JC01184](#)  
1473 [Dong, S., Sprintall, J., Gille, S.T., Talley, L., 2008. Southern Ocean mixed-layer depth from](#)  
1474 [Argo float profiles. \*J. Geophys. Res. Oceans\* 113.](#)  
1475 [https://doi.org/10.1029/2006JC004051](#)

1476 [Dunphy, M., Lamb, K.G., 2014. Focusing and vertical mode scattering of the first mode internal](#)  
1477 [tide by mesoscale eddy interaction. J. Geophys. Res. Oceans 119, 523–536.](#)  
1478 <https://doi.org/10.1002/2013JC009293>

1479 [Egbert, G.D., Ray, R.D., 2000. Significant dissipation of tidal energy in the deep ocean inferred](#)  
1480 [from satellite altimeter data. Nature 405, 775–778. https://doi.org/10.1038/35015531](#)

1481 [Fassoni-Andrade, A.C., Durand, F., Azevedo, A., Bertin, X., Santos, L.G., Khan, J.U., Testut,](#)  
1482 [L., Moreira, D.M., 2023. Seasonal to interannual variability of the tide in the Amazon](#)  
1483 [estuary. Cont. Shelf Res. 255, 104945. https://doi.org/10.1016/j.csr.2023.104945](#)

1484 [Fontes, R.F.C., Castro, B.M., Beardsley, R.C., 2008. Numerical study of circulation on the inner](#)  
1485 [Amazon Shelf. Ocean Dyn. 58, 187–198. https://doi.org/10.1007/s10236-008-0139-4](#)

1486 [Gabioux, M., Vinzon, S.B., Paiva, A.M., 2005. Tidal propagation over fluid mud layers on the](#)  
1487 [Amazon shelf. Cont. Shelf Res. 25, 113–125. https://doi.org/10.1016/j.csr.2004.09.001](#)

1488 [Garzoli, S.L., Ffield, A., Yao, Q., 2003. North Brazil Current rings and the variability in the](#)  
1489 [latitude of retroflection, in: Goni, G.J., Malanotte-Rizzoli, P. \(Eds.\), Elsevier](#)  
1490 [Oceanography Series, Interhemispheric Water Exchange in the Atlantic Ocean.](#)  
1491 [Elsevier, pp. 357–373. https://doi.org/10.1016/S0422-9894\(03\)80154-X](#)

1492 [Gévaudan, M., Durand, F., Jouanno, J., 2022. Influence of the Amazon-Orinoco Discharge](#)  
1493 [Interannual Variability on the Western Tropical Atlantic Salinity and Temperature. J.](#)  
1494 [Geophys. Res. Oceans 127, e2022JC018495. https://doi.org/10.1029/2022JC018495](#)

1495 [Hernandez, O., Jouanno, J., Durand, F., 2016. Do the Amazon and Orinoco freshwater plumes](#)  
1496 [really matter for hurricane-induced ocean surface cooling? J. Geophys. Res. Oceans](#)  
1497 [121, 2119–2141. https://doi.org/10.1002/2015JC011021](#)

1498 [Hernandez, O., Jouanno, J., Echevin, V., Aumont, O., 2017. Modification of sea surface](#)  
1499 [temperature by chlorophyll concentration in the Atlantic upwelling systems. J. Geophys.](#)  
1500 [Res. Oceans 122, 5367–5389. https://doi.org/10.1002/2016JC012330](#)

1501 [Hersbach, H., Bell, B., Berrisford, P., Hirahara, S., Horányi, A., Muñoz-Sabater, J., Nicolas, J.,](#)  
1502 [Peubey, C., Radu, R., Schepers, D., Simmons, A., Soci, C., Abdalla, S., Abellan, X.,](#)  
1503 [Balsamo, G., Bechtold, P., Biavati, G., Bidlot, J., Bonavita, M., De Chiara, G.,](#)  
1504 [Dahlgren, P., Dee, D., Diamantakis, M., Dragani, R., Flemming, J., Forbes, R., Fuentes,](#)  
1505 [M., Geer, A., Haimberger, L., Healy, S., Hogan, R.J., Hólm, E., Janisková, M., Keeley,](#)  
1506 [S., Laloyaux, P., Lopez, P., Lupu, C., Radnoti, G., de Rosnay, P., Rozum, I., Vamborg,](#)  
1507 [F., Villaume, S., Thépaut, J.-N., 2020. The ERA5 global reanalysis. Q. J. R. Meteorol.](#)  
1508 [Soc. 146, 1999–2049. https://doi.org/10.1002/qj.3803](#)

1509 [Jayakrishnan, P.R., Babu, C.A., 2013. Study of the Oceanic Heat Budget Components over the](#)  
1510 [Arabian Sea during the Formation and Evolution of Super Cyclone, Gonu 2013.](#)  
1511 <https://doi.org/10.4236/acs.2013.33030>

1512 [Jithin, A.K., Francis, P.A., 2020. Role of internal tide mixing in keeping the deep Andaman Sea](#)  
1513 [warmer than the Bay of Bengal. Sci. Rep. 10, 11982. https://doi.org/10.1038/s41598-](#)  
1514 [020-68708-6](#)

1515 [Johns, W.E., Lee, T.N., Beardsley, R.C., Candela, J., Limeburner, R., Castro, B., 1998. Annual](#)  
1516 [Cycle and Variability of the North Brazil Current. J. Phys. Oceanogr. 28, 103–128.](#)  
1517 [https://doi.org/10.1175/1520-0485\(1998\)028<0103:ACAVOT>2.0.CO;2](https://doi.org/10.1175/1520-0485(1998)028<0103:ACAVOT>2.0.CO;2)

1518 [Johns, W.E., Lee, T.N., Schott, F.A., Zantopp, R.J., Evans, R.H., 1990. The North Brazil](#)  
1519 [Current retroflection: Seasonal structure and eddy variability. J. Geophys. Res. Oceans](#)  
1520 [95, 22103–22120. https://doi.org/10.1029/JC095iC12p22103](#)

1521 [Jouanno, J., Marin, F., du Penhoat, Y., Sheinbaum, J., Molines, J.-M., 2011. Seasonal heat](#)  
1522 [balance in the upper 100 m of the equatorial Atlantic Ocean. J. Geophys. Res. Oceans](#)  
1523 [116. https://doi.org/10.1029/2010JC006912](#)

1524 [Kara, A.B., Rochford, P.A., Hurlburt, H.E., 2003. Mixed layer depth variability over the global](#)  
1525 [ocean. J. Geophys. Res. Oceans 108. https://doi.org/10.1029/2000JC000736](#)

1526 [Kelly, S.M., Nash, J.D., Kunze, E., 2010. Internal-tide energy over topography. J. Geophys. Res. Oceans 115. <https://doi.org/10.1029/2009JC005618>](#)

1527

1528 [Koch-Larrouy, A., Atmadipoera, A., van Beek, P., Madec, G., Aucan, J., Lyard, F., Grelet, J., Souhaut, M., 2015. Estimates of tidal mixing in the Indonesian archipelago from multidisciplinary INDOMIX in-situ data. Deep Sea Res. Part Oceanogr. Res. Pap. 106. 136–153. <https://doi.org/10.1016/j.dsr.2015.09.007>](#)

1531

1532 [Koch-Larrouy, A., Lengaigne, M., Terray, P., Madec, G., Masson, S., 2010. Tidal mixing in the Indonesian Seas and its effect on the tropical climate system. Clim. Dyn. 34, 891–904. <https://doi.org/10.1007/s00382-009-0642-4>](#)

1533

1534 [Koch-Larrouy, A., Madec, G., Bouruet-Aubertot, P., Gerkema, T., Bessières, L., Molcard, R., 2007. On the transformation of Pacific Water into Indonesian Throughflow Water by internal tidal mixing. Geophys. Res. Lett. 34. <https://doi.org/10.1029/2006GL028405>](#)

1537

1538 [Koch-Larrouy, A., Madec, G., Iudicone, D., Atmadipoera, A., Molcard, R., 2008. Physical processes contributing to the water mass transformation of the Indonesian Throughflow. Ocean Dyn. 58, 275–288. <https://doi.org/10.1007/s10236-008-0154-5>](#)

1539

1540

1541 [Kosuth, P., Callède, J., Laraque, A., Filizola, N., Guyot, J.L., Seyler, P., Fritsch, J.M., Guimarães, V., 2009. Sea-tide effects on flows in the lower reaches of the Amazon River. Hydrol. Process. 23, 3141–3150. <https://doi.org/10.1002/hyp.7387>](#)

1542

1543

1544 [Kunze, E., MacKay, C., McPhee-Shaw, E.E., Morrice, K., Girton, J.B., Terker, S.R., 2012. Turbulent Mixing and Exchange with Interior Waters on Sloping Boundaries. J. Phys. Oceanogr. 42, 910–927. <https://doi.org/10.1175/JPO-D-11-075.1>](#)

1546

1547 [Lambeck, K., Runcorn, S.K., 1977. Tidal dissipation in the oceans: astronomical, geophysical and oceanographic consequences. Philos. Trans. R. Soc. Lond. Ser. Math. Phys. Sci. 287, 545–594. <https://doi.org/10.1098/rsta.1977.0159>](#)

1548

1549

1550 [Lascaratos, A., 1993. Estimation of deep and intermediate water mass formation rates in the Mediterranean Sea. Deep Sea Res. Part II Top. Stud. Oceanogr. 40, 1327–1332. \[https://doi.org/10.1016/0967-0645\\(93\\)90072-U\]\(https://doi.org/10.1016/0967-0645\(93\)90072-U\)](#)

1551

1552

1553 [Laurent, L.S., Garrett, C., 2002. The Role of Internal Tides in Mixing the Deep Ocean. J. Phys. Oceanogr. 32, 2882–2899. \[https://doi.org/10.1175/1520-0485\\(2002\\)032<2882:TROITI>2.0.CO;2\]\(https://doi.org/10.1175/1520-0485\(2002\)032<2882:TROITI>2.0.CO;2\)](#)

1554

1555

1556 [Leclair, M., Madec, G., 2009. A conservative leapfrog time stepping method. Ocean Model. 30, 88–94. <https://doi.org/10.1016/j.ocemod.2009.06.006>](#)

1557

1558 [Lellouche, J.-M., Greiner, E., Le Galloudec, O., Garric, G., Regnier, C., Drevillon, M., Benkiran, M., Testut, C.-E., Bourdalle-Badie, R., Gasparin, F., Hernandez, O., Levier, B., Drillet, Y., Remy, E., Le Traon, P.-Y., 2018. Recent updates to the Copernicus Marine Service global ocean monitoring and forecasting real-time 1/12° high-resolution system. Ocean Sci. 14, 1093–1126. <https://doi.org/10.5194/os-14-1093-2018>](#)

1561

1562

1563 [Lentini, C.A.D., Magalhães, J.M., da Silva, J.C.B., Lorenzetti, J.A., 2016. Transcritical Flow and Generation of Internal Solitary Waves off the Amazon River: Synthetic Aperture Radar Observations and Interpretation. Oceanography 29, 187–195.](#)

1564

1565

1566 [Lentz, S.J., Limeburner, R., 1995. The Amazon River Plume during AMASSEDS: Spatial characteristics and salinity variability. J. Geophys. Res. Oceans 100, 2355–2375. <https://doi.org/10.1029/94JC01411>](#)

1567

1568

1569 [Li, C., Zhou, W., Jia, X., Wang, X., 2006. Decadal/interdecadal variations of the ocean temperature and its impacts on climate. Adv. Atmospheric Sci. 23, 964–981. <https://doi.org/10.1007/s00376-006-0964-7>](#)

1570

1571

1572 [Li, Y., Curchitser, E.N., Wang, J., Peng, S., 2020. Tidal Effects on the Surface Water Cooling Northeast of Hainan Island, South China Sea. J. Geophys. Res. Oceans 125. e2019JC016016. <https://doi.org/10.1029/2019JC016016>](#)

1573

1574

1575 [Lyard, F.H., Allain, D.J., Cancet, M., Carrère, L., Picot, N., 2021. FES2014 global ocean tide](#)  
1576 [atlas: design and performance. Ocean Sci. 17, 615–649. \[https://doi.org/10.5194/os-17-\]\(https://doi.org/10.5194/os-17-615-2021\)](#)  
1577 [615-2021](#)

1578 [Magalhaes, J.M., da Silva, J.C.B., Buijsman, M.C., Garcia, C. a. E., 2016. Effect of the North](#)  
1579 [Equatorial Counter Current on the generation and propagation of internal solitary waves](#)  
1580 [off the Amazon shelf \(SAR observations\). Ocean Sci. 12, 243–255.](#)  
1581 [https://doi.org/10.5194/os-12-243-2016](#)

1582 [Mei, W., Xie, S.-P., Primeau, F., McWilliams, J.C., Pasquero, C., 2015. Northwestern Pacific](#)  
1583 [typhoon intensity controlled by changes in ocean temperatures. Sci. Adv. 1, e1500014.](#)  
1584 [https://doi.org/10.1126/sciadv.1500014](#)

1585 [Moisan, J.R., Niiler, P.P., 1998. The Seasonal Heat Budget of the North Pacific: Net Heat Flux](#)  
1586 [and Heat Storage Rates \(1950–1990\). J. Phys. Oceanogr. 28, 401–421.](#)  
1587 [https://doi.org/10.1175/1520-0485\(1998\)028<0401:TSHBOT>2.0.CO;2](#)

1588 [Muller-Karger, F.E., McClain, C.R., Richardson, P.L., 1988. The dispersal of the Amazon’s](#)  
1589 [water. Nature 333, 56–59. <https://doi.org/10.1038/333056a0>](#)

1590 [Munk, W., Wunsch, C., 1998. Abyssal recipes II: energetics of tidal and wind mixing. Deep](#)  
1591 [Sea Res. Part Oceanogr. Res. Pap. 45, 1977–2010. \[https://doi.org/10.1016/S0967-\]\(https://doi.org/10.1016/S0967-0637\(98\)00070-3\)](#)  
1592 [0637\(98\)00070-3](#)

1593 [Nagai, T., Hibiya, T., 2015. Internal tides and associated vertical mixing in the Indonesian](#)  
1594 [Archipelago. J. Geophys. Res. Oceans 120, 3373–3390.](#)  
1595 [https://doi.org/10.1002/2014JC010592](#)

1596 [Madec, G., Bourdallé-Badie, R., Chanut, J., Clementi, E., Coward, A., Ethé, C., Iovino, D., Lea,](#)  
1597 [D., Lévy, C., Lovato, T., Martin, N., Masson, S., Mocavero, S., Rousset, C., Storkey,](#)  
1598 [D., Vancoppenolle, M., Müeller, S., Nurser, G., Bell, M., & Samson, G., 2019. NEMO](#)  
1599 [ocean engine. In Notes du Pôle de modélisation de l'Institut Pierre-Simon Laplace](#)  
1600 [\(IPSL\) \(v4.0, Numéro 27\). Zenodo. <https://doi.org/10.5281/zenodo.3878122>](#)

1601 [Neto, A.V.N., da Silva, A.C., 2014. Seawater temperature changes associated with the North](#)  
1602 [Brazil current dynamics. Ocean Dyn. 64, 13–27. \[https://doi.org/10.1007/s10236-013-\]\(https://doi.org/10.1007/s10236-013-0667-4\)](#)  
1603 [0667-4](#)

1604 [Niwa, Y., Hibiya, T., 2011. Estimation of baroclinic tide energy available for deep ocean mixing](#)  
1605 [based on three-dimensional global numerical simulations. J. Oceanogr. 67, 493–502.](#)  
1606 [https://doi.org/10.1007/s10872-011-0052-1](#)

1607 [Nugroho, D., Koch-Larrouy, A., Gaspar, P., Lyard, F., Reffray, G., Tranchant, B., 2018.](#)  
1608 [Modelling explicit tides in the Indonesian seas: An important process for surface sea](#)  
1609 [water properties. Mar. Pollut. Bull., Special Issue: Indonesia seas management 131, 7–](#)  
1610 [18. <https://doi.org/10.1016/j.marpolbul.2017.06.033>](#)

1611 [Peng, S., Liao, J., Wang, X., Liu, Z., Liu, Y., Zhu, Y., Li, B., Khokiattiwong, S., Yu, W., 2021.](#)  
1612 [Energetics Based Estimation of the Diapycnal Mixing Induced by Internal Tides in the](#)  
1613 [Andaman Sea. J. Geophys. Res. Oceans 126. <https://doi.org/10.1029/2020JC016521>](#)

1614 [Prestes, Y.O., Silva, A.C. da, Jeandel, C., 2018. Amazon water lenses and the influence of the](#)  
1615 [North Brazil Current on the continental shelf. Cont. Shelf Res. 160, 36–48.](#)  
1616 [https://doi.org/10.1016/j.csr.2018.04.002](#)

1617 [Richardson, P.L., Hufford, G.E., Limeburner, R., Brown, W.S., 1994. North Brazil Current](#)  
1618 [retroreflection eddies. J. Geophys. Res. Oceans 99, 5081–5093.](#)  
1619 [https://doi.org/10.1029/93JC03486](#)

1620 [Rosenthal, Y., Boyle, E.A., Slowey, N., 1997. Temperature control on the incorporation of](#)  
1621 [magnesium, strontium, fluorine, and cadmium into benthic foraminiferal shells from](#)  
1622 [Little Bahama Bank: Prospects for thermocline paleoceanography. Geochim.](#)  
1623 [Cosmochim. Acta 61, 3633–3643. \[https://doi.org/10.1016/S0016-7037\\(97\\)00181-6\]\(https://doi.org/10.1016/S0016-7037\(97\)00181-6\)](#)

1624 [Ruault, V., Jouanno, J., Durand, F., Chanut, J., Benshila, R., 2020. Role of the Tide on the](#)  
1625 [Structure of the Amazon Plume: A Numerical Modeling Approach. \*J. Geophys. Res.\*](#)  
1626 [Oceans 125, e2019JC015495. <https://doi.org/10.1029/2019JC015495>](#)

1627 [Salamena, G.G., Whinney, J.C., Heron, S.F., Ridd, P.V., 2021. Internal tidal waves and deep-](#)  
1628 [water renewal in a tropical fjord: Lessons from Ambon Bay, eastern Indonesia. \*Estuar.\*](#)  
1629 [Coast. Shelf Sci. 253, 107291. <https://doi.org/10.1016/j.ecss.2021.107291>](#)

1630 [Schott, F.A., Dengler, M., Brandt, P., Affler, K., Fischer, J., Bourlès, B., Gouriou, Y., Molinari,](#)  
1631 [R.L., Rhein, M., 2003. The zonal currents and transports at 35°W in the tropical](#)  
1632 [Atlantic. \*Geophys. Res. Lett.\* 30. <https://doi.org/10.1029/2002GL016849>](#)

1633 [Sharples, J., Moore, C.M., Hickman, A.E., Holligan, P.M., Tweddle, J.F., Palmer, M.R.,](#)  
1634 [Simpson, J.H., 2009. Internal tidal mixing as a control on continental margin](#)  
1635 [ecosystems. \*Geophys. Res. Lett.\* 36. <https://doi.org/10.1029/2009GL040683>](#)

1636 [Sharples, J., Tweddle, J.F., Green, J.A.M., Palmer, M.R., Kim, Y.-N., Hickman, A.E., Holligan,](#)  
1637 [P.M., Moore, C.M., Rippeth, T.P., Simpson, J.H., Krivtsov, V., 2007. Spring-neap](#)  
1638 [modulation of internal tide mixing and vertical nitrate fluxes at a shelf edge in summer.](#)  
1639 [Limnol. Oceanogr. 52, 1735–1747. <https://doi.org/10.4319/lo.2007.52.5.1735>](#)

1640 [Silva, A., Araujo, M., Medeiros, C., Silva, M., Bourles, B., 2005. Seasonal changes in the mixed](#)  
1641 [and barrier layers in the western Equatorial Atlantic. \*Braz. J. Oceanogr.\* 53, 83–98.](#)

1642 [Smith, J.E., Smith, C.M., Vroom, P.S., Beach, K.L., Miller, S., 2004. Nutrient and growth](#)  
1643 [dynamics of Halimeda tuna on Conch Reef, Florida Keys: Possible influence of internal](#)  
1644 [tides on nutrient status and physiology. \*Limnol. Oceanogr.\* 49, 1923–1936.](#)  
1645 [https://doi.org/10.4319/lo.2004.49.6.1923](#)

1646 [Smith, K.A., Rocheleau, G., Merrifield, M.A., Jaramillo, S., Pawlak, G., 2016. Temperature](#)  
1647 [variability caused by internal tides in the coral reef ecosystem of Hanauma bay, Hawai'i.](#)  
1648 [Cont. Shelf Res. 116, 1–12. <https://doi.org/10.1016/j.csr.2016.01.004>](#)

1649 [Speer, K.G., Isemer, H.-J., Biastoch, A., 1995. Water mass formation from revised COADS](#)  
1650 [data. \*J. Phys. Oceanogr.\* 25, 2444–2457.](#)

1651 [Sprintall, J., Gordon, A.L., Koch-Larrouy, A., Lee, T., Potemra, J.T., Pujiana, K., Wijffels, S.E.,](#)  
1652 [2014. The Indonesian seas and their role in the coupled ocean–climate system. \*Nat.\*](#)  
1653 [Geosci. 7, 487–492. <https://doi.org/10.1038/ngeo2188>](#)

1654 [Sprintall, J., Gordon, A.L., Wijffels, S.E., Feng, M., Hu, S., Koch-Larrouy, A., Phillips, H.,](#)  
1655 [Nugroho, D., Napitu, A., Pujiana, K., Susanto, R.D., Sloyan, B., Peña-Molino, B., Yuan,](#)  
1656 [D., Riama, N.F., Siswanto, S., Kuswardani, A., Arifin, Z., Wahyudi, A.J., Zhou, H.,](#)  
1657 [Nagai, T., Ansong, J.K., Bourdalle-Badié, R., Chanut, J., Lyard, F., Arbic, B.K.,](#)  
1658 [Ramdhani, A., Setiawan, A., 2019. Detecting Change in the Indonesian Seas. \*Front.\*](#)  
1659 [Mar. Sci. 6.](#)

1660 [Swift, J.H., Aagaard, K., 1981. Seasonal transitions and water mass formation in the Iceland](#)  
1661 [and Greenland seas. \*Deep Sea Res. Part Oceanogr. Res. Pap.\* 28, 1107–1129.](#)  
1662 [https://doi.org/10.1016/0198-0149\(81\)90050-9](#)

1663 [Tchilibou, M., Gourdeau, L., Lyard, F., Morrow, R., Koch Larrouy, A., Allain, D., Djath, B.,](#)  
1664 [2020. Internal tides in the Solomon Sea in contrasted ENSO conditions. \*Ocean Sci.\* 16,](#)  
1665 [615–635. <https://doi.org/10.5194/os-16-615-2020>](#)

1666 [Tchilibou, M., Gourdeau, L., Morrow, R., Serazin, G., Djath, B., Lyard, F., 2018. Spectral](#)  
1667 [signatures of the tropical Pacific dynamics from model and altimetry: a focus on the](#)  
1668 [meso-/submesoscale range. \*Ocean Sci.\* 14, 1283–1301. \[https://doi.org/10.5194/os-14-\]\(https://doi.org/10.5194/os-14-1283-2018\)](#)  
1669 [1283-2018](#)

1670 [Tchilibou, M., Koch-Larrouy, A., Barbot, S., Lyard, F., Morel, Y., Jouanno, J., Morrow, R.,](#)  
1671 [2022. Internal tides off the Amazon shelf during two contrasted seasons: interactions](#)  
1672 [with background circulation and SSH imprints. \*Ocean Sci.\* 18, 1591–1618.](#)  
1673 [https://doi.org/10.5194/os-18-1591-2022](#)



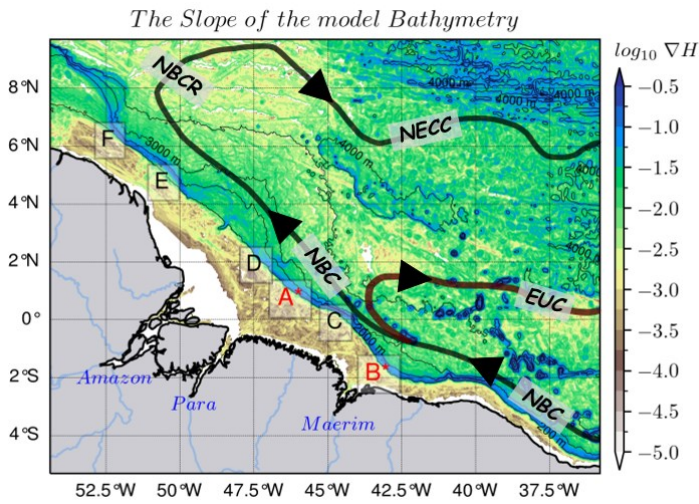
1674 [Varona, H.L., Veleda, D., Silva, M., Cintra, M., Araujo, M., 2019. Amazon River plume](#)  
1675 [influence on Western Tropical Atlantic dynamic variability. \*Dyn. Atmospheres Oceans\*](#)  
1676 [85, 1–15. <https://doi.org/10.1016/j.dynatmoce.2018.10.002>](#)  
1677 [Vlasenko, V., Stashchuk, N., 2006. Amplification and Suppression of Internal Waves by Tides](#)  
1678 [over Variable Bottom Topography. \*J. Phys. Oceanogr.\* 36, 1959–1973.](#)  
1679 [https://doi.org/10.1175/JPO2958.1](#)  
1680 [Wang, X., Peng, S., Liu, Z., Huang, R.X., Qian, Y.-K., Li, Y., 2016. Tidal Mixing in the South](#)  
1681 [China Sea: An Estimate Based on the Internal Tide Energetics. \*J. Phys. Oceanogr.\* 46,](#)  
1682 [107–124. <https://doi.org/10.1175/JPO-D-15-0082.1>](#)  
1683 [Wentz, F.J., 2015. A 17-Yr Climate Record of Environmental Parameters Derived from the](#)  
1684 [Tropical Rainfall Measuring Mission \(TRMM\) Microwave Imager. \*J. Clim.\* 28, 6882–](#)  
1685 [6902. <https://doi.org/10.1175/JCLI-D-15-0155.1>](#)  
1686 [Whalen, C.B., Talley, L.D., MacKinnon, J.A., 2012. Spatial and temporal variability of global](#)  
1687 [ocean mixing inferred from Argo profiles. \*Geophys. Res. Lett.\* 39,](#)  
1688 [https://doi.org/10.1029/2012GL053196](#)  
1689 [Xie, S.-P., Carton, J.A., 2004. Tropical Atlantic variability: Patterns, mechanisms, and impacts.](#)  
1690 [Wash. DC Am. Geophys. Union Geophys. Monogr. Ser. 147, 121–142.](#)  
1691 [https://doi.org/10.1029/147GM07](#)  
1692 [Xu, P., Yang, W., Zhu, B., Wei, H., Zhao, L., Nie, H., 2020. Turbulent mixing and vertical](#)  
1693 [nitrate flux induced by the semidiurnal internal tides in the southern Yellow Sea. \*Cont.\*](#)  
1694 [Shelf Res. 208, 104240. <https://doi.org/10.1016/j.csr.2020.104240>](#)  
1695 [Yadidya, B., Rao, A.D., 2022. Projected climate variability of internal waves in the Andaman](#)  
1696 [Sea. \*Commun. Earth Environ.\* 3, 1–12. <https://doi.org/10.1038/s43247-022-00574-8>](#)  
1697 [Zalesak, S.T., 1979. Fully multidimensional flux-corrected transport algorithms for fluids. \*J.\*](#)  
1698 [Comput. Phys. 31, 335–362. \[https://doi.org/10.1016/0021-9991\\(79\\)90051-2\]\(https://doi.org/10.1016/0021-9991\(79\)90051-2\)](#)  
1699 [Zaron, E.D., 2019. Baroclinic Tidal Sea Level from Exact-Repeat Mission Altimetry. \*J. Phys.\*](#)  
1700 [Oceanogr. 49, 193–210. <https://doi.org/10.1175/JPO-D-18-0127.1>](#)  
1701

1702  
1703  
1704  
1705  
1706  
1707  
1708  
1709  
1710  
1711  
1712  
1713  
1714  
1715

a mis en forme : Anglais (États-Unis)

a mis en forme : Normal

1716



1717

1718

1719

1720

1721

1722

1723

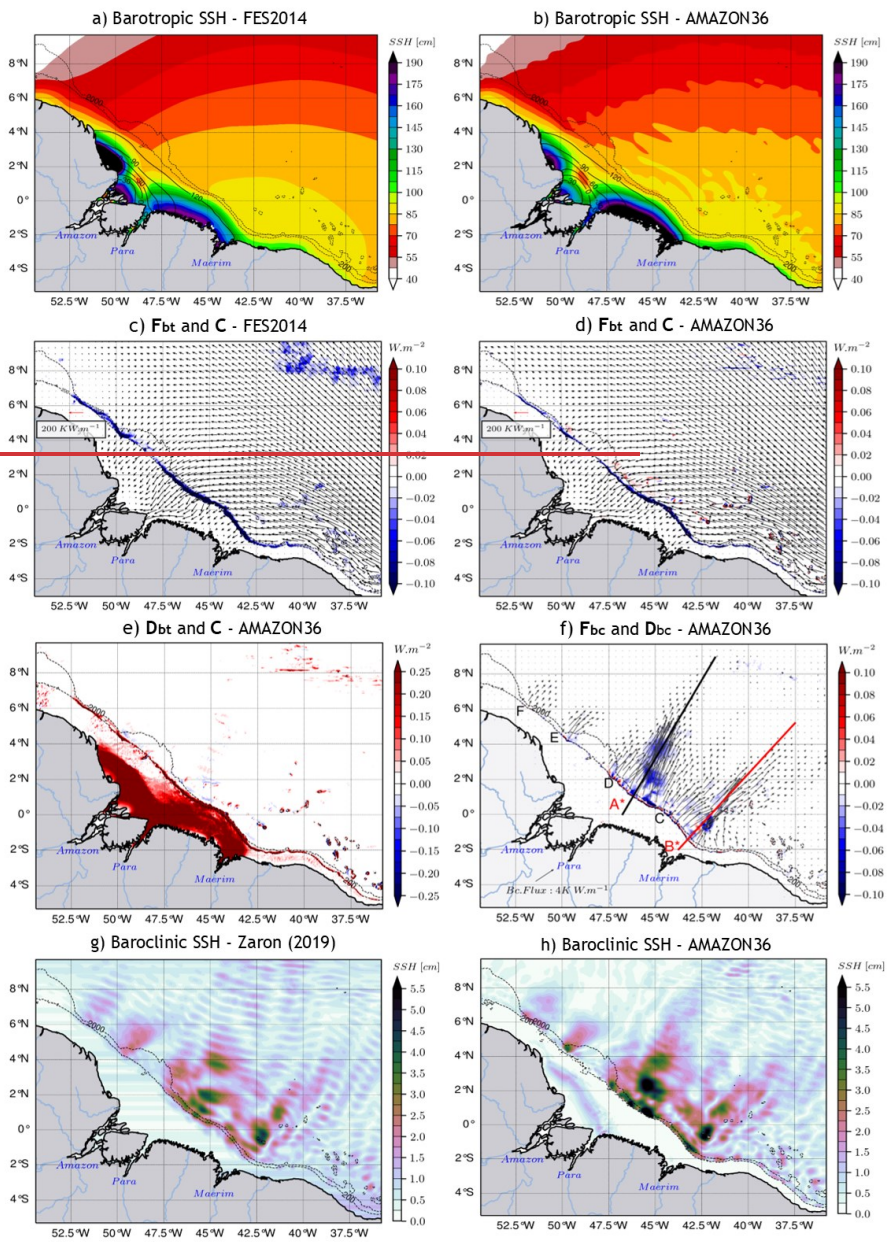
1724

1725

Figure 1. The horizontal gradient ( $\nabla H$ ) of the model's bathymetry with different internal tides generation sites ( $A^*$ ,  $B^*$ , C, D, E and F) along the high slope (blue color shading) of the shelf break, with the two main sites  $A^*$  and  $B^*$  (in red), as reported in Magalhaes et al. (2016) and Tchilibou et al. (2022). Solid bold lines represent a schematic view of the circulation (as described by Didden and Schott, 1993; Richardson et al., 1994; Johns et al., 1998; Bourles et al., 1999a; Schott et al., 2003; Garzoli et al., 2004) with NBC, NBCR and NECC tracks in black, and the EUC track in brown red. Tin black contours are 200 m, 2000 m, 3000 m and 4000 m isobaths.

a mis en forme : Espace Avant : 0 pt, Après : 0 pt

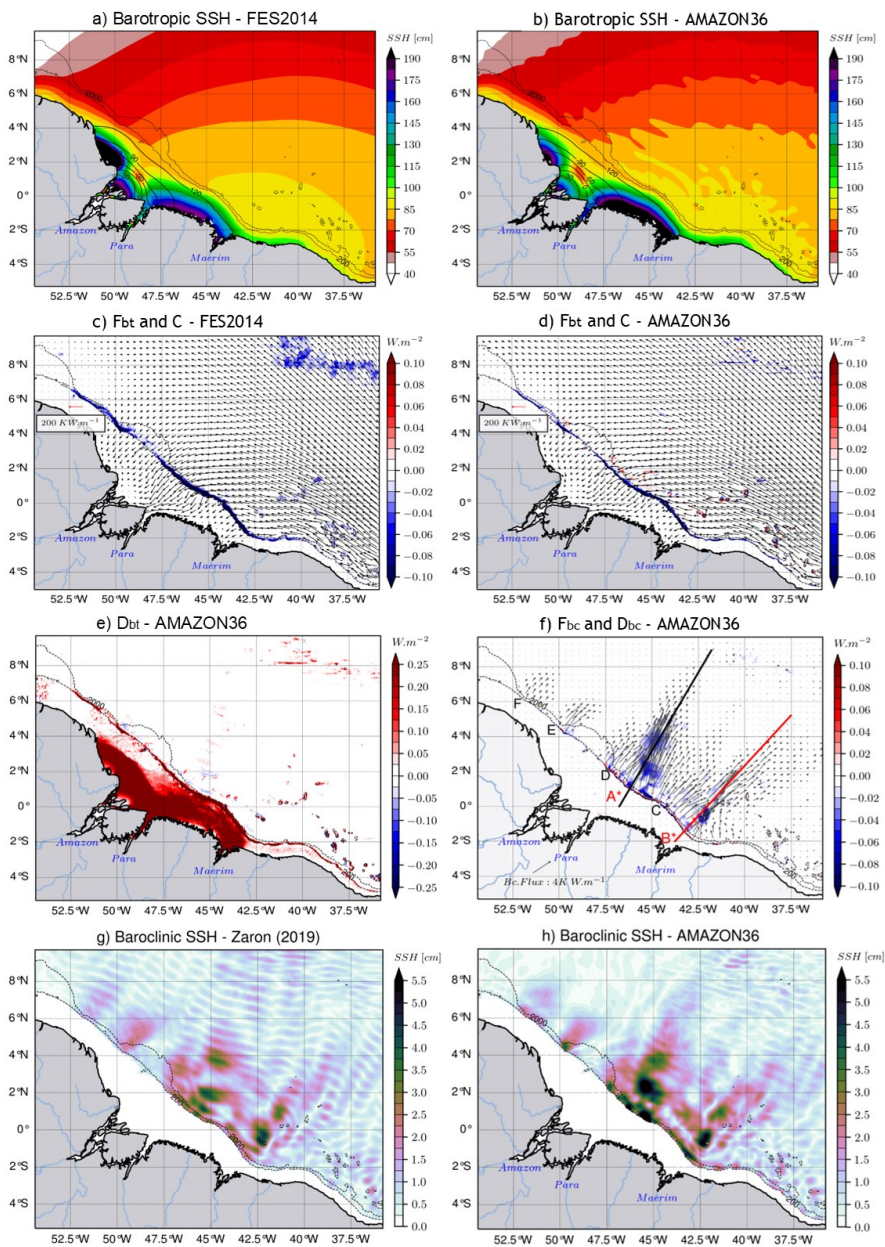
a mis en forme : Police :Non Italique



**bt** : barotropic ; **bc** : baroclinic  
**F** : energy flux ; **C** : barotropic-to-baroclinic energy conversion ; **D** : energy dissipation

1726  
 1727

1728  
1729  
1730  
1731  
1732  
1733  
1734



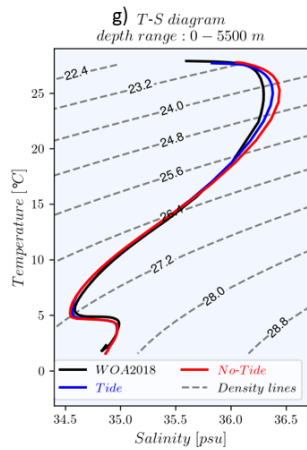
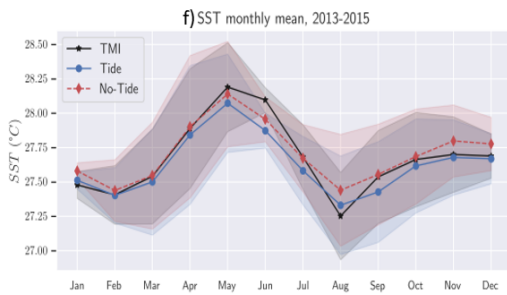
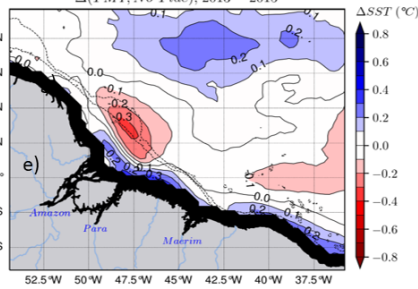
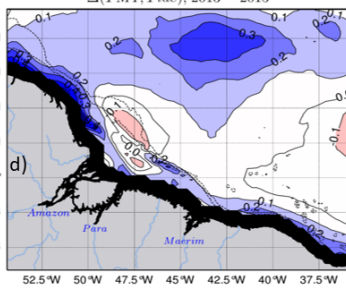
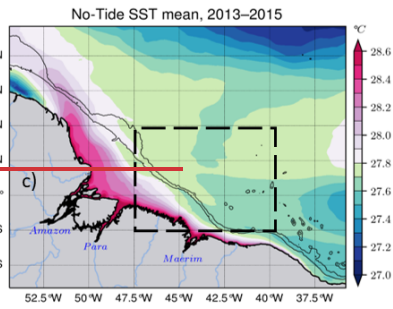
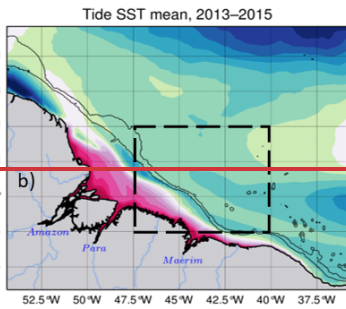
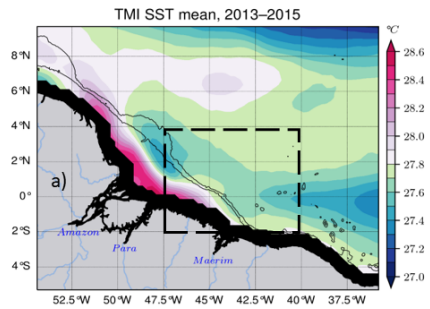
bt : barotropic ; bc : baroclinic  
 F : energy flux ; C : barotropic-to-baroclinic energy conversion ; D : dissipation

1735  
 1736 Figure 2: Coherent (or stationary) characteristics of the  $M_2$  tides. Barotropic sea surface

a mis en forme : Indice

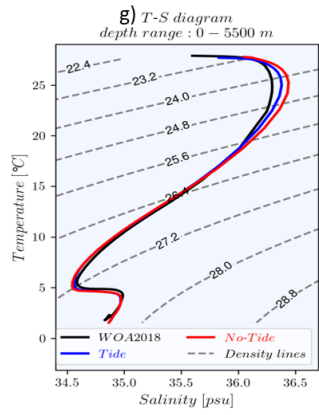
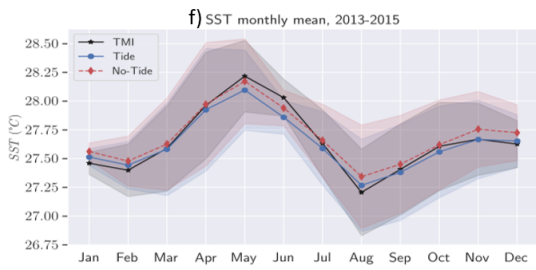
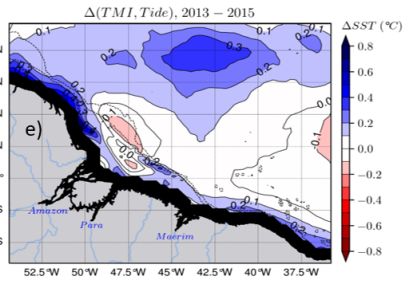
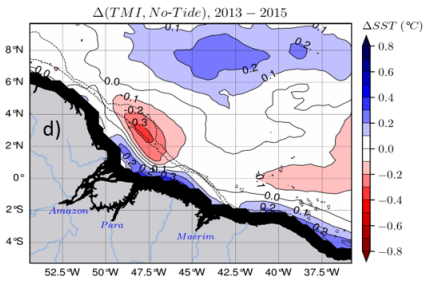
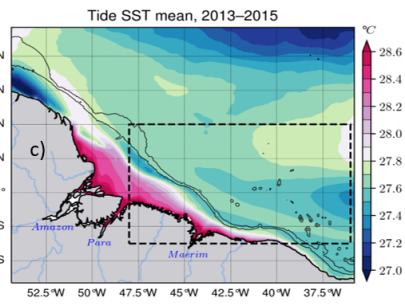
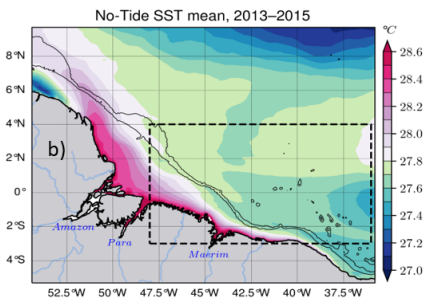
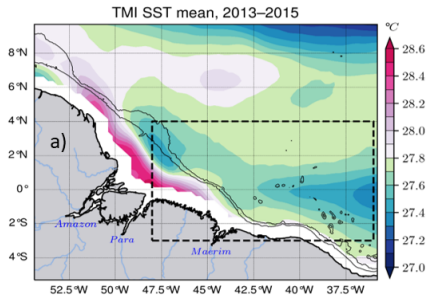
1737 height (color shading) and its phase (solid ~~4m~~-contours) for (a) FES2014 and (b) the model,  
1738 barotropic energy flux (black arrows) with the energy conversion rate (color shading) for (c)  
1739 FES2014 and (d) the model, (e) the model depth-integrated barotropic energy dissipation, (f)  
1740 the model depth-integrated baroclinic energy flux (black arrows) and the depth-integrated  
1741 baroclinic energy dissipation (color shading) with transect lines along ~~HSIT~~ trajectories A\*  
1742 (black) and B\* (red), the baroclinic sea surface height from (g) Zaron (2019) and (h) the model.  
1743 Data from the model are the mean value over the year 2015. For all panels, dashed black lines  
1744 represent the 200 m and 2000 m isobaths of the model bathymetry. ▲

**a mis en forme** : Police :Italique, Couleur de police :  
Automatique



1746  
1747  
1748  
1749  
1750  
1751  
1752  
1753  
1754  
1755  
1756  
1757  
1758  
1759  
1760  
1761  
1762  
1763  
1764  
1765  
1766  
1767

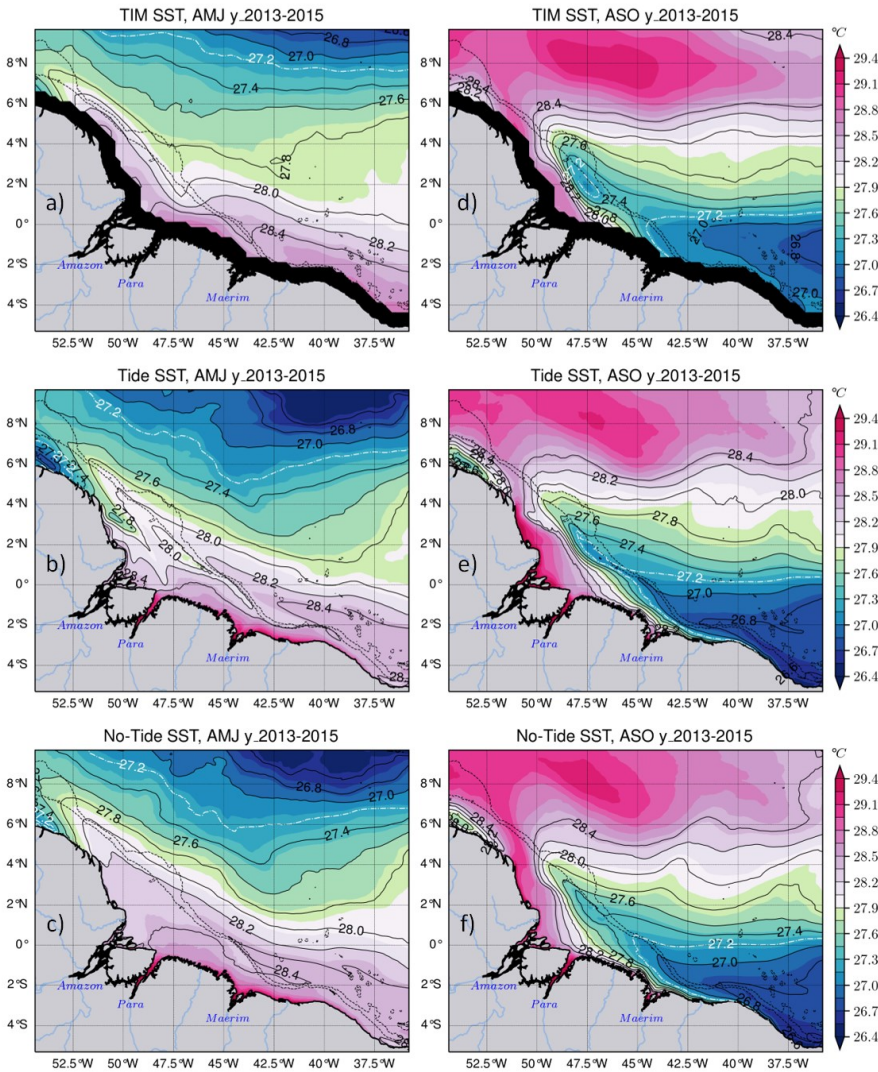




1769 Figure 3: Validation of the model temperature for the whole period 2013-2015. Mean SST for  
1770 (a) TMI with its black coastal mask, (b) the tidal simulation, (c) the non-tidal simulation, the  
1771 difference (bias) in SST between TMI and (d) the tidal simulation and (e) the non-tidal  
1772 simulation, (f) the seasonal cycle of the SST of the three products averaged within the dashed  
1773 line box in upper panels (covering ~~FFIT~~ pathways ~~emanating from the main generation sites~~  
1774 ~~A and B~~) with values masked below the 200 m isobath, bands ~~indieiate~~indicate variability  
1775 according to standard deviation. Solid black lines in panels a-c and dashed black lines in  
1776 panels d-e represent the 200 m and 2000 m isobaths from the model bathymetry, while solid  
1777 black lines in panels d-e represent bias contours. (g) Temperature-Salinity (T-S) diagram of  
1778 the mean properties in the same area as (e) from observed WOA2018 climatology (black line),  
1779 the tidal simulation (blue line) and non-tidal simulation (red line) for the water column from  
1780 surface to 5500 m depth, dashed gray lines represent density ( $\sigma_\theta$ ) contours. ~~For panels a-e~~  
1781 ~~and hereinafter (unless otherwise stated), the solid black lines represent the 200 m and 2000~~  
1782 ~~m isobaths from the model bathymetry: contours.~~  
1783  
1784  
1785  
1786

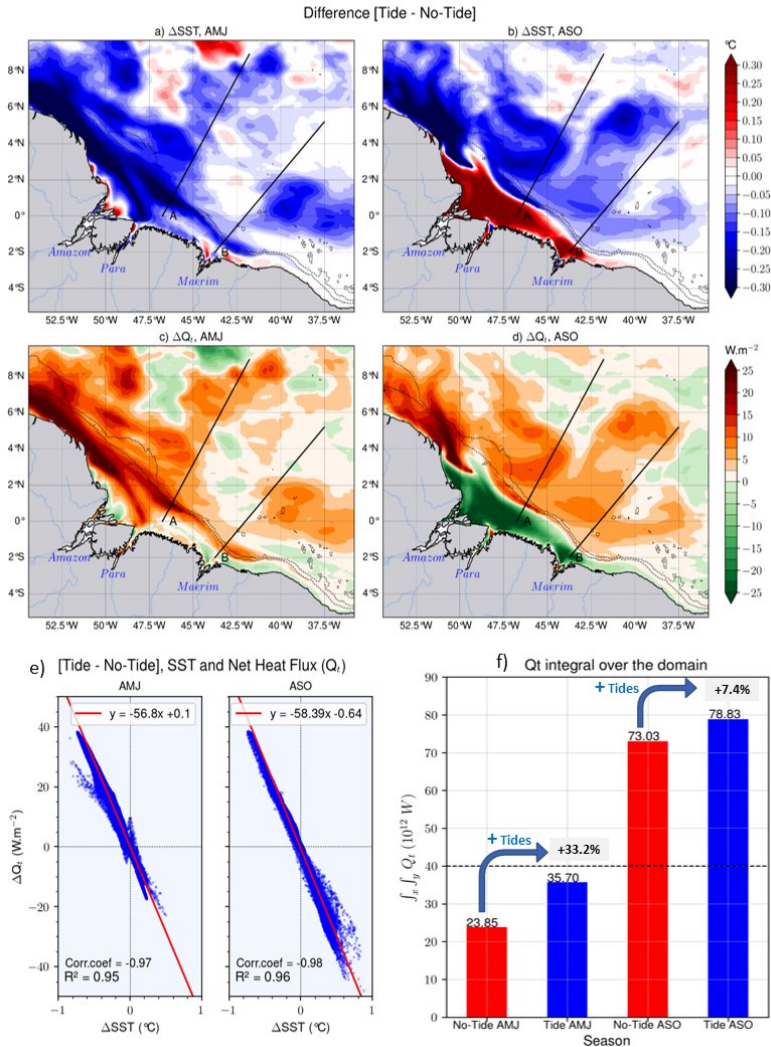
a mis en forme : Interligne : simple

a mis en forme : Police :Italique



1787  
 1788 *Figure 4: 2013-2015 seasonal SST mean. The left panels stand for the AMJ season for TMI*  
 1789 *with its black coastal mask, the tidal simulation and the non-tidal simulation, respectively for*  
 1790 *the upper-left, center-left and lower-left panel; the same in the panels on the right but for the*  
 1791 *ASO season. The dashed white and black solid lines represent the temperature contours.*  
 1792 *Dashed black lines in all panels stand for the 200 m and 2000 m isobaths from the model*  
 1793 *bathymetry.*

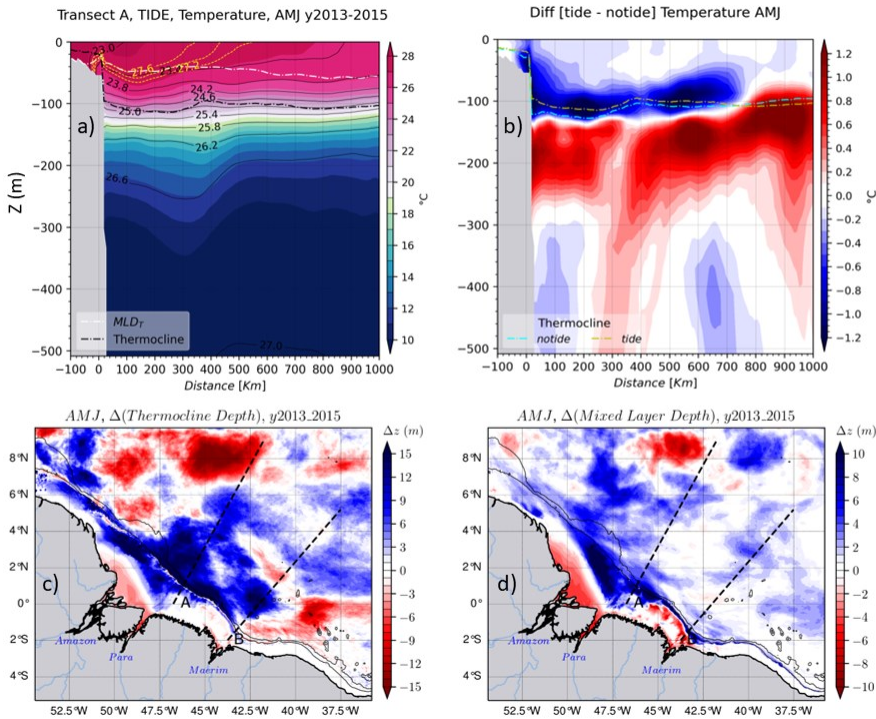
1794  
1795



1796  
1797  
1798  
1799  
1800  
1801  
1802  
1803

Figure 5: Relationship between the SST and the atmosphere-to-ocean net heat flux ( $Q_t$ ): SST anomaly [Tide - No-Tide] in AMJ (a) and ASO (b) seasons,  $Q_t$  anomaly in AMJ (c) and ASO (d) seasons, (e) correlation between  $Q_t$  anomaly and SST anomaly for each season, (f) domain integrated  $Q_t$  for both seasons of each simulation. *Hereinafter, anomaly refers to what is described hereabove.*

a mis en forme : Interligne : simple



1805

1806

1807

1808

1809

1810

1811

1812

1813

1814

1815

1816

1817

1818

1819

1820

Figure 6. Some water mass properties for the AMJ season: (a) vertical section of the temperature of the tidal simulation following the transect A, the yellow dashed and the solid black lines are the temperature and density ( $\sigma_\theta$ ) isobars respectively, the black and white ticked dashed lines are the thermocline and MLD respectively, (b) the temperature anomaly for the same vertical section, yellow and cyan dashed lines are the thermocline depth for the tidal and non-tidal simulations respectively, (c) thermocline depth anomaly and (d) MLD anomaly for the whole domain. When the MLD or the Thermocline depth anomaly are colored in blue (vs red) it means that the tides rise (vs deepen) them. Solid black lines in lower panels stand for the 200 m and 2000 m isobaths from the model bathymetry.

a mis en forme : Interligne : simple

a mis en forme : Police : 12 pt, Italique, Couleur de police : Texte 1

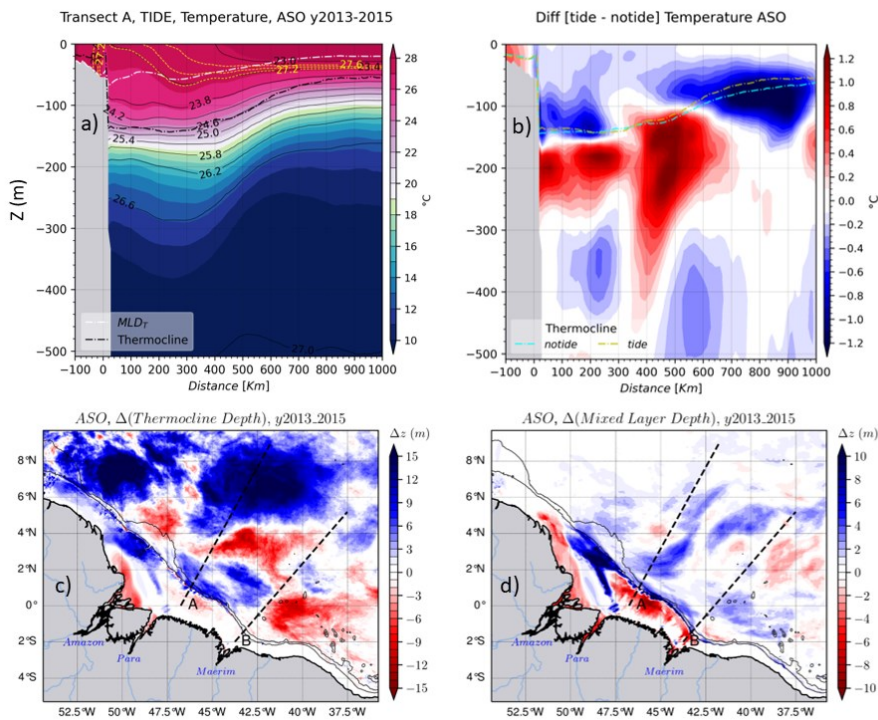
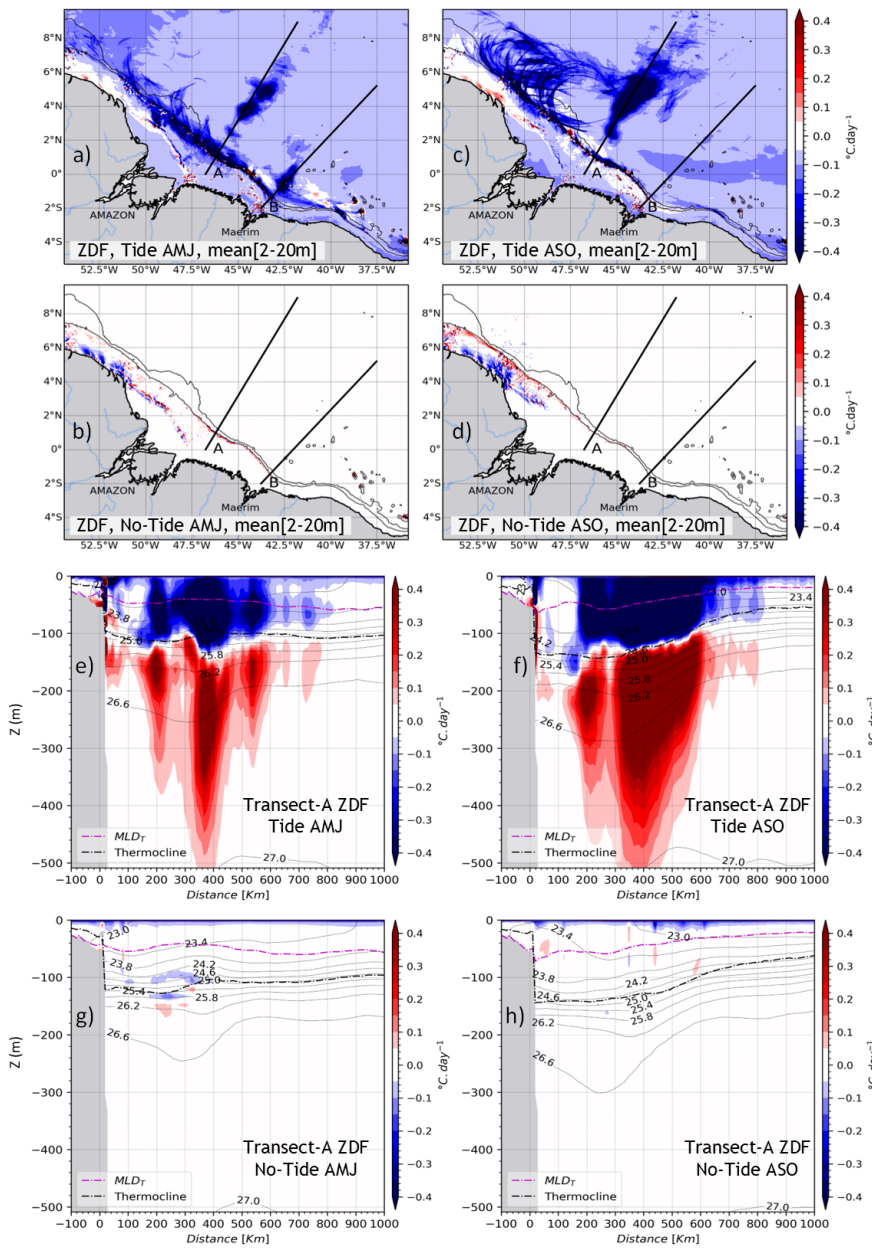


Figure 7—~~same~~. Same as figure 6 but for the ASO season.

a mis en forme : Espace Avant : 0 pt, Après : 0 pt

1821  
1822  
1823  
1824  
1825  
1826  
1827  
1828  
1829  
1830  
1831  
1832  
1833  
1834  
1835  
1836



1837

1838

1839

Figure 8: The vertical diffusion tendency of temperature (ZDF) for both seasons. The vertical mean between 2–20 m for AMJ season in tidal (a) and non-tidal (b) simulation; then for ASO

a mis en forme : Interligne : simple

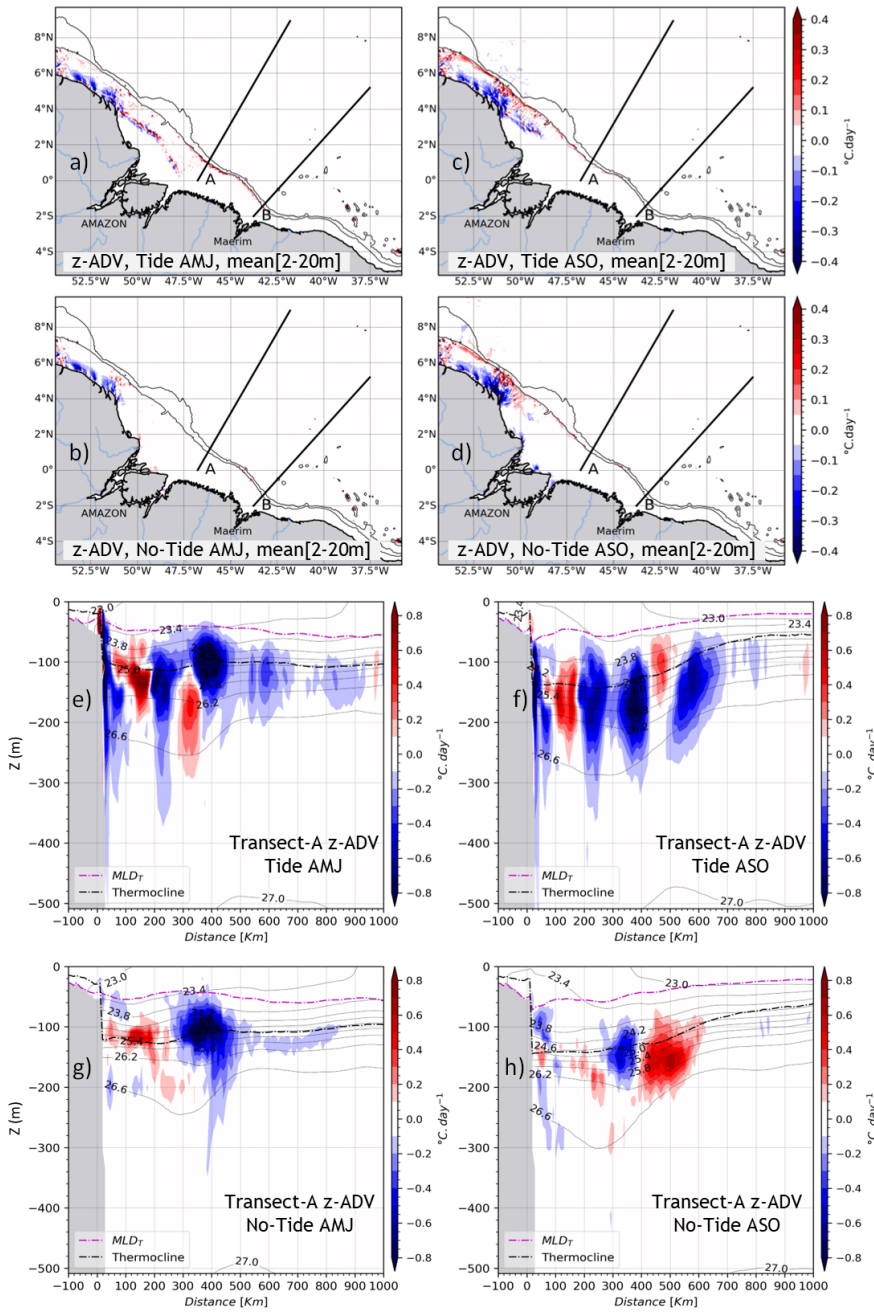
1840 season in tidal (c) and non-tidal (d) simulations. Vertical sections of ZDF following the transect  
1841 A for AMJ season in the tidal (e), for ASO season in non-tidal (f) simulations; then for AMJ  
1842 season in the non-tidal (g) and for ASO season in the non-tidal (h) simulations. The black and  
1843 magenta dashed lines are the thermocline depth and MLD respectively. Solid black lines in  
1844 panels a-d stand for the 200 m and 2000 m isobaths from the model bathymetry, while in panels  
1845 e-h, they represent the density ( $\sigma_\theta$ ) ~~isoecontours~~ contours.▲

a mis en forme : Couleur de police : Texte 1

a mis en forme : Police :12 pt, Italique

1847  
1848  
1849  
1850  
1851  
1852  
1853  
1854  
1855  
1856  
1857  
1858  
1859  
1860  
1861  
1862  
1863  
1864  
1865  
1866  
1867  
1868  
1869  
1870  
1871  
1872



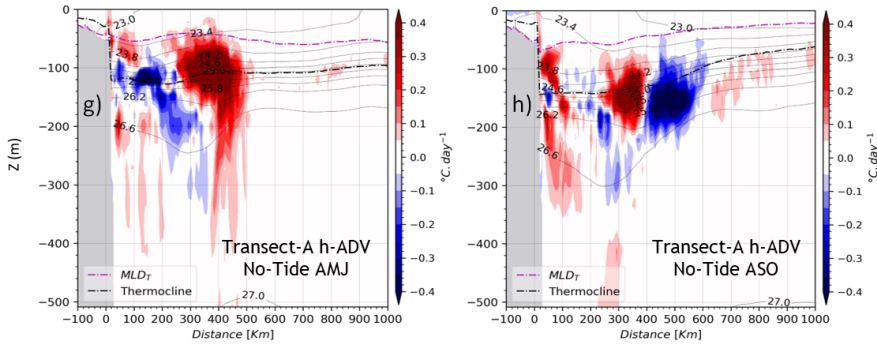
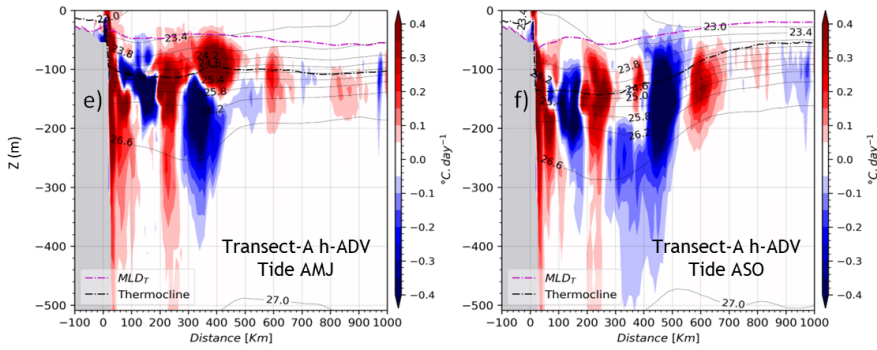
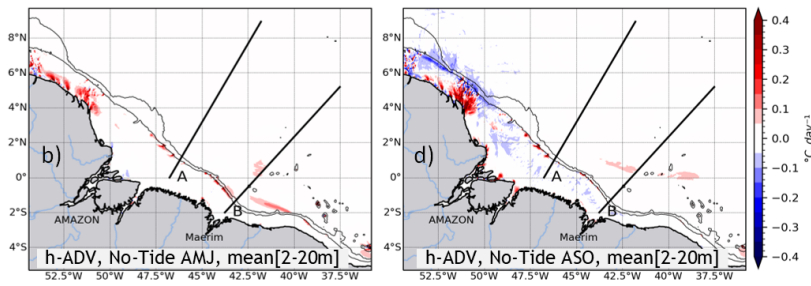
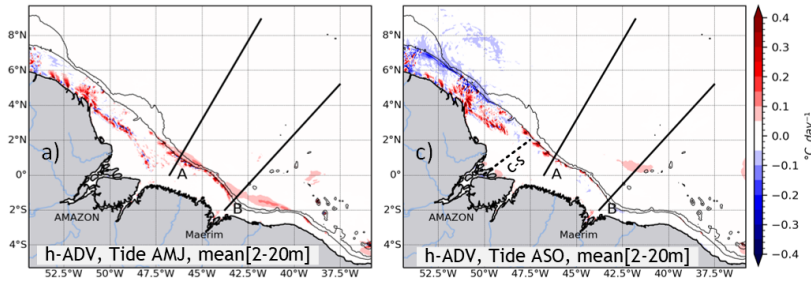


1874 Figure 9 ~~same~~ Same as figure 8, but for the vertical advection tendency of temperature ( $z$ -  
1875  $ADV$ ).

1876  
1877  
1878  
1879  
1880  
1881  
1882  
1883  
1884  
1885  
1886  
1887  
1888  
1889  
1890  
1891  
1892  
1893  
1894  
1895  
1896  
1897  
1898  
1899  
1900  
1901  
1902  
1903  
1904  
1905  
1906

a mis en forme : Police :Italique

1p07

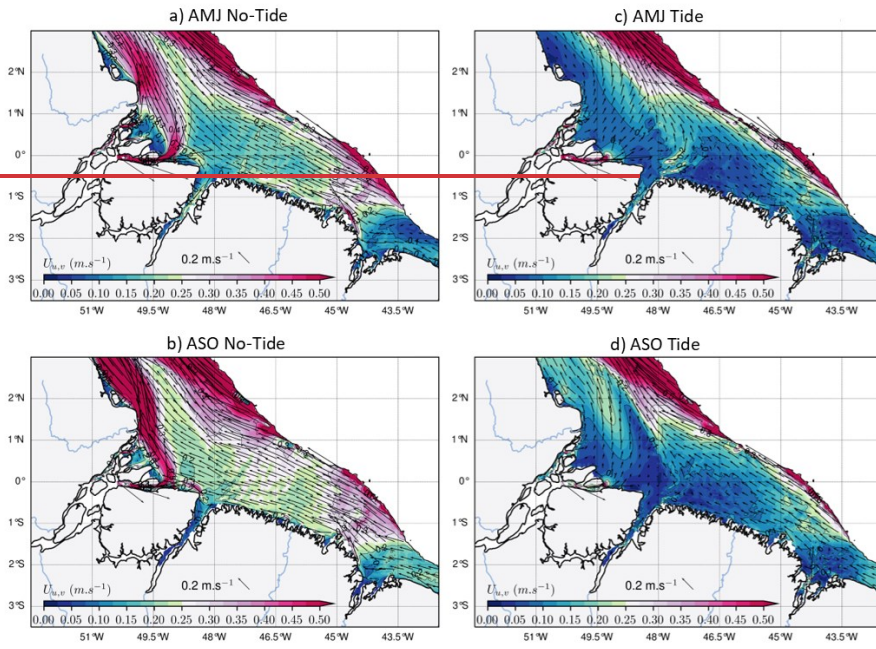


1909  
1910  
1911  
1912

Figure 10: ~~same~~ Same as figure 8 but for the horizontal advection of temperature ( $h\text{-ADV} = x\text{-ADV} + y\text{-ADV}$ ). The dashed line from the Amazon River mouth toward the outer shelf in the panel (b) indicates the cross-shore transect (C-S) used further on.

a mis en forme : Interligne : simple

a mis en forme : Espace Avant : 0 pt, Après : 0 pt

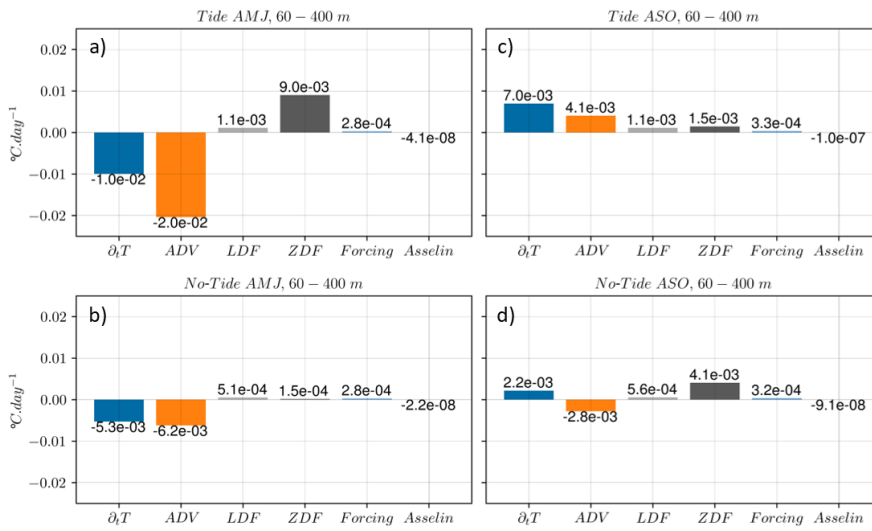


1913

1914

Figure

11



1915

1916

1917

1918

1919

1920

*Figure 11. Trends balance averaged in region around IT trajectories between 48°W–40°W and 0°N–6°N, and below the MLD between 60-400 m depth. Upper panels are for the tidal simulation and lower panels for the non-tidal simulation, while left and right panels are for the AMJ and ASO seasons respectively. ZDF is the dominant term of the heat budget equation (see section II.3.2) within the mixed-layer to explain temperature changes in upper layers.*

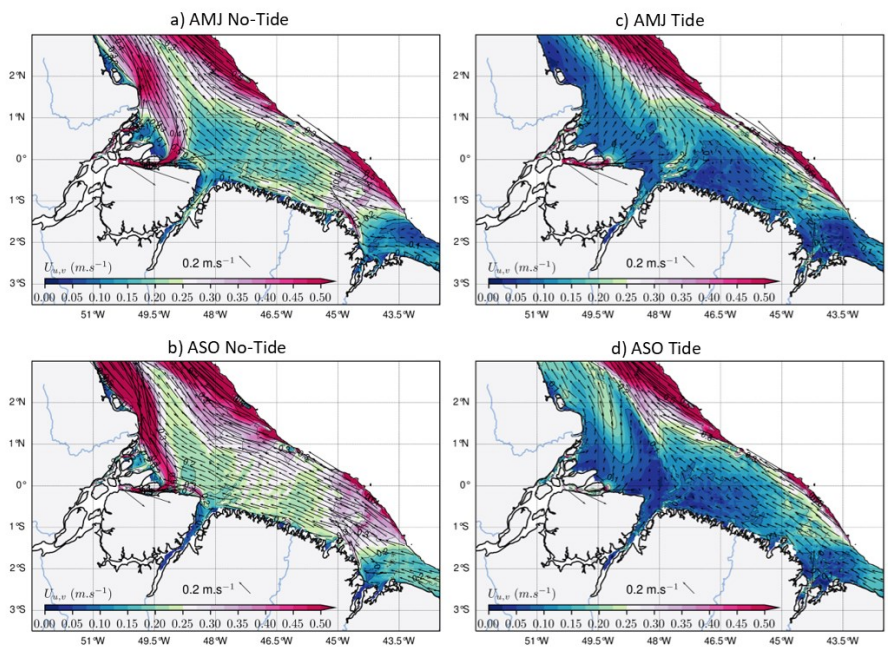
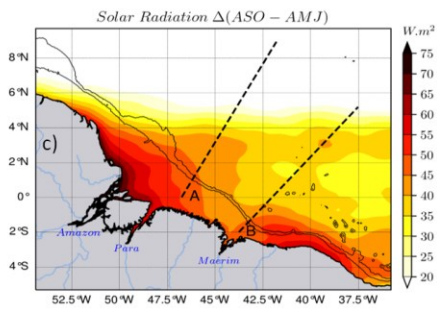
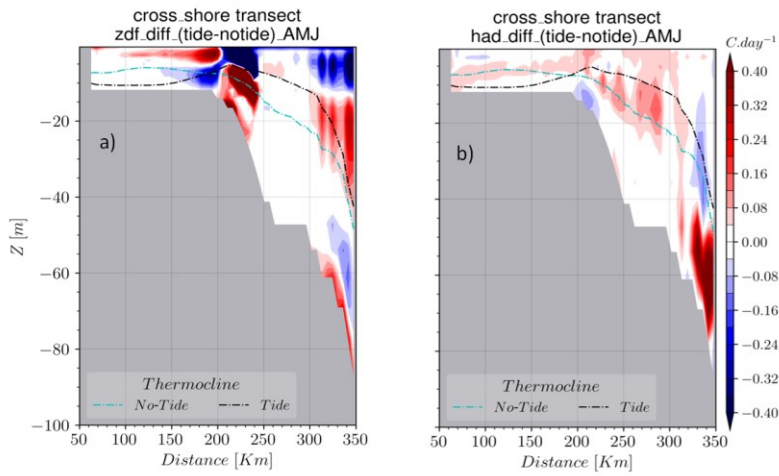


**Figure 12.** The seasonal mean of the current ( $U_{u,v}$ ) at the shelf averaged between the surface and 50 m: the non-tidal simulation in the left panels and the tidal simulation in the right panels. The upper panels stand for the AMJ season, while the lower stand for the ASO season. The color shading is the modulus of the current and the black arrows represent its direction. Values beyond the 200 m isobath are masked.

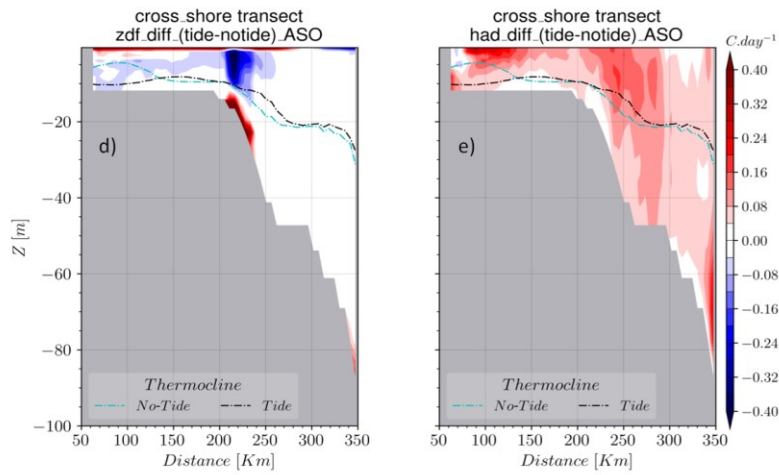
a mis en forme : Interligne : simple

a mis en forme : Police :italique, Couleur de police : Texte 1

1921  
1922  
1923  
1924  
1925  
1926  
1927  
1928  
1929  
1930  
1931  
1932  
1933



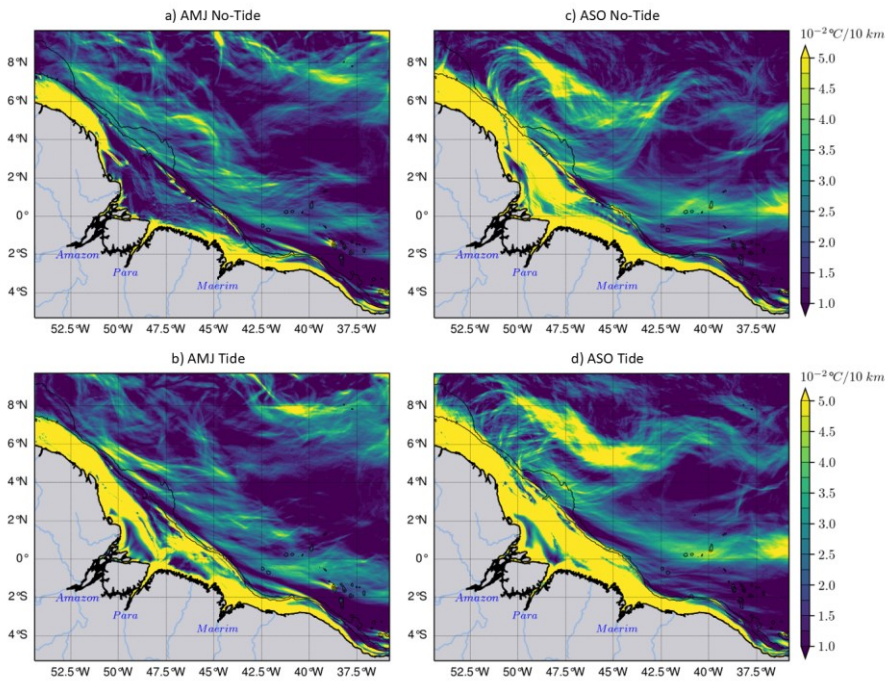
Solar radiation ( $Q_s$ ) increases in the ASO season:  
 > 30  $W.m^2$  offshore  
 > 60  $W.m^2$  over the shelf





1935 Figure 12-13. The cross-shore transect of ZDF anomaly for (a) AMJ and (b) ASO seasons,  
 1936 then for h-ADV anomaly for (d) AMJ and (e) ASO seasons ; (c) Difference in solar radiation  
 1937 between ASO and AMJ seasons. Solar radiation increases during the ASO season, with greater  
 1938 intensity on the shelf.  
 1939

a mis en forme : Interligne : simple



1940  
 1941 Figure 13-14. The horizontal gradient of the Temperature ( $\nabla T$ ) averaged between 2–20 m :  
 1942 the AMJ season in the left panels and ASO season in the right panels, the simulations without  
 1943 the tides in the upper panels, and with tides in the lower panels. During the ASO season, the  
 1944 NBC retroflects and eddy activity intensifies in the north-west. Therefore,  $\nabla T$  emphasizes eddy-  
 1945 like fronts at the same location as eddy-like patterns in ZDF (see Fig. 8b)–9b).  
 1946

1947  
 1948  
 1949  
 1950  
 1951